Progressive Failure Analysis of Composite Laminates Using Non-linear and Stochastic FEA

Daying Zhang

A Thesis in The Department of
Mechanical and Industrial Engineering

Presented in Partial Fulfillment of the Requirements
For the
Degree of Master of Applied Science
At
Concordia University
Montreal, Quebec, Canada

September, 2002

Acknowledgements

I wish to express my gratitude and indebtedness to my supervisor, Dr. Rajamohan Ganesan for his invaluable guidance, financial support and encouragement throughout the development of my thesis. He was devoting his valuable time for me always in spite of his busy schedule. I also wish to express here that Dr. Ganesan has been my constant source of inspiration for the past two years.

I would like to thank Mr. Qi Zhao for his valuable suggestions and patient discussions. I also would like to thank my fiancé Dr. Michael Collins for his understand and support during the past two years.

Abstract

Daying Zhang

The objectives of the present work are: (1) to derive the non-linear finite element formulation for the analysis of composite laminates based on the application of minimum potential energy principle; (2) to study the deterministic progressive failure and stochastic progressive failure of symmetric and unsymmetric laminates under the action of uni-axial compressive load; (3) to study the deterministic progressive failure and stochastic progressive failure of symmetric and unsymmetric laminates under the action of bi-axial compressive load; (4) to study the deterministic progressive failure of symmetric and unsymmetric laminates under the action of bi-axial compression combined with in-plane positive shear load; and (5) to study the deterministic progressive failure of symmetric and unsymmetric laminates under the action of bi-axial compression combined with in-plane negative shear load.

The first-order shear deformation theory and the von Karman geometric non-linearity hypothesis are used to develop the finite element formulation. For the stochastic failure analysis, a stochastic finite element methodology based on the Monte Carlo Simulation is used. For the case of uni-axial compression and bi-axial compression, the tensor polynomial form of the maximum stress criterion is used to predict the failure of the lamina. For the case of bi-axial compression combined with in-plane positive or negative shear loadings, the tensor polynomial form of the 3-D Tsai-Hill criterion is used to predict the failure of the lamina. The maximum stress criterion is used to predict the onset of delamination at the interface between two adjacent layers. The influences of plate aspect ratio, symmetric and unsymmetric lay-ups, and fiber orientations on the deflection response, the first-ply failure load, the ultimate failure load, the failure mode and the maximum deflection associated with failure loads are determined. In addition, progressive failure of $(\pm 45/0/90)_{2s}$, $(\pm 45)_{4s}$ and $(0/90)_{4s}$ laminates are analyzed. In the case of stochastic material properties, the mean values and the standard deviation values of failure loads are calculated.

Table of Contents

List of Figures

Chapter 1

Introduction

1.1 The First-Order Shear Deformation Theory (FSDT)

Plate structures made of laminated composite materials are often modeled as an equivalent single layer using classical laminate theory, in which the thickness direction stress components are ignored. The classical laminate theory is a direct extension of classical plate theory that is based on the Kirchhoff hypothesis for homogeneous plates. This theory is adequate when the thickness is small. However, laminated plates made of advanced composite materials, such as graphite-epoxy, are susceptible to thickness effects because their effective transverse and shear moduli are significantly smaller than the effective elastic modulus along the fibre direction. The first-order shear deformation theory is a theory for plate analysis in which the transverse stresses are taken into account. The first-order shear deformation theory is based on a displacement-based theory in which the three-dimensional elasticity theory is reduced to a two-dimensional laminate theory by assuming an approximation of the displacements through the thickness [1].

1.2 The von Karman Theory for Geometric Nonlinear Analysis

The analysis of structures involves three basic steps: (1) satisfaction of equilibrium; (2) use of material force-deformation or stress-strain relations; and (3) enforcement of continuity and compatibility in the deformed structure. In most of the familiar types of

structures, it is sufficiently accurate to consider the equilibrium with respect to the unstrained structures. The equilibrium is considered to be satisfied by assuming that all the forces involved in the final stressed structure, are acting on the undeformed structure. This is permissible since in such cases all deformations are small. Further if the material stress-strain law is also linear, the result is that the structure's behaviour and its analysis are linear.

For some materials, however, the stress-strain characteristics are nonlinear, even though they may be approximately linear for small strains. In such cases, even when the deformations of the structure and the resulting strains can be considered small from the point of view of equilibrium, the nonlinear nature of the stress-strain law is reflected in the behaviour of the structure through the force-displacement characteristics of the structure which are nonlinear. For these cases, even though it is still legitimate to consider equilibrium with respect to the undeformed configuration of the structure, the resulting analysis is nonlinear. In another class of problems, even though the stress-strain characteristics of the material are linear, the structure deformations are not small enough to allow the consideration of equilibrium in the undeformed configuration to be a valid approximation. In such cases, satisfaction of equilibrium must be discussed with respect to the final deformed configuration of the structure. Again the associated analysis is nonlinear, the nonlinearity being geometric in nature. Geometric nonlinearity is associated with large deflection and structural stability problems.

The von Karman assumption: u and v are small displacements and w is large displacement. In the analysis, consider only the nonlinearity of w.

1.3 Progressive Failure Analysis of Laminated Composite Plates

It is well known that the total failure of a laminated composite plate does not always occur at the load corresponding to the first–ply failure. The plate failure in a broad sense can be considered to have occurred when a structural element ceased to function satisfactorily; thus the definition of failure varies from one case to another. The failure characteristics of heterogeneous and anisotropic composite laminates are completely different from that of the isotropic plates. The appearance of detectable cracks in metals is generally considered to be unsafe since a slight amount of damage can rapidly progress into a catastrophic fracture. However, this is not true in the case of composite materials, although internal damage might appear very early, its propagation is arrested by the internal configuration of the structure. Therefore, composite laminates can still sustain a much higher load after the occurrence of localized damage such as matrix cracking, fiber breaks or delamination. Hence the knowledge of the first–ply failure load and the ultimate load of such structures is essential so that these plates can be designed efficiently and economically by fully utilizing its post-initial-failure strength with appropriate reliability and safety. Thus, to accurately predict the failure loads of such structures, the progressive failure analysis has become an important subject of research.

1.4 Randomness in Failure Properties

The parameters of any mechanical or structural system possess a random variation as a function of space and / or time. The randomness in failure parameters encompasses the uncertainties involved at the design and manufacturing stages, as well as the uncertain nature of the operating conditions. At the design stage, randomness is present in the test data regarding material strength values, elastic constants, engineering constants, and the material properties pertinent to the service life. The randomness in material properties significantly affects the functioning of the mechanical component and is unavoidable even with the best quality control measures.

Tests on a single material specimen or structure yield a definite value for each material parameter such as the elastic constant, engineering constant, etc. But when a number of specimens are tested, (1) the parameter values randomly fluctuate from specimen to specimen; (2) within the same structure itself, the values of any parameter display an uncertain spatial variation; (3) due to environmental degradation the parameters have uncertain fluctuations. The sample to sample variation, spatial fluctuations within the structure, structure to structure variations, and variations due to environmental effects in strength, deterioration and deformation parameters are particularly present in the case of fiber reinforced composite materials. Variations in fiber size, fiber volume fraction, fiber orientation, matrix properties, interfaces and thickness of lamina are always present and unavoidable. As a result, the elastic constants, engineering constants and deformation parameters of fiber reinforced composite materials possess a random variatio.

1.5 Overview of Literature

Among the early investigations related to the failure of laminated plates are the works by Turvey [2, 3], in which analytical solutions for the first–ply failure load are presented for symmetric and antisymmetric laminates with simply supported boundary condition under the action of transverse loads. The finite element procedure for the prediction of linear first-ply failure loads of composite laminates subjected to transverse and in-plane (tensile) load was presented by Reddy and Pandey [4]. Another study by Reddy and Reddy [5] used the first-order shear deformation theory in the finite element modeling to conduct the linear and nonlinear failure analysis. Engelstad *et al* [6] investigated the postbuckling response and failure characteristics of graphite-epoxy panels with and without circular hole in axial compression using a progressive damage failure mechanism in conjunction with a 3-D degenerated shell element. Lee and Hyer [7] studied postbuckling failure characteristics of square, symmetrically laminated plate with a circular hole under uni-axial compression using the maximum stress failure criterion. Recently, Kam and Sher [8] studied the nonlinear behaviour and the first-ply failure strength of centrally loaded laminated composite plates with semi-clamped edges using a method developed from the von Karman-Mindlin plate theory in conjunction with the Ritz method.

One of the early studies related to the shear postbuckling response of laminated plates is the work of Kaminski and Ashton [9], who presented an experimental study on rectangular boron/epoxy plates clamped on each edge. Kobayashi *et al* [10] also presented an experimental study on graphite/epoxy laminated plates in which the ultimate

load was found to be considerably greater than the buckling load. Agrawal [11] examined the postbuckling behaviour of multibay composite shear webs and studied the failure modes typical of composite panels using a NASTRAN finite element model. The investigation of Zhang and Matthews [12] on postbuckling analysis of anisotropic plates under combined compression and shear loads revealed the importance of the direction of applied shear force on the postbuckling behaviour of anisotropic laminates. Stein [13] conducted the analysis of long orthotropic plates subjected to combined shear and compression using the method developed in his earlier investigation [14] dealing with longitudinally compressed plates. Prabakar and Kennedy [15] examined theoretically the postbuckling behaviour of antisymmetric angle-ply laminates. Kosteletos [16] using the stress function approach investigated the postbuckling response of thin, flat, rectangular generally layered laminates with clamped edges under the action of shear and combined in-plane loads. Lee and Hyer [17] studied the postbuckling failure characteristics of a square symmetrically laminated plate with circular hole under uniaxial compression using the maximum stress failure criterion. Singh *et al* [18] have presented a detailed study of the progressive failure of square symmetric laminates subjected to uni-axial compression. Singh *et al* [19], [20] have also presented a study of the progressive failure of symmetric laminates under the action in-plane shear.

Stock *et al* [21], and Fukuda [22] carried out the probabilistic analysis of composite strength and effective properties using the Monte Carlo simulation technique. The simulation procedure required extensive computational resources for any new set of structural parameters and properties of the constituents.

Composites have inherent scatter in elastic and strength properties. A probabilistic model utilizing random material characteristic to predict damage evolution in orthotropic laminated composites is presented by Dzenis *et al* [23], Joshi and Frantziskonis [24] and Larder [25]. Cassenti [26] investigated the probabilistic static failure of composite materials. Probabilistic failure strength analysis of graphite/epoxy cross-ply composite laminates has been performed by Fukunaga and Chou [27]. This paper treats the failure characteristics of (0/90/0) and (90/0/90) cross-ply laminate based upon the statistical strength analysis. The stress redistributions at the failure of the 90^0 ply are analyzed using a shear-lag model.

The well-known probabilistic theories for the tensile strength of unidirectional composites have been proposed by Rosen [28] and Zweben [29] and further developments have been reported in detail in Refs. [30, 31]. These models give us a satisfactory strength estimation when the failure of the composite material is predominantly affected by the stochastic strength distribution of reinforcement fibres.

The analysis of structures, whether subjected to random or deterministic external loads, has been developed mainly under the assumption that the structure's parameters are deterministic quantities. In a significant number of circumstances, this assumption is not valid, and the probabilistic aspects of the structure need to be taken into account. The necessity to account for random effects in determining the response of a mechanical system is due, in general, to three different sources: random external loadings, random boundary conditions, and random material parameters. In the last twenty years the

powerful finite element method has undergone various new developments to incorporate the randomness, and is now termed as Stochastic Finite Element Method (SFEM). The developments in this field are reviewed by Contreras [32], Vanmarcke *et al* [33], Benaroya and Rehak [34], Yamazaki *et al* [35], Ostoja-Starzewshi [36], and Vanmarcke [37]. The stochastic finite element method is capable of dealing with random structural properties described by random fields very efficiently. Recent developments, such as the weighted integral technique [38] and [39], provide an accurate and consistent transition from continuous type random fields to discrete type stochastic finite elements.

Ramu and Ganesan [40] developed a new finite element method to analyze the structures with more than one parameter behaving in a stochastic manner using the Galerkin weighted residual method. The stochastic finite element analysis based on the local averages of random vector fields is formulated by Zhu *et al* [41] for eigenvalue problems. Jensen and Iwan [42] presented a method for the dynamic analysis of linear systems with uncertain parameters to stochastic excitation. Liu *et al* [43] studied the application of the SFEM in elastic/plastic dynamics with random material properties. Ghanem and Spanos [44] proposed a new method for the solution of problems involving material variability. The material property is modeled as a stochastic process. The method makes use of a convergent orthogonal expansion of the process. Ganesan *et al* [45] developed a stochastic finite element method to solve the more general non-self-adjoint eigenvalue problems. Shinozuka *et al* [46] developed a method for the estimation of the structural reliability when a structure is subjected to loads that can be idealized in terms of a Gaussian random vector process. Ramu and Ganesan [47] analyzed the free vibrational

characteristics of a beam-column, which is having randomly varying Young's modulus and mass density and subjected to randomly distributed axial loading. In their study, Hamilton's principle is used to formulate the problem using stochastic FEM. Ren *et al* [48] proposed a new version of finite element method for the mean and covariance functions of the displacement for bending of beams with spatially random stiffness based on the variational principles. Sankar, Ramu and Ganesan [49] derived the sensitivities of SIF and COD of cracked structural systems to fluctuations in material property values and external loadings. In their study, a Taylor series expansion is used to express the SIF and COD in terms of averaged values. Sankar, Ramu and Ganesan [50] described an effective method for integrating the concepts of probabilistic structural mechanics with the finite element analysis for dynamic systems.

The successful application of the mechanics of composites for achieving safer and reliable designs is hindered by the inherent uncertain distributions of material and geometric properties. In recent years, composite structures involving random material properties have been studied by many researchers. Among them Liaw and Yang [51] developed a 16-dof quadrilateral stochastic laminated thin-plate element. Ganesan and Hoa [52] presented the stress analysis of composite structures with stochastic parameters. Nakagiri, Takabatake and Tani [53] presented a methodology of stochastic finite element method applied to the uncertain eigenvalue problem of linear vibration which arises from the fluctuation of the overall stiffness due to uncertain variation of the stacking sequence of composite laminates. Engelstad and Reddy [54] developed a probabilistic finite element analysis procedure for laminated composite shells. In their study, a total

Lagrangian finite element formulation, employing a degenerated three-dimensional laminated composite shell element with the full Green-Lagrange strains and first-order shear deformable kinematics, is used. Chang and Yang [55] formulated a geometrically non-linear stochastic thin-plate finite element to study the reliability of fiber-reinforced laminates made of advanced composite materials. The modeling involves two steps: a micro-mechanical simulation of the degradation of a small cell of the composite and a random-damage finite element simulation of material failure.

Studies on the reliability of the static strength of fibrous composites can be classified into three groups: 1) studies that investigate experimentally the factors that effect the variation or the scatter of the strength using a number of specimens, 2) studies that analyze the variation of the strength theoretically using micro-mechanical models, 3) studies that analyze the reliability of the strength of unidirectional and laminated composites using a macroscopic failure criterion and fundamental data on the variations of the strengths along the principal directions. The strength and stiffness of composite materials change remarkably by changing the kinds, volume contents and orientations of the reinforcing fibers and stacking sequences, therefore, the optimum material design can be performed under a given loading condition. Mitsunori *et al* [56] have presented a method to evaluate the reliability of unidirectional fibrous composites under any plane stress condition, and the effects of various factors on the reliability are investigated. It has been found that the orientation angle that results in the maximum reliability and the optimum angle that corresponds to the design criterion vary with the variation in the applied stress in some cases. It has been found that the optimum fiber orientations of unidirectional composite

materials under probabilistic loading conditions are found to be different from those under deterministic loading conditions. Mitsunori *et al* [57] also proposed a simple and intuitive method called the interior tangent ellipsoid (ITE) method for the optimum design of composites under the action of loads with variations. Shaowen *et al* [58] presented a discussion on the optimum design of multiaxially laminated fibrous composites under probabilistic conditions of loads and material conditions. The first-ply failure criterion is adopted for conducting the reliability analysis. Mitsunori *et al* [59] have presented a discussion on the optimum fiber orientation angles of multiaxial laminates based on reliability analysis. The probabilistic properties of the applied loads and the elastic constants of the ply material are discussed from the viewpoint of reliability and optimum design. The effects of the correlation between various random variables on the reliability and reliability-based design of composite plates subjected to buckling have been discussed by Nozomu *et al* [60], and the reliability have been maximised in terms of the mean ply orientation angles. The study shows that reliability-based design ignoring correlation is sometimes less safe than even a deterministic buckling load maximization design when random variables are correlated. By viewing the composite lamina as a homogeneous solid whose directional strengths are random variables, Thomas and Wetherhold [61] proposed some physically plausible phenomenological rules for the redistribution of load after a lamina has failed within the confines of a laminate. Using a non-interactive criterion for demonstration purposes, laminate reliabilities are calculated assuming previously established load sharing rules for the redistribution of the load as the failure of the lamina occurs. Cohen [62] presented a composite vessel design approach that is based on the reliability and the probabilistic failure strength distribution concepts.

This method is based on fiber strain-strength interference reliability theory. The fiber statistical strength distribution is analyzed using the Weibull distribution function.

1.6 Scope and Objectives of the Thesis

In the present study, the principle of minimum potential energy is used to derive the nonlinear finite element formulation. The finite element formulation is based on the first-order shear deformation theory and employs a nine-node Lagrangian element having five degrees of freedom (two in-plane displacements, one transverse displacement and two rotational degrees of freedom) per node. The resulting nonlinear equations are solved using the Newton-Raphson technique. Failure models based on the tensor polynomial failure criterion are used in the progressive failure procedure, while the maximum stress criterion is used for predicting the onset of delamination.

The objectives of the present work are: (1) to derive the non-linear finite element formulation for the analysis of composite laminates based on the application of minimum potential energy principle; (2) to study the deterministic progressive failure and stochastic progressive failure of symmetric and unsymmetric laminates under the action of uni-axial compressive load; (3) to study the deterministic progressive failure and stochastic progressive failure of symmetric and unsymmetric laminates under the action of bi-axial compressive load; (4) to study the deterministic progressive failure of symmetric and unsymmetric laminates under the action of bi-axial compression combined with in-plane positive shear load; and (5) to study the deterministic progressive failure of symmetric and unsymmetric laminates under the action of bi-axial compression combined with in-

plane negative shear load. In all cases, the load-deflection curve is determined. One can estimate the linearized buckling load from the load-deflection curve. The progressive failure analysis is conducted until the ultimate failure is reached and thus encompasses the post-buckling behavior of the laminate.

1.7 Organization of the Thesis

The present chapter provided a brief introduction and also, the scope and the objectives of the thesis. In Chapter 2, the first-order shear deformation theory is described and the corresponding finite element formulation is developed. The geometric nonlinearity is incorporated into the formulation using the von Karman hypothesis. The Newton-Raphson technique that can be used to solve the nonlinear algebraic equations is described.

In Chapter 3, the details about the failure criteria are presented. The tensor polynomial failure criterion, from which the maximum stress criterion and Tsai-Hill criterion are derived, is used to predict the failure of the lamina. The maximum stress criterion is used to predict the onset of delamination at the interface between two adjacent layers. The progressive failure analysis procedure is described. Example applications are described. Comparison of the results obtained in the present work with that given in relevant reference works are given in this Chapter.

A detailed parametric study regarding the progressive failure of various types of laminates subjected to different types of loads is described in Chapter 4.

In Chapter 5, the analytical modeling of material properties as stochastic processes is described. The Markov model is applied to stochastic finite element analysis. The program that has been developed in Chapters 2 and 3 is extended so as to incorporate the stochastic description of material properties and the stochastic finite element analysis. The influences of randomness in material properties on the distribution of failure loads are studied in Chapter 5. A stochastic finite element failure analysis procedure is developed and described in this Chapter.

In Chapter 6, the conclusions of the present work and suggestions for the future work are given.

Chapter 2

Finite Element Formulation and Analysis

2.1 The First-order Shear Deformation Theory

Plates are structural elements whose thickness (or height) is small compared to the other two geometric dimensions. Plate structures made of laminated composite materials are often modeled as an equivalent single-layer with anisotropic properties using classical laminate theory, in which the thickness-direction stress components are ignored. In the classical plate theory (the Kirchhoff hypothesis) holds that:

(1) Straight lines perpendicular to mid-surface (i.e., transverse normal) before deformation remain straight after deformation.

(2) The straight lines do not undergo axial deformation (i.e.inextensible).

(3) The straight line rotates such that they remain perpendicular to the mid-surface after deformation.

The first two assumptions imply that the transverse displacement is independent of the transverse (or thickness) coordinate and the transverse normal strain is zero. The third assumption results in zero transverse shear strains. Thus, in the classical plate theory all transverse stresses are neglected. The classical plate theory is adequate for many engineering problems. However, laminated plates made of advanced filamentary

composite materials, whose elastic to shear modulus ratios are very large, are susceptible to thickness effects because their effective transverse shear moduli are significantly smaller than the effective elastic moduli along the fiber direction. These high ratios of elastic to shear moduli render the classical theories inadequate for the analysis of thick or composite plates. The first order shear deformation theory is a single-layer theory in which the transverse shear stresses are taken into account. In this theory it is assumed that the strain normal to the mid-plane of the plate is negligible when compared to the in-plane strains ($\varepsilon_z \approx 0$) and that straight lines normal to the plate mid-plane before deformation remain straight but not necessarily normal to the mid-surface after deformation.

The displacement field in the first–order theory is assumed to be of the form [1]

$$u(x,y,z) = u_0(x,y) + z\phi_x(x,y) \tag{2.1}$$

$$v(x,y,z) = v_0(x,y) + z\phi_y(x,y) \tag{2.2}$$

$$w(x,y,z) = w_0(x,y) \tag{2.3}$$

where (u_0, v_0, w_0) denote the displacements along the (x,y,z) directions of a point $(x,y,0)$ on the mid-plane, and (ϕ_x, ϕ_y) are the rotations (counter clockwise rotation is +ve) of the transverse normal about Y and X axes, respectively.

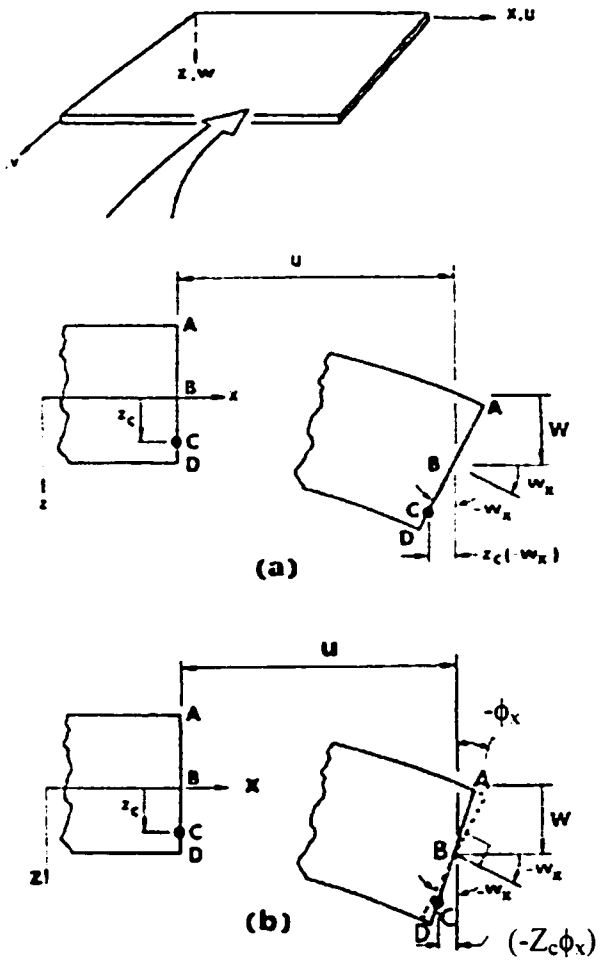

Figure 2-1 Geometry of deformation in the xz-plane for the (a) classical and (b) first-order plate theories [1]

2.2 The Nonlinear Strain-displacement Relations

The von Karman assumption: the displacements u and v are small and the displacement w is large. Correspondingly, the products and square of the in-plane displacement gradients are neglected in the nonlinear strain-displacement relations.

The nonlinear strain-displacement relations [1]:

$$\varepsilon_x = \frac{\partial u}{\partial x} + \frac{1}{2}\left[\left(\frac{\partial u}{\partial x}\right)^2 + \left(\frac{\partial v}{\partial x}\right)^2 + \left(\frac{\partial w}{\partial x}\right)^2\right] = \frac{\partial u}{\partial x} + \frac{1}{2}\left(\frac{\partial w}{\partial x}\right)^2 \tag{2.4}$$

$$\varepsilon_y = \frac{\partial v}{\partial y} + \frac{1}{2}\left[\left(\frac{\partial u}{\partial x}\right)^2 + \left(\frac{\partial v}{\partial x}\right)^2 + \left(\frac{\partial w}{\partial x}\right)^2\right] = \frac{\partial v}{\partial y} + \frac{1}{2}\left(\frac{\partial w}{\partial y}\right)^2 \tag{2.5}$$

$$\varepsilon_z = \frac{\partial w}{\partial z} + \frac{1}{2}\left[\left(\frac{\partial u}{\partial z}\right)^2 + \left(\frac{\partial v}{\partial z}\right)^2 + \left(\frac{\partial w}{\partial z}\right)^2\right] = \frac{\partial w}{\partial z} + \frac{1}{2}\left(\frac{\partial w}{\partial z}\right)^2 = 0 \tag{2.6}$$

$$\gamma_{xy} = \frac{\partial v}{\partial x} + \frac{\partial u}{\partial y} + \frac{\partial u}{\partial x}\frac{\partial u}{\partial y} + \frac{\partial v}{\partial x}\frac{\partial v}{\partial y} + \frac{\partial w}{\partial x}\frac{\partial w}{\partial y} = \frac{\partial v}{\partial x} + \frac{\partial u}{\partial y} + \frac{\partial w}{\partial x}\frac{\partial w}{\partial y} \tag{2.7}$$

$$\gamma_{yz} = \frac{\partial w}{\partial y} + \frac{\partial v}{\partial z} + \frac{\partial u}{\partial z}\frac{\partial u}{\partial y} + \frac{\partial v}{\partial z}\frac{\partial v}{\partial y} + \frac{\partial w}{\partial z}\frac{\partial w}{\partial y} = \frac{\partial w}{\partial y} + \frac{\partial v}{\partial z} + \frac{\partial w}{\partial z}\frac{\partial w}{\partial y} \tag{2.8}$$

$$\gamma_{xz} = \frac{\partial w}{\partial x} + \frac{\partial u}{\partial z} + \frac{\partial u}{\partial z}\frac{\partial u}{\partial x} + \frac{\partial v}{\partial z}\frac{\partial v}{\partial x} + \frac{\partial w}{\partial z}\frac{\partial w}{\partial x} = \frac{\partial w}{\partial x} + \frac{\partial u}{\partial z} + \frac{\partial w}{\partial z}\frac{\partial w}{\partial x} \tag{2.9}$$

Substituting equations (2.1-2.3) into the nonlinear strain-displacement relations (2.4-2.9) referred to an orthogonal coordinate system, and retaining only those nonlinear terms that involve the transverse deflection (i.e., the von Karman assumption), we obtain

$$\varepsilon_x = \frac{\partial u}{\partial x} + \frac{1}{2}\left(\frac{\partial w}{\partial x}\right)^2 = \frac{\partial u_0}{\partial x} + z\frac{\partial \phi_x}{\partial x} + \frac{1}{2}\left(\frac{\partial w_0}{\partial x}\right)^2 = \varepsilon_x{}^0 + zk_x \tag{2.10}$$

$$\varepsilon_y = \frac{\partial v}{\partial y} + \frac{1}{2}\left(\frac{\partial w}{\partial y}\right)^2 = \frac{\partial v_0}{\partial y} + z\frac{\partial \phi_y}{\partial y} + \frac{1}{2}\left(\frac{\partial w_0}{\partial y}\right)^2 = \varepsilon_y{}^0 + zk_y \tag{2.11}$$

$$\varepsilon_z = 0 \tag{2.12}$$

$$\gamma_{xy} = \frac{\partial v}{\partial x} + \frac{\partial u}{\partial y} + \frac{\partial w}{\partial x}\frac{\partial w}{\partial y} = \frac{\partial v_0}{\partial x} + \frac{\partial u_0}{\partial y} + \frac{\partial w_0}{\partial x}\frac{\partial w_0}{\partial y} + z\left(\frac{\partial \phi_x}{\partial y} + \frac{\partial \phi_y}{\partial x}\right) = \gamma_{xy}^{\ 0} + zk_{xy} \tag{2.13}$$

$$\gamma_{yz} = \frac{\partial w}{\partial y} + \frac{\partial v}{\partial z} + \frac{\partial w}{\partial z}\frac{\partial w}{\partial y} = \frac{\partial w_0}{\partial y} + \phi_y + 0 = \gamma_{yz}^{\ 0} \qquad (\frac{\partial w}{\partial z} = 0) \tag{2.14}$$

$$\gamma_{xz} = \frac{\partial w}{\partial x} + \frac{\partial u}{\partial z} + \frac{\partial w}{\partial z}\frac{\partial w}{\partial x} = \frac{\partial w_0}{\partial x} + \phi_x + 0 = \gamma_{xz}^{\ 0} \tag{2.15}$$

where

$$\varepsilon_x^{\ 0} = \frac{\partial u_0}{\partial x} + \frac{1}{2}\left(\frac{\partial w_0}{\partial x}\right)^2 \tag{2.16}$$

$$k_x = \frac{\partial \phi_x}{\partial x} \tag{2.17}$$

$$\varepsilon_y^{\ 0} = \frac{\partial v_0}{\partial y} + \frac{1}{2}\left(\frac{\partial w_0}{\partial y}\right)^2 \tag{2.18}$$

$$k_y = \frac{\partial \phi_y}{\partial y} \tag{2.19}$$

$$\gamma_{xy}^{\ 0} = \frac{\partial v_0}{\partial x} + \frac{\partial u_0}{\partial y} + \frac{\partial w_0}{\partial x}\frac{\partial w_0}{\partial y} \tag{2.20}$$

$$k_{xy} = \frac{\partial \phi_x}{\partial y} + \frac{\partial \phi_y}{\partial x} \tag{2.21}$$

$$\gamma_{yz}^{0} = \frac{\partial w_0}{\partial y} + \phi_y \tag{2.22}$$

$$\gamma_{xz}^{0} = \frac{\partial w_0}{\partial x} + \phi_x \tag{2.23}$$

2.3 Constitutive Equations

If the plate is made of several orthotropic layers, with their material axes oriented arbitrarily with respect to the plate coordinates, the constitutive equations of laminated plate can be derived by integrating the lamina relations through the thickness. The constitutive relations for a linear elastic body are given by [1]

$$\sigma_i = c_{ij}\varepsilon_j \qquad \text{(sum on j)} \tag{2.24}$$

where

$\sigma_1 = \sigma_x$, $\sigma_2 = \sigma_y$, $\sigma_3 = \sigma_z$, $\sigma_6 = \tau_{xy}$, $\sigma_4 = \tau_{yz}$, $\sigma_5 = \tau_{xz}$

$\varepsilon_1 = \varepsilon_x$, $\varepsilon_2 = \varepsilon_y$, $\varepsilon_3 = \varepsilon_z$, $\varepsilon_6 = 2\varepsilon_{xy}$, $\varepsilon_4 = 2\varepsilon_{zy}$, $\varepsilon_5 = 2\varepsilon_{xz}$

and c_{ij} are the elastic constants of the material.

The stress-strain relations for an orthotropic material in its material coordinates are given by [1]

$$\begin{Bmatrix} \bar{\sigma}_1 \\ \bar{\sigma}_2 \\ \bar{\sigma}_6 \\ \bar{\sigma}_4 \\ \bar{\sigma}_5 \end{Bmatrix} = \begin{bmatrix} \bar{Q}_{11} & \bar{Q}_{12} & 0 & 0 & 0 \\ \bar{Q}_{21} & \bar{Q}_{22} & 0 & 0 & 0 \\ 0 & 0 & \bar{Q}_{66} & 0 & 0 \\ 0 & 0 & 0 & \bar{Q}_{44} & 0 \\ 0 & 0 & 0 & 0 & \bar{Q}_{55} \end{bmatrix} \begin{Bmatrix} \bar{\varepsilon}_1 \\ \bar{\varepsilon}_2 \\ \bar{\varepsilon}_6 \\ \bar{\varepsilon}_4 \\ \bar{\varepsilon}_5 \end{Bmatrix} \tag{2.25}$$

where $\bar{Q}_{ij}$ are the plane stress reduced stiffness coefficients of the plate in its material coordinate system, and $(\bar{\sigma}_j, \bar{\varepsilon}_j)$ are the stress and strain components referred to material coordinate system.

The coefficients $\bar{Q}_{ij}$ can be expressed in terms of the engineering constants as [1]

$$\bar{Q}_{11} = \frac{E_1}{1 - \nu_{12}\nu_{21}} \tag{2.26}$$

$$\bar{Q}_{12} = \frac{\nu_{12}E_2}{1 - \nu_{12}\nu_{21}} = \frac{\nu_{21}E_1}{1 - \nu_{12}\nu_{21}} \tag{2.27}$$

$$\bar{Q}_{22} = \frac{E_2}{1 - \nu_{12}\nu_{21}} \tag{2.28}$$

$$\bar{Q}_{44} = G_{23} \tag{2.29}$$

$$\bar{Q}_{55} = G_{13} \tag{2.30}$$

$$\bar{Q}_{66} = G_{12} \tag{2.31}$$

To determine the laminate constitutive equations, equation (2.25) should be transformed to the plate coordinates. We have [1]

$$\begin{Bmatrix}\sigma_1\\ \sigma_2\\ \sigma_6\end{Bmatrix}=\begin{bmatrix}Q_{11} & Q_{12} & Q_{16}\\ Q_{21} & Q_{22} & Q_{26}\\ Q_{61} & Q_{62} & Q_{66}\end{bmatrix}\begin{Bmatrix}\varepsilon_1\\ \varepsilon_2\\ \varepsilon_6\end{Bmatrix} \tag{2.32}$$

$$\begin{Bmatrix}\sigma_4\\ \sigma_5\end{Bmatrix}=\begin{bmatrix}Q_{44} & Q_{45}\\ Q_{45} & Q_{55}\end{bmatrix}\begin{Bmatrix}\varepsilon_4\\ \varepsilon_5\end{Bmatrix} \tag{2.33}$$

where

$$Q_{11}=\overline{Q}_{11}\cos^4\theta+2(\overline{Q}_{12}+2\overline{Q}_{66})\sin^2\theta\cos^2\theta+\overline{Q}_{22}\sin^4\theta \tag{2.34}$$

$$Q_{12}=(\overline{Q}_{11}+\overline{Q}_{22}-4\overline{Q}_{66})\sin^2\theta\cos^2\theta+\overline{Q}_{12}(\sin^4\theta+\cos^4\theta) \tag{2.35}$$

$$Q_{22}=\overline{Q}_{11}\sin^4\theta+2(\overline{Q}_{12}+2\overline{Q}_{66})\sin^2\theta\cos^2\theta+\overline{Q}_{22}\cos^4\theta \tag{2.36}$$

$$Q_{16}=(\overline{Q}_{11}-\overline{Q}_{12}-2\overline{Q}_{66})\sin\theta\cos^3\theta+(\overline{Q}_{12}-\overline{Q}_{22}+2\overline{Q}_{66})\sin^3\theta\cos\theta \tag{2.37}$$

$$Q_{26}=(\overline{Q}_{11}-\overline{Q}_{12}-2\overline{Q}_{66})\sin^3\theta\cos\theta+(\overline{Q}_{12}-\overline{Q}_{22}+2\overline{Q}_{66})\sin\theta\cos^3\theta \tag{2.38}$$

$$Q_{66}=(\overline{Q}_{11}+\overline{Q}_{22}-2\overline{Q}_{12}-2\overline{Q}_{66})\sin^2\theta\cos^2\theta+\overline{Q}_{66}(\sin^4\theta+\cos^4\theta) \tag{2.39}$$

$$Q_{44}=\overline{Q}_{44}\cos^2\theta+\overline{Q}_{55}\sin^2\theta \tag{2.40}$$

$$Q_{45}=(\overline{Q}_{55}-\overline{Q}_{44})\cos\theta\sin\theta \tag{2.41}$$

$$Q_{55}=\overline{Q}_{55}\cos^2\theta+\overline{Q}_{44}\sin^2\theta \tag{2.42}$$

The angle θ is measured counter-clockwise between the $\bar{x}_1$ and x_1 axes.

The force and moment resultants N_i and M_i are defined as

$$(N_i, M_i) = \int_{-\frac{h}{2}}^{\frac{h}{2}} \sigma_i(1, z)dz \qquad (i, j = 1,2,6) \tag{2.43}$$

Similarly,

$$(Q_1, Q_2) = \int_{-\frac{h}{2}}^{\frac{h}{2}} (\sigma_5, \sigma_4)dz \tag{2.44}$$

Note that

$$\int_{-\frac{h}{2}}^{\frac{h}{2}} \sigma_5 z dz = \int_{-\frac{h}{2}}^{\frac{h}{2}} \sigma_4 z dz = 0 \tag{2.45}$$

The resultants (N_i, M_i, Q_i) can be expressed in terms of the strain components using equations (2.10-2.15), equation (2.32) and equation (2.33) in equation (2.43) and equation (2.44). We obtain

$$N_i = A_{ij}\varepsilon_j^{\,0} + B_{ij}k_j \qquad (i, j = 1,2,6) \tag{2.46}$$

$$M_i = B_{ij}\varepsilon_j^{\,0} + D_{ij}k_j \qquad (i, j = 1,2,6) \tag{2.47}$$

$$Q_1 = A_{4j}\varepsilon_j^0 \qquad (j = 4,5) \tag{2.48}$$

$$Q_2 = A_{5j}\varepsilon_j^0 \qquad (j = 4,5) \tag{2.49}$$

where A_{ij}, B_{ij} and D_{ij} are the laminate stiffness coefficients.

$$(A_{ij}, B_{ij}, D_{ij}) = \int_{-\frac{h}{2}}^{\frac{h}{2}} Q_{ij}(1, z, z^2)dz \text{ , (i, j=1,2,6)} \tag{2.50}$$

Written in matrix form

$$\begin{Bmatrix} N_1 \\ N_2 \\ N_6 \\ M_1 \\ M_2 \\ M_6 \\ Q_1 \\ Q_2 \end{Bmatrix} = \begin{bmatrix} A_{11} & A_{12} & A_{16} & B_{11} & B_{12} & B_{16} & 0 & 0 \\ A_{21} & A_{22} & A_{26} & B_{21} & B_{22} & B_{26} & 0 & 0 \\ A_{61} & A_{62} & A_{66} & B_{61} & B_{62} & B_{66} & 0 & 0 \\ B_{11} & B_{12} & B_{16} & D_{11} & D_{12} & D_{16} & 0 & 0 \\ B_{21} & B_{22} & B_{26} & D_{21} & D_{22} & D_{26} & 0 & 0 \\ B_{61} & B_{62} & B_{66} & D_{61} & D_{62} & D_{66} & 0 & 0 \\ 0 & 0 & 0 & 0 & 0 & 0 & A_{44} & A_{45} \\ 0 & 0 & 0 & 0 & 0 & 0 & A_{54} & A_{55} \end{bmatrix} \begin{Bmatrix} \varepsilon_1^0 \\ \varepsilon_2^0 \\ \varepsilon_6^0 \\ k_1 \\ k_2 \\ k_6 \\ \varepsilon_4^0 \\ \varepsilon_5^0 \end{Bmatrix} \tag{2.51}$$

Written in short form

$$\{N\} = [C]\{\varepsilon\} \tag{2.52}$$

where $[C]^T = [C]$

For convenience, u_0, v_0 and w_0 will be written as u, v and w respectively in the following formulation. The strain matrix is decomposed into two parts:

$$\{\varepsilon\} = \{\varepsilon_L\} + \{\varepsilon_N\} = \begin{Bmatrix} \frac{\partial u}{\partial x} \\ \frac{\partial v}{\partial y} \\ \frac{\partial u}{\partial y} + \frac{\partial v}{\partial x} \\ \frac{\partial \phi_x}{\partial x} \\ \frac{\partial \phi_y}{\partial y} \\ \frac{\partial \phi_y}{\partial x} + \frac{\partial \phi_x}{\partial y} \\ \phi_y + \frac{\partial w}{\partial y} \\ \phi_x + \frac{\partial w}{\partial x} \end{Bmatrix} + \begin{Bmatrix} \frac{1}{2}\left(\frac{\partial w}{\partial x}\right)^2 \\ \frac{1}{2}\left(\frac{\partial w}{\partial y}\right)^2 \\ \frac{\partial w}{\partial y}\frac{\partial w}{\partial x} \\ 0 \\ 0 \\ 0 \\ 0 \\ 0 \end{Bmatrix} \tag{2.53}$$

2.4 Energy Formulation

Here, we consider the application of minimum potential energy principle to the analysis of laminated plates. First of all, the equation for the total potential energy is set up so that the strain energy of the laminated plate in element coordinate system is given by

$$U = \frac{1}{2}\int_{\Omega} \{N\}^T \{\varepsilon\} d\Omega = \frac{1}{2}\int_{\Omega} \{\varepsilon\}^T [C]^T \{\varepsilon\} d\Omega = \frac{1}{2}\int_{\Omega} \{\varepsilon\}^T [C]\ \{\varepsilon\} d\Omega \tag{2.54}$$

If a distributed loading q (x,y) is applied on the plate, the potential energy of external loads is

$$W = -\int_{\Omega} qw dx dy \tag{2.55}$$

Total potential energy is obtained as

$$\pi = \frac{1}{2}\int_{\Omega}\{\varepsilon\}^T[C]\{\varepsilon\}d\Omega - \int_{\Omega} qwd\Omega$$

$$= \frac{1}{2}\int_{\Omega}(\{\varepsilon_L\}+\{\varepsilon_N\})^T[C](\{\varepsilon_L\}+\{\varepsilon_N\})d\Omega - \int_{\Omega} qwd\Omega$$

$$= \frac{1}{2}\int_{\Omega}\{\varepsilon_L\}^T[C]\{\varepsilon_L\}d\Omega + \frac{1}{2}\int_{\Omega}\{\varepsilon_L\}^T[C]\{\varepsilon_N\}d\Omega + \frac{1}{2}\int_{\Omega}\{\varepsilon_N\}^T[C]\{\varepsilon_L\}d\Omega + \frac{1}{2}\int_{\Omega}\{\varepsilon_N\}^T[C]\{\varepsilon_N\}d\Omega - \int_{\Omega} qwd\Omega$$

$$= \frac{1}{2}\int_{\Omega}\{\varepsilon_L\}^T[C]\{\varepsilon_L\}d\Omega + \int_{\Omega}\{\varepsilon_L\}^T[C]\{\varepsilon_N\}d\Omega + \frac{1}{2}\int_{\Omega}\{\varepsilon_N\}^T[C]\{\varepsilon_N\}d\Omega - \int_{\Omega} qwd\Omega$$

$$= U_L + U_{N1} + U_{N2} + W \tag{2.56}$$

where the linear part is expressed as:

$$U_L = \frac{1}{2}\int_{\Omega}\{\varepsilon_L\}^T[C]\{\varepsilon_L\}d\Omega \tag{2.57}$$

Next we have nonlinear part 1:

$$U_{N1} = \int_{\Omega}\{\varepsilon_L\}^T[C]\{\varepsilon_N\}d\Omega \tag{2.58}$$

Nonlinear part 2 is:

$$U_{N2} = \frac{1}{2}\int_{\Omega}\{\varepsilon_N\}^T[C]\{\varepsilon_N\}d\Omega \tag{2.59}$$

In equation (2.56), we consider:

$$\frac{1}{2}\int_{\Omega}\{\varepsilon_L\}^T[C]\{\varepsilon_N\}d\Omega = \frac{1}{2}\int_{\Omega}\{\varepsilon_N\}^T[C]\{\varepsilon_L\}d\Omega \tag{2.60}$$

2.5 Displacement Fields

The displacement field for a 9-node laminate element can be described as

$$u = \sum_{i=1}^{9} \overline{N}_i u_i \tag{2.61}$$

$$v = \sum_{i=1}^{9} \overline{N}_i v_i \tag{2.62}$$

$$w = \sum_{i=1}^{9} \overline{N}_i w_i \tag{2.63}$$

$$\phi_x = \sum_{i=1}^{9} \overline{N}_i \phi_{xi} \tag{2.64}$$

$$\phi_y = \sum_{i=1}^{9} \overline{N}_i \phi_{yi} \tag{2.65}$$

where $\overline{N}_i(x, y)$ are the shape functions that are giveN below.

$$\overline{N}_1 = \frac{(x - x_2)(x - x_3)(y - y_4)(y - y_7)}{(x_1 - x_2)(x_1 - x_3)(y_1 - y_4)(y_1 - y_7)} \tag{2.66}$$

$$\overline{N}_2 = \frac{(x - x_1)(x - x_3)(y - y_4)\ (y - y_7)}{(x_2 - x_1)(x_2 - x_3)(y_2 - y_4)(y_2 - y_7)} \tag{2.67}$$

$$\overline{N}_3 = \frac{(x - x_1)(x - x_2)(y - y_4)(y - y_7)}{(x_3 - x_2)(x_3 - x_2)(y_3 - y_4)(y_3 - y_7)} \tag{2.68}$$

$$\overline{N}_4 = \frac{(x - x_2)(x - x_3)(y - y_1)(y - y_7)}{(x_4 - x_2)(x_4 - x_3)(y_4 - y_1)(y_4 - y_7)} \tag{2.69}$$

$$\overline{N}_5 = \frac{(x - x_1)\ (x - x_3)(y - y_1)(y - y_7)}{(x_5 - x_1)(x_5 - x_3)(y_5 - y_1)(y_5 - y_7)} \tag{2.70}$$

$$\overline{N}_6 = \frac{(x - x_1)(x - x_2)(y - y_1)(y - y_7)}{(x_6 - x_1)(x_6 - x_2)(y_6 - y_1)(y_6 - y_7)} \tag{2.71}$$

$$\overline{N}_7 = \frac{(x - x_2)(x - x_3)(y - y_1)(y - y_4)}{(x_7 - x_2)(x_7 - x_3)(y_7 - y_1)(y_7 - y_4)} \tag{2.72}$$

$$\overline{N}_8 = \frac{(x - x_1)(x - x_3)(y - y_1)(y - y_4)}{(x_8 - x_1)(x_8 - x_3)(y_8 - y_1)(y_8 - y_4)} \tag{2.73}$$

$$\overline{N}_9 = \frac{(x - x_1)(x - x_2)(y - y_1)(y - y_4)}{(x_9 - x_1)(x_9 - x_2)(y_9 - y_1)(y_9 - y_4)} \tag{2.74}$$

In the above, x_i and y_i denote the i-th nodal coordinates in the element coordinate system (X_e, Y_e). The element is shown in Figure 2-1.

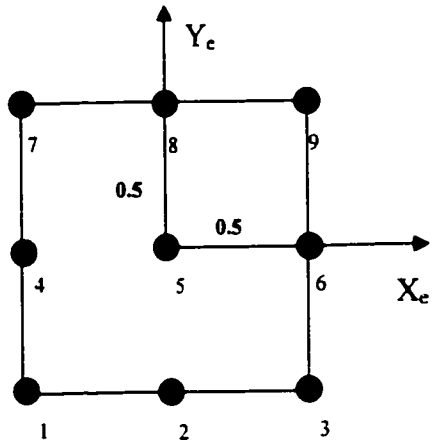

Figure 2-2 The 9-node element

2.6 Finite Element Equations

This section is concerned with the principle of minimum potential energy: Let a body be in equilibrium under the action of specified body forces and surface tractions. Of all

displacements satisfying the given boundary conditions those which satisfy the equilibrium equations make the potential energy an absolute minimum.

The principle of minimum potential energy is applied to derive nonlinear algebraic equations which will be solved using Newton-Raphson technique. This technique needs the stiffness matrix and the tangent matrix which can be obtained respectively through the first-order and second-order differentials of the elastic energy. Substitution of the displacement interpolation into the strain-displacement relations leads to

$$\{\varepsilon_L\} = [\overline{B}_L]\{\overline{u}\} \tag{2.75}$$

where the element nodal displacement vector $\{\overline{u}\}$ and matrix $[\overline{B}_L]$ are given by

$$\{\overline{u}\} = [u_1, v_1, w_1, \phi_{1x}, \phi_{1y}, \cdots \quad \cdots \quad , u_9, v_9, w_9, \phi_{9x}, \phi_{9y}]^T \tag{2.76}$$

$$[\overline{B}_L] = [[\overline{B}_L{}^1] \quad [\overline{B}_L{}^2] \quad \cdots \quad \cdots \quad [\overline{B}_L{}^9]] \tag{2.77}$$

$$[\overline{B}_L{}^i] = \begin{bmatrix} \frac{\partial \overline{N}_i}{\partial x} & 0 & 0 & 0 & 0 \\ 0 & \frac{\partial \overline{N}_i}{\partial y} & 0 & 0 & 0 \\ \frac{\partial \overline{N}_i}{\partial y} & \frac{\partial \overline{N}_i}{\partial x} & 0 & 0 & 0 \\ 0 & 0 & 0 & \frac{\partial \overline{N}_i}{\partial x} & 0 \\ 0 & 0 & 0 & 0 & \frac{\partial \overline{N}_i}{\partial y} \\ 0 & 0 & 0 & \frac{\partial \overline{N}_i}{\partial y} & \frac{\partial \overline{N}_i}{\partial x} \\ 0 & 0 & \frac{\partial \overline{N}_i}{\partial y} & 0 & \overline{N}_i \\ 0 & 0 & \frac{\partial \overline{N}_i}{\partial x} & \overline{N}_i & 0 \end{bmatrix} \tag{2.78}$$

Linear part of the strain energy:

$$U_L = \frac{1}{2}\int_\Omega \{\varepsilon_L\}^T [C]\{\varepsilon_L\} d\Omega = \frac{1}{2}\{\bar{u}\}^T \left(\int_\Omega [\bar{B}_L]^T [C][\bar{B}_L] d\Omega\right)\{\bar{u}\} \tag{2.79}$$

$$\delta U_L = \delta\{\bar{u}\}^T \left(\int_\Omega [\bar{B}_L]^T [C][\bar{B}_L] d\Omega\right)\{\bar{u}\} \tag{2.80}$$

$$\delta^2 U_L = \delta\{\bar{u}\}^T \left(\int_\Omega [\bar{B}_L]^T [C][\bar{B}_L] d\Omega\right)\delta\{\bar{u}\} \tag{2.81}$$

Nonlinear part 1 of the strain energy:

$$U_{N1} = \int_\Omega \{\varepsilon_L\}^T [C]\{\varepsilon_N\} d\Omega \tag{2.82}$$

$$\delta U_{N1} = \int_\Omega \delta\{\varepsilon_L\}^T [C]\{\varepsilon_N\} d\Omega + \int_\Omega \delta\{\varepsilon_N\}^T [C]\{\varepsilon_L\} d\Omega \tag{2.83}$$

$$\delta^2 U_{N1} = \int_\Omega \delta\{\varepsilon_L\}^T [C]\delta\{\varepsilon_N\} d\Omega + \int_\Omega \delta\{\varepsilon_N\}^T [C]\delta\{\varepsilon_L\} d\Omega + \int_\Omega \delta^2\{\varepsilon_N\}^T [C]\{\varepsilon_L\} d\Omega \tag{2.84}$$

First of all, derive equations for $\{\varepsilon_N\}$, $\delta\{\varepsilon_N\}$ and $\delta^2\{\varepsilon_N\}$.

$$\{\varepsilon_N\} = \begin{Bmatrix} \frac{1}{2}\left(\frac{\partial w}{\partial x}\right)^2 \\ \frac{1}{2}\left(\frac{\partial w}{\partial y}\right)^2 \\ \frac{\partial w}{\partial x}\frac{\partial w}{\partial y} \\ 0 \\ 0 \\ 0 \\ 0 \\ 0 \end{Bmatrix} = \begin{bmatrix} \frac{1}{2}\frac{\partial w}{\partial x} & 0 \\ 0 & \frac{1}{2}\frac{\partial w}{\partial y} \\ \frac{1}{2}\frac{\partial w}{\partial y} & \frac{1}{2}\frac{\partial w}{\partial x} \\ 0 & 0 \\ 0 & 0 \\ 0 & 0 \\ 0 & 0 \\ 0 & 0 \end{bmatrix} \begin{Bmatrix} \frac{\partial w}{\partial x} \\ \frac{\partial w}{\partial y} \end{Bmatrix} \tag{2.85}$$

$$\delta\{\varepsilon_N\}=\begin{Bmatrix} \frac{\partial w}{\partial x}\delta\left(\frac{\partial w}{\partial x}\right) \\ \frac{\partial w}{\partial y}\delta\left(\frac{\partial w}{\partial y}\right) \\ \delta\left(\frac{\partial w}{\partial x}\right)\left(\frac{\partial w}{\partial y}\right)+\left(\frac{\partial w}{\partial x}\right)\delta\left(\frac{\partial w}{\partial y}\right) \\ 0 \\ 0 \\ 0 \\ 0 \\ 0 \end{Bmatrix}=\begin{bmatrix} \frac{\partial w}{\partial x} & 0 \\ 0 & \frac{\partial w}{\partial y} \\ \frac{\partial w}{\partial y} & \frac{\partial w}{\partial x} \\ 0 & 0 \\ 0 & 0 \\ 0 & 0 \\ 0 & 0 \\ 0 & 0 \end{bmatrix}_{8*2} \begin{Bmatrix} \delta\left(\frac{\partial w}{\partial x}\right) \\ \delta\left(\frac{\partial w}{\partial y}\right) \end{Bmatrix} \tag{2.86}$$

Let

$$[H]=\begin{bmatrix} \frac{\partial w}{\partial x} & 0 \\ 0 & \frac{\partial w}{\partial y} \\ \frac{\partial w}{\partial y} & \frac{\partial w}{\partial x} \\ 0 & 0 \\ 0 & 0 \\ 0 & 0 \\ 0 & 0 \\ 0 & 0 \end{bmatrix}_{8*2} \tag{2.87}$$

and

$$\delta\{\overline{W}\}=\begin{Bmatrix} \delta\left(\frac{\partial w}{\partial x}\right) \\ \delta\left(\frac{\partial w}{\partial y}\right) \end{Bmatrix}=\begin{bmatrix} 0 & 0 & \frac{\partial N_1}{\partial x} & 0 & 0 & \cdots & \cdots & 0 & 0 & \frac{\partial N_9}{\partial x} & 0 & 0 \\ 0 & 0 & \frac{\partial N_1}{\partial y} & 0 & 0 & \cdots & \cdots & 0 & 0 & \frac{\partial N_9}{\partial y} & 0 & 0 \end{bmatrix}_{2*45} \delta\{\overline{u}\} \tag{2.88}$$

Let

$$[S]=\begin{bmatrix} 0 & 0 & \frac{\partial N_1}{\partial x} & 0 & 0 & \cdots & \cdots & 0 & 0 & \frac{\partial N_9}{\partial x} & 0 & 0 \\ 0 & 0 & \frac{\partial N_1}{\partial y} & 0 & 0 & \cdots & \cdots & 0 & 0 & \frac{\partial N_9}{\partial y} & 0 & 0 \end{bmatrix}_{2*45} \tag{2.89}$$

$$\delta^2\{\varepsilon_N\} = \begin{bmatrix} \delta\left(\frac{\partial w}{\partial x}\right) & 0 \\ 0 & \delta\left(\frac{\partial w}{\partial y}\right) \\ \delta\left(\frac{\partial w}{\partial y}\right) & \delta\left(\frac{\partial w}{\partial x}\right) \\ 0 & 0 \\ 0 & 0 \\ 0 & 0 \\ 0 & 0 \\ 0 & 0 \end{bmatrix}_{8*2} \begin{Bmatrix} \delta\left(\frac{\partial w}{\partial x}\right) \\ \delta\left(\frac{\partial w}{\partial y}\right) \end{Bmatrix}_{2*1} \tag{2.90}$$

Let

$$\{N_L\}_{8*1} = [C]_{8*8}\{\varepsilon_L\}_{8*1}$$

With equations (2.85), (2.86) and (2.90), parts of δU_{N1} and $\delta^2 U_{N1}$ are obtained as:

$$\int_\Omega \delta^2\{\varepsilon_N\}^T[C]\{\varepsilon_L\}d\Omega = \int_\Omega \delta^2\{\varepsilon_N\}^T\{N_L\}d\Omega = \int_\Omega \begin{bmatrix} \delta\left(\frac{\partial w}{\partial x}\right) & \delta\left(\frac{\partial w}{\partial y}\right) \end{bmatrix} \begin{Bmatrix} N_{L1}\delta\left(\frac{\partial w}{\partial x}\right) + N_{L3}\delta\left(\frac{\partial w}{\partial y}\right) \\ N_{L3}\delta\left(\frac{\partial w}{\partial x}\right) + N_{L2}\delta\left(\frac{\partial w}{\partial y}\right) \end{Bmatrix} d\Omega$$

$$= \int_\Omega \begin{bmatrix} \delta\left(\frac{\partial w}{\partial x}\right) & \delta\left(\frac{\partial w}{\partial y}\right) \end{bmatrix} \begin{bmatrix} N_{L1} & N_{L3} \\ N_{L3} & N_{L2} \end{bmatrix} \begin{Bmatrix} \delta\left(\frac{\partial w}{\partial x}\right) \\ \delta\left(\frac{\partial w}{\partial y}\right) \end{Bmatrix} d\Omega = \int_\Omega \delta\{\bar{u}\}^T[S]^T \begin{bmatrix} N_{L1} & N_{L3} \\ N_{L3} & N_{L2} \end{bmatrix} [S]\delta\{\bar{u}\}d\Omega$$

$$= \delta\{\bar{u}\}^T\left(\int_\Omega [S]^T \begin{bmatrix} N_{L1} & N_{L3} \\ N_{L3} & N_{L2} \end{bmatrix} [S]d\Omega\right)\delta\{\bar{u}\} \tag{2.91}$$

$$\int_\Omega \delta\{\varepsilon_N\}^T[C]\delta\{\varepsilon_L\}d\Omega$$

$$= \int_\Omega (([H][S]\delta\{\bar{u}\})^T[C][\bar{B}_L]\delta\{\bar{u}\}d\Omega = \delta\{\bar{u}\}^T\left(\int_\Omega [S]^T[H]^T[C][\bar{B}_L]d\Omega\right)\delta\{\bar{u}\} \tag{2.92}$$

$$\int_{\Omega} \delta\{\varepsilon_L\}^T [C] \delta\{\varepsilon_N\} d\Omega$$

$$= \int_{\Omega} \left([\bar{B}_L] \delta\{\bar{u}\} \right)^T [C][H][S] \delta\{\bar{u}\} d\Omega = \delta\{\bar{u}\}^T \left(\int_{\Omega} [\bar{B}_L]^T [C][H][S] d\Omega \right) \delta\{\bar{u}\} \tag{2.93}$$

$$\int_{\Omega} \delta\{\varepsilon_N\}^T [C] \{\varepsilon_L\} d\Omega$$

$$= \int_{\Omega} \left([H][S] \delta\{\bar{u}\} \right)^T [C][\bar{B}_L] \{\bar{u}\} d\Omega = \delta\{\bar{u}\}^T \left(\int_{\Omega} [S]^T [H]^T [C][\bar{B}_L] d\Omega \right) \{\bar{u}\} \tag{2.94}$$

$$\int_{\Omega} \delta\{\varepsilon_L\}^T [C] \{\varepsilon_N\} d\Omega$$

$$= \int_{\Omega} \left([\bar{B}_L] \delta\{\bar{u}\} \right)^T [C] \left(\frac{1}{2} [H][S] \{\bar{u}\} \right) d\Omega = \delta\{\bar{u}\}^T \left(\frac{1}{2} \int_{\Omega} [\bar{B}_L]^T [C][H][S] d\Omega \right) \{\bar{u}\} \tag{2.95}$$

Combining the above equations, δU_{N1} and $\delta^2 U_{N1}$ are written as below:

$$\delta U_{N1} = \delta\{\bar{u}\}^T \left[\left(\frac{1}{2} \int_{\Omega} [\bar{B}_L]^T [C][H][S] d\Omega \right) + \left(\int_{\Omega} [S]^T [H]^T [C][\bar{B}_L] d\Omega \right) \right] \{\bar{u}\} \tag{2.96}$$

$$\delta^2 U_{N1} = \delta\{\bar{u}\}^T \left[\left(\int_{\Omega} [\bar{B}_L]^T [C][H][S] d\Omega \right) + \left(\int_{\Omega} [S]^T [H]^T [C][\bar{B}_L] d\Omega \right) + \left(\int_{\Omega} [S]^T \begin{bmatrix} N_{L1} & N_{L3} \\ N_{L3} & N_{L2} \end{bmatrix} [S] d\Omega \right) \right] \delta\{\bar{u}\} \tag{2.97}$$

Nonlinear part 2 of the strain energy:

$$U_{N2} = \frac{1}{2}\int_{\Omega}\{\varepsilon_N\}^T[C]\{\varepsilon_N\}d\Omega \tag{2.98}$$

$$\delta U_{N2} = \int_{\Omega}\delta\{\varepsilon_N\}^T[C]\{\varepsilon_N\}d\Omega$$

$$= \int_{\Omega}([H][S]\delta\{\bar{u}\})^T[C]\left(\frac{1}{2}[H][S]\{\bar{u}\}\right)d\Omega = \delta\{\bar{u}\}^T\left(\frac{1}{2}\int_{\Omega}[S]^T[H]^T[C][H][S]d\Omega\right)\{\bar{u}\} \tag{2.99}$$

$$\delta^2 U_{N2} = \int_{\Omega}\delta\{\varepsilon_N\}^T[C]\delta\{\varepsilon_N\}d\Omega + \int_{\Omega}\delta^2\{\varepsilon_N\}^T[C]\{\varepsilon_N\}d\Omega \tag{2.100}$$

where

$$\int_{\Omega}\delta\{\varepsilon_N\}^T[C]\delta\{\varepsilon_N\}d\Omega = \int_{\Omega}([H][S]\delta\{\bar{u}\})^T[C][H][S]\delta\{\bar{u}\})d\Omega$$

$$= \delta\{\bar{u}\}^T\left(\int_{\Omega}[S]^T[H]^T[C][H][S]d\Omega\right)\{\bar{u}\} \tag{2.101}$$

$$\int_{\Omega}\delta^2\{\varepsilon_N\}^T[C]\{\varepsilon_N\}d\Omega = \int_{\Omega}\delta^2\{\varepsilon_N\}^T\{N_N\}d\Omega$$

$$= \int_{\Omega}\left[\delta\left(\frac{\partial w}{\partial x}\right) \quad \delta\left(\frac{\partial w}{\partial y}\right)\right]\begin{Bmatrix} N_{N1}\delta\left(\frac{\partial w}{\partial x}\right) + N_{N3}\delta\left(\frac{\partial w}{\partial y}\right) \\ N_{N3}\delta\left(\frac{\partial w}{\partial x}\right) + N_{N2}\delta\left(\frac{\partial w}{\partial y}\right)\end{Bmatrix}d\Omega$$

$$= \int_{\Omega}\left[\delta\left(\frac{\partial w}{\partial x}\right) \quad \delta\left(\frac{\partial w}{\partial y}\right)\right]\begin{bmatrix} N_{N1} & N_{N3} \\ N_{N3} & N_{N2}\end{bmatrix}\begin{Bmatrix}\delta\left(\frac{\partial w}{\partial x}\right) \\ \delta\left(\frac{\partial w}{\partial y}\right)\end{Bmatrix}d\Omega$$

$$= \int_{\Omega}\delta\{\bar{u}\}^T[S]^T\begin{bmatrix} N_{N1} & N_{N3} \\ N_{N3} & N_{N2}\end{bmatrix}[S]\delta\{\bar{u}\}d\Omega$$

$$= \delta\{\bar{u}\}^T\left(\int_{\Omega}[S]^T\begin{bmatrix} N_{N1} & N_{N3} \\ N_{N3} & N_{N2}\end{bmatrix}[S]d\Omega\right)\delta\{\bar{u}\} \qquad (2.102)$$

Therefore, $\delta^2 U_{N2}$ can be expressed further as:

$$\delta^2 U_{N2} = \delta\{\bar{u}\}^T\left[\left(\int_{\Omega}[S]^T[H]^T[C][H][S]d\Omega\right) + \left(\int_{\Omega}[S]^T\begin{bmatrix} N_{N1} & N_{N3} \\ N_{N3} & N_{N2}\end{bmatrix}[S]d\Omega\right)\right]\{\bar{u}\} \qquad (2.103)$$

Finally, putting the linear part, the nonlinear part 1 and part 2 together, δU and $\delta^2 U$ are obtained as:

$$\delta U = \delta\{\bar{u}\}^T[K_e]\{\bar{u}\} \qquad (2.104)$$

$$\delta^2 U = \delta\{\bar{u}\}^T[K_{eT}]\delta\{\bar{u}\} \qquad (2.105)$$

where the stiffness matrix is:

$$[K_e]=\begin{bmatrix}(\int_\Omega[\bar{B}_L]^T[\bar{Q}][\bar{B}_L]d\Omega)+\\ \left(\frac{1}{2}\int_\Omega[\bar{B}_L]^T[\bar{Q}][H][S]d\Omega\right)+\left(\int_\Omega[S]^T[H]^T[\bar{Q}][\bar{B}_L]d\Omega\right)+\\ \left(\frac{1}{2}\int_\Omega[S]^T[H]^T[\bar{Q}][H][S]d\Omega\right)\end{bmatrix}_{45\times45} \tag{2.106}$$

The tangent stiffness matrix is:

$$[K_{eT}]=\begin{bmatrix}(\int_\Omega[\bar{B}_L]^T[\bar{Q}][\bar{B}_L]d\Omega)+\\ \left(\int_\Omega[\bar{B}_L]^T[\bar{Q}][H][S]d\Omega\right)+\left(\int_\Omega[S]^T[H]^T[\bar{Q}][\bar{B}_L]d\Omega\right)+\left(\int_\Omega[S]^T\begin{bmatrix}N_{L1} & N_{L3}\\ N_{L3} & N_{L2}\end{bmatrix}[S]d\Omega\right)+\\ \left(\int_\Omega[S]^T[H]^T[\bar{Q}][H][S]d\Omega\right)+\left(\int_\Omega[S]^T\begin{bmatrix}N_{N1} & N_{N3}\\ N_{N3} & N_{N2}\end{bmatrix}[S]d\Omega\right)\end{bmatrix}_{45\times45} \tag{2.107}$$

Once the element stiffness matrix is obtained, equilibrium equations for the element can be expressed as

$$[K_e]\{\bar{u}\}=\{P_e\} \tag{2.108}$$

Here subscript e denotes that the corresponding quantity is relevant to the element. $\{P_e\}$ is the nodal force matrix corresponding to nodal displacement matrix $\{\bar{u}\}$.

$$\{P_e\}=[f_{u1},f_{v1},f_{w1},m_{1x},m_{1y},\cdots\ \cdots\ ,f_{u9},f_{v9},f_{w9},m_{9x},m_{9y}]^T \tag{2.109}$$

Numerical integration is applied to evaluate the stiffness matrix and the tangent stiffness matrix using Gauss quadrature with (3×3=) 9 point rule or (2×2=) 4 point rule. Gauss points are shown below:

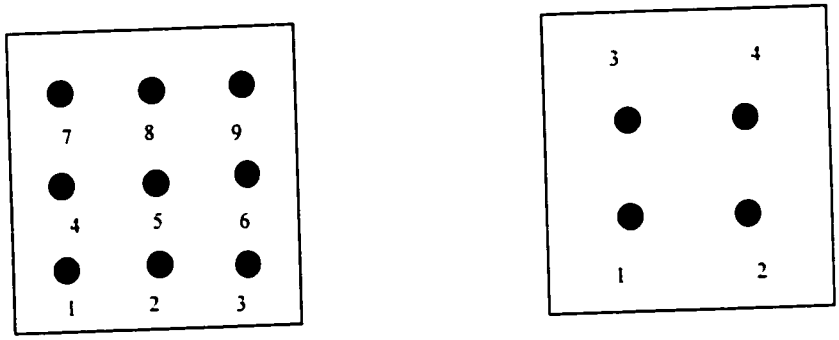

Figure 2-3 Location of Gauss points in the element

2.7 Newton-Raphson Iterative Method

In the solution of linear problems by finite element method one always needs to solve a set of simultaneous algebraic equations of the form

$$Ka = f \tag{2.110}$$

Provided the coefficient matrix is non-singular the solution to these equations is unique. In the solution of non-linear problems we will obtain a set of algebraic equations, these are generally non-linear, in the form

$$\psi(a) = f - P(a) = 0 \tag{2.111}$$

where a is the set of discretization parameters, f is a vector which is independent of parameters and P is a vector dependent on the parameters. These equations may have

multiple solutions [i.e. more than one set of a may satisfy equation (2.111)]. Thus, if a solution is achieved it may not necessarily be the solution sought. Physical insight into the nature of the problem and, usually, small-step incremental approaches are essential to obtaining realistic answers. Such increments are indeed always required if the constitutive law relating stress and strain changes is path dependent or if the load-displacement path has bifurcations or multiple branches at certain load levels.

The general problem should always be formulated [1] as the solution of

$$\psi_{n+1} = \psi(a_{n+1}) = f_{n+1} - P(a_{n+1}) = 0 \tag{2.112}$$

which starts from a nearby solution at

$$a = a_n, \qquad \psi_n = 0, \qquad f = f_n$$

and often arises from changes in the forcing function f_n to

$$f_{n+1} = f_n + \Delta f_n \tag{2.113}$$

The determination of the change Δf_n is performed such that

$$a_{n+1} = a_n + \Delta a_n \tag{2.114}$$

will be the objective and generally the increments of Δf will be kept reasonably small so that path dependence can be followed. Further, such incremental procedures will be useful in avoiding excessive numbers of iterations and in following the physically correct path.

It is possible to obtain solutions in a single increment of f only in the case of mild non-linearity (and no path dependence), that is with

$$f_n = 0$$

$$\Delta f_n = f_{n+1} = f \tag{2.115}$$

The Newton-Raphson method provides the most rapidly converging solutions for problems in which only one evaluation of ψ is made in each iteration. Of course, this assumes that the initial solution is within the zone of attraction and, thus, divergence does not occur. Indeed, the Newton-Raphson method is the only process described here in which the asymptotic rate of convergence is quadratic.

In this iterative method we note that, to the first order, equation (2.112) can be approximated as

$$\psi(a_{n+1}^{i+1}) \approx \psi(a_{n+1}^{i}) + (\frac{\partial \psi}{\partial a})_{n+1}^{i} da_n^i = 0 \tag{2.116}$$

Here the iteration counter i usually starts by assuming

$$a_{n+1}^{i} = a_n \tag{2.117}$$

in which a_n is a converged solution at a previous load level or time step. The Jacobian matrix (or in structural mechanics terms the stiffness matrix) corresponding to a tangent direction is given by

$$K_T = \frac{\partial P}{\partial a} = -\frac{\partial \psi}{\partial a} \tag{2.118}$$

Equation (2.116) gives immediately the iterative correction as

$$K_T^i da_n^i = \psi_{n+1}^i \tag{2.119}$$

or

$$da_n^i = (K_T^i)^{-1} \psi_{n+1}^i \tag{2.120}$$

A series of successive approximations gives

$$a_{n+1}^{i+1} = a_{n+1}^i + da_{n+1}^i = a_n + \Delta a_n^i \tag{2.121}$$

where

$$\Delta a_n^i = \sum_{k=1}^{i} da_n^k \tag{2.122}$$

The process is illustrated in Figure 2-3 and shows the very rapid convergence that can be achieved.

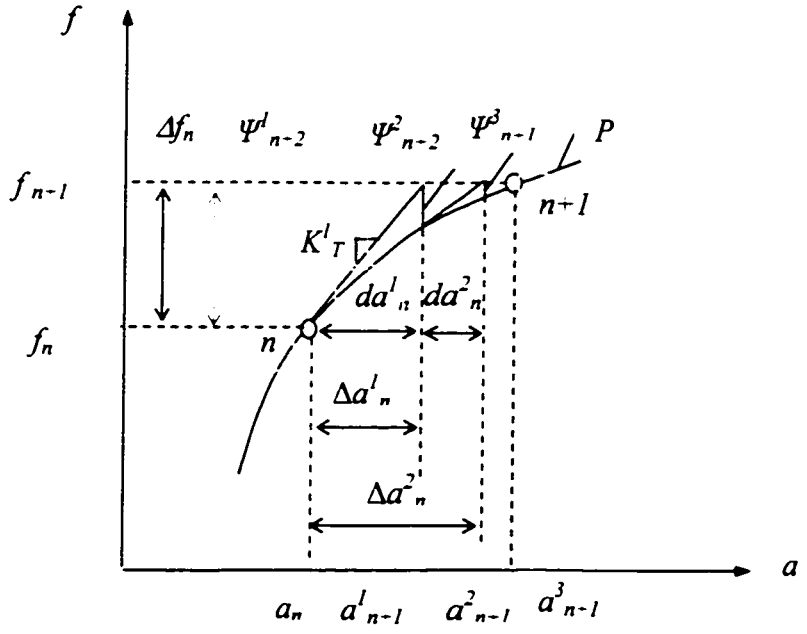

Figure 2-4 The Newton-Raphson method

The Newton-Raphson iterative process, despite its rapid convergence, has some negative features:

1. A new K_T matrix has to be computed at each iteration;
2. If direct solution for equation (2.120) is used the matrix needs to be factored at each iteration;
3. On some occasions the tangent matrix is symmetric at a solution state but unsymmetric otherwise (e.g. in some schemes for integrating large rotation parameters or in the case of non-associated plasticity). In these cases an unsymmetric solver is needed in general.

Some of these drawbacks are absent in alternative procedures, although generally then a quadratic asymptotic rate of convergence is lost.

2.8 Failure Analysis Methodology

The finite element formulation is based on the first order shear deformation theory with the nine-node Lagrangian element having five degrees of freedom per node. Geometric nonlinearity based on von Karman's assumptions has been incorporated. The nonlinear algebraic equations are solved using Newton-Raphson technique. The calculation of stresses is done at the Gauss points for the cases of uni-axial compression and bi-axial compression. The calculation of stresses is done at the nodal points in the case of combined in-plane loads (bi-axial compression and shear). All the six stress components are calculated at the Gauss point or nodal point. However, to predict the failure of a lamina only five stress components (three in-plane stresses and two transverse shear

stresses) are used in the selected failure criterion. To predict the onset of delamination, two transverse shear stress components and one transverse normal stress component are used in the maximum stress failure criterion or Tsai-Hill criterion. Delamination at any interface is said to have occurred when any of the transverse stress components in any of the two layers adjacent to the interface becomes equal to or greater than its corresponding strength. Ply failure is said to have occurred when the state of stress at any point within the lamina satisfies the selected failure criterion. The first-ply failure refers to the first instant at which one or more than one plies fail at the same load. After the first–ply failure, the progressive failure analysis is carried out using progressive failure procedure appropriate to the selected failure criterion. Tensor polynomial form of the maximum stress criterion is used in the case of uni-axial compression and bi-axial compression. The tensor polynomial form of the Tsai-Hill criterion is used in the case of combined bi-axial compression and shear. Tangent stiffness coefficients are obtained by numerical integration. The order of the Gauss quadrature used is based on the selective integration rule, i.e. the 3×3 rule is used for terms associated with membrane and bending action while the 2×2 rule is used for terms associated with transverse shear behavior. The convergence tolerance used for computations is 0.001. A shear correction factor of value K1=K2=5/6 is used. The laminate dimensions employed in the analysis are 279 mm×279 mm×2.16 mm. Since the laminate under consideration is symmetrically disposed with respect to mid-surface, a very small lateral load is applied to create initial deflection in order to calculate the tangent stiffness coefficients and residual forces for the increment of loading applied as a first guess.

Chapter 3

Progressive Failure Analysis

3.1 Introduction

Failure of a mechanical component can be defined as the inability of the component to carry any further load. Failure of composite materials is complex, and studies of failure are a ongoing activity. There are many issues and controversies surrounding the subject of failure of composite materials.

Clearly, we must consider many mechanisms when studying failure, for failure is often a combination of several of these mechanisms, or modes. Failure can simply be the final event in a complex and difficult-to-understand process of damage initiation and accumulation within the material. A structure consists of multiple layers of fiber-reinforced material, and there are multiple fiber directions and a range of load levels and load types. Thus even with a single layer of material, the issues can be quite complicated. As a result, there have been many studies of failure. In the interest of utility, a failure criterion should be reducible to a level that can provide a means of judging whether or not a structure is safe from failure by knowing that a particular stress or combinations of stresses, or combination of strains, is less than some predetermined critical value.

The failure criterion should be accurate without being overly conservative, it should be understandable by those using it, and it should be substantiated by experiment. A number of criteria have been proposed. Some are rather straightforward and some are quite involved. The maximum stress criterion accounts for interaction among the stress components. This is because of the physical bases that underlie this criterion. In addition, many of the other criteria are simple variations of this criterion, and the variations are based on experimental observations.

A review of the tensor polynomial failure criterion, with its various degenerate cases, has been presented by Reddy and Reddy [5], and Singh *et al* [18]. Here, because of its simplicity, the tensor polynomial form of the maximum stress failure criterion is used for the cases of uni-axial compression and bi-axial compression.

A detailed review of various failure criteria used for the prediction of failure loads of laminated composite plates for the case of in-plane shear has been made by Singh *et al.* [19] and [20]. It was observed that the difference in failure loads predicted by various failure criteria is strongly dependent on plate lay-up and boundary conditions. It was also observed that the Hashin criterion and the tensor polynomial form of the maximum strain criterion give the most inconsistent results as compared with other criteria. Moreover, the difference in failure loads predicted by tensor polynomial form of the Tsai-Hill criterion and Tsai-Wu criterion is small. Owing to lack of experimental data, it is not possible to say which criterion is best for the prediction of failure loads. Here, the tensor polynomial

form of the 3D Tsai-Hill criterion is used as one of the failure models for a lamina failure in the case of in-plane shear.

In contrast, the maximum stress criterion is used to predict the onset of delamination because of its simplicity.

3.2 Tensor Polynomial Failure Criterion

The most general polynomial failure criterion is expressed as [63]

$$F_1\sigma_1 + F_2\sigma_2 + F_3\sigma_3 + 2F_{12}\sigma_1\sigma_2 + 2F_{13}\sigma_1\sigma_3 + 2F_{23}\sigma_2\sigma_3 + F_{11}\sigma_1^2 + F_{22}\sigma_2^2 + F_{33}\sigma_3^2 + F_{44}\sigma_4^2 + F_{55}\sigma_5^2 + F_{66}\sigma_6^2 + \cdots \geq 1 \quad (3.1)$$

In the above expression σ_1, σ_2 and σ_3 are the normal stress components, σ_4, σ_5 and σ_6 are the shear stress components in the principal material directions (the subscript 1 refers to the fiber direction). Particular cases of the above criterion differ from one another by their strength tensors F_{ij}. Hence, various degenerate cases of the tensor polynomial criterion can be obtained by substituting the appropriate tensor strength factors F_{ij} in the equation (3.1). Tensor strength factors appropriate to the various polynomial criteria are given below:

(a) Maximum stress criterion [64]:

$$F_1 = \frac{1}{X_T} - \frac{1}{X_c} \tag{3.2}$$

$$F_2 = \frac{1}{Y_T} - \frac{1}{Y_c} \tag{3.3}$$

$$F_3 = \frac{1}{Z_T} - \frac{1}{Z_c} \tag{3.4}$$

$$F_{11} = \frac{1}{X_T X_c} \tag{3.5}$$

$$F_{22} = \frac{1}{Y_T Y_c} \tag{3.6}$$

$$F_{33} = \frac{1}{Z_T Z_c} \tag{3.7}$$

$$F_{44} = \frac{1}{R^2} \tag{3.8}$$

$$F_{55} = \frac{1}{S^2} \tag{3.9}$$

$$F_{66} = \frac{1}{T^2} \tag{3.10}$$

$$F_{12} = -\frac{F_1 F_2}{2} \tag{3.11}$$

$$F_{13} = -\frac{F_1 F_3}{2} \tag{3.12}$$

$$F_{23} = -\frac{F_2 F_3}{2} \tag{3.13}$$

The remaining strength tensor terms are equal to zero.

In the above expressions X_t and Y_t are the tensile strengths of the lamina in the fiber direction and in the direction transverse to it, respectively: X_c and Y_c are the

corresponding compressive strengths; Z_t and Z_c are the tensile and the compressive strength, respectively, in the principal direction 3 of the lamina. R and T are the shear strengths of lamina in planes 2-3 and 1-2 respectively. The shear strength in plane 1-3 is designated as S.

(b) Tsai-Hill criterion [65]:

$$F_1 = F_2 = F_3 = 0 \tag{3.14}$$

$$F_{11} = \frac{1}{X^2} \tag{3.15}$$

$$F_{22} = \frac{1}{Y^2} \tag{3.16}$$

$$F_{33} = \frac{1}{Z^2} \tag{3.17}$$

$$F_{44} = \frac{1}{R^2} \tag{3.18}$$

$$F_{55} = \frac{1}{S^2} \tag{3.19}$$

$$F_{66} = \frac{1}{T^2} \tag{3.20}$$

$$F_{12} = -\frac{1}{2}\left(\frac{1}{X^2} + \frac{1}{Y^2} - \frac{1}{Z^2}\right) \tag{3.21}$$

$$F_{13} = -\frac{1}{2}\left(\frac{1}{Z^2} + \frac{1}{X^2} - \frac{1}{Y^2}\right) \tag{3.22}$$

$$F_{23} = -\frac{1}{2}\left(\frac{1}{Y^2} + \frac{1}{Z^2} - \frac{1}{X^2}\right) \tag{3.23}$$

The values of X, Y and Z are taken as either X_t, Y_t and Z_t, or as X_c, Y_c and Z_c, depending upon the sign of σ_1, σ_2 and σ_3

3.3 Failure of the Lamina

Lamina failure in the cases of uni-axial compression and bi-axial compression is said to have occurred when the state of stress at any Gauss point with in the lamina satisfies the tensor polynomial form of the maximum stress criterion.

Lamina failure in the case of bi-axial compression combined with in-plane shear loading is said to have occurred when the state of stress at any nodal point within the lamina (at mid-thickness) satisfies the tensor polynomial form of the Tsai-Hill criterion in which the terms associated with the normal stress component in the third principal material direction are omitted.

3.4 Onset of Delamination

Delamination at any interface between two adjacent layers is said to have occurred when any of the three transverse stress components (adjacent to the interface) in any of the two layers becomes equal to or greater than its corresponding allowable strength (the transverse interlaminar normal strength is taken to be the tensile strength of lamina in principal material direction 3).

3.5 Progressive Failure Analysis

At each load step, Gauss point stresses are used in the maximum stress criterion in the cases of uni-axial compression and bi-axial compression. The nodal point stresses are used in the Tsai-Hill failure criterion in the case of bi-axial compression combined with in-plane shear loading. When failure occurs at a Gauss point according to the maximum stress criterion in the cases of uni-axial compression and bi-axial compression, and when failure occurs at a nodal point in a layer in the case of bi-axial compression combined with in-plane shear loading, a reduction in the appropriate lamina moduli is introduced everywhere in the lamina as per the mode of failure, which causes the change in overall laminate stiffness. Following terms are used to determine the failure modes.

$$H_1 = F_1\sigma_1 + F_{11}\sigma_1^2 \tag{3.24}$$

$$H_2 = F_2\sigma_2 + F_{22}\sigma_2^2 \tag{3.25}$$

$$H_4 = F_{44}\sigma_4^2 \tag{3.26}$$

$$H_5 = F_{55}\sigma_5^2 \tag{3.27}$$

$$H_6 = F_{66}\sigma_6^2 \tag{3.28}$$

Terms in the above expressions are defined in the section 3.2 (Tensor Polynomial Failure Criterion).

The largest H_i term is selected to correspond to the dominant failure mode and the corresponding modulus is reduced to zero. H_1 corresponds to the modulus E_1; H_2 to E_2; H_4 to G_{23}; H_5 to G_{13} and H_6 to G_{12}. Here E_1 and E_2 are, respectively, the moduli in the fiber direction and in the direction transverse to it; G_{12} ,G_{23} and G_{13} are the principal shear moduli in planes 1-2, 2-3 and 1-3, respectively.

The failure analysis procedure can be described as follows:

(1) After iterative convergence is achieved in the nonlinear analysis, calculate the stresses at the middle of each layer and at its interfaces with the adjacent layers at each Gauss point in the case of uni-axial compression and bi-axial compression, or at each nodal point in the case of bi-axial compression combined with in-plane shear loading.

(2) Transform the stresses to principal material directions.

(3) Compute failure indices, H_1, H_2, ..., H_6.

(4) If failure occurs reduce the appropriate lamina moduli and recompute laminate stiffness and restart nonlinear analysis at the same load step.

(5) If no failure occurs, proceed to the next load step.

(6) Final failure is said to have occurred when delamination occurs or when the plate is no longer able to carry any further load because of very large deflection.

3.6 Numerical Examples and Verification

A square laminate consisting of (0/90) plygroups and subjected to a uniformly distributed loading is considered. The plate has simply-supported boundary conditions. The sides of the plate a and b are taken to be 243.8 cm and thickness h to be 0.635 cm.

The material properties of the laminate are:

$E_1/E_2 = 24$ $\quad E_2 = 7.031\times10^5$ N/cm^2

$G_{12}/E_2 = 0.5$ $\quad G_{13} = G_{12}$

$G_{23}/E_2 = 0.2$ $\quad \nu_{12} = 0.25$

The boundary conditions are given below:

$u = w = \theta_y = 0$ $\quad$ at $x = \pm a/2$

$v = w = \theta_x = 0$ $\quad$ at $y = \pm a/2$

$v = \theta_y = 0$ $\quad$ at $y = 0$

$u = \theta_x = 0$ $\quad$ at $x = 0$

A 4 by 4 type finite element mesh is considered. Here, the first number refers to the number of elements in X direction (dimension of the plate in X direction is a) and the second number corresponds to Y direction (dimension of the plate in Y direction is b). The 4 by 4 type finite element mesh for the plate is shown in Figure 3-1. Figure 3-2 shows the results obtained using the present formulation. The present results are compared with that given in the work of Reddy *et al* [1]. It is observed that the results

obtained in the present study compare very well with the results given in the work of Reddy *et al* [1].

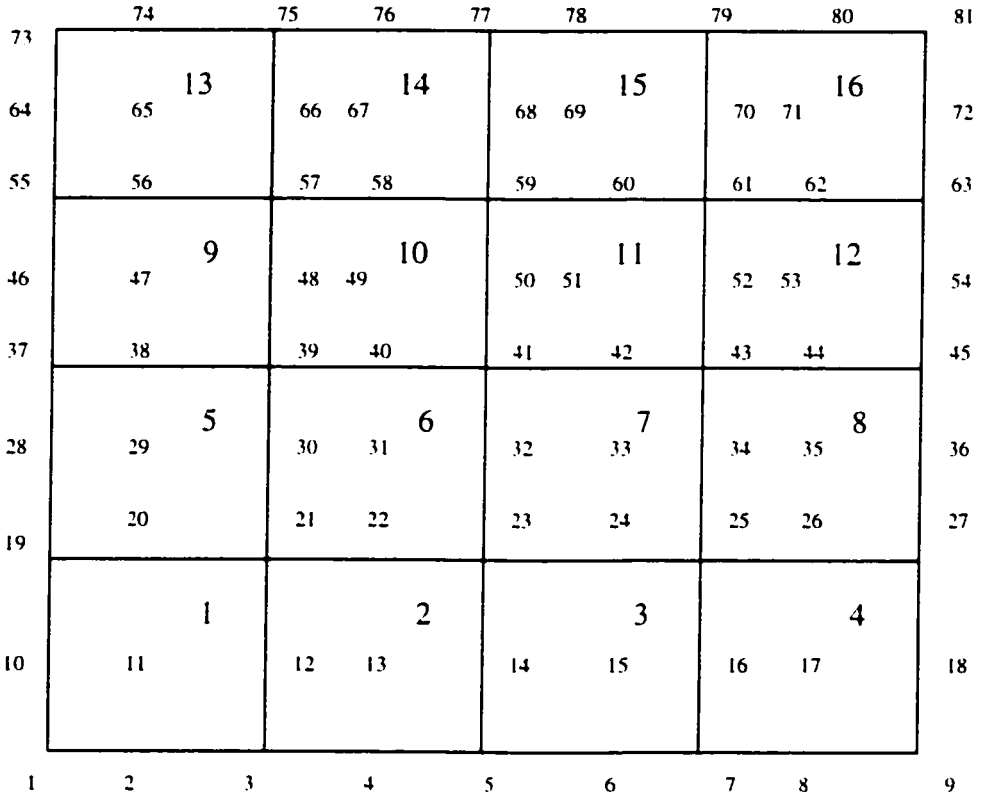

Figure 3-1 4 by 4 type finite element mesh for the plate

Now different laminates with simply-supported boundary condition under the action of uni-axial compression are analyzed and the results are compared with the results given in the work of Singh *et al* [18].

The dimensions of the plate are: a = 279 mm, b = 279 mm and h = 2.16 mm. Ply thickness is 0.135 mm.

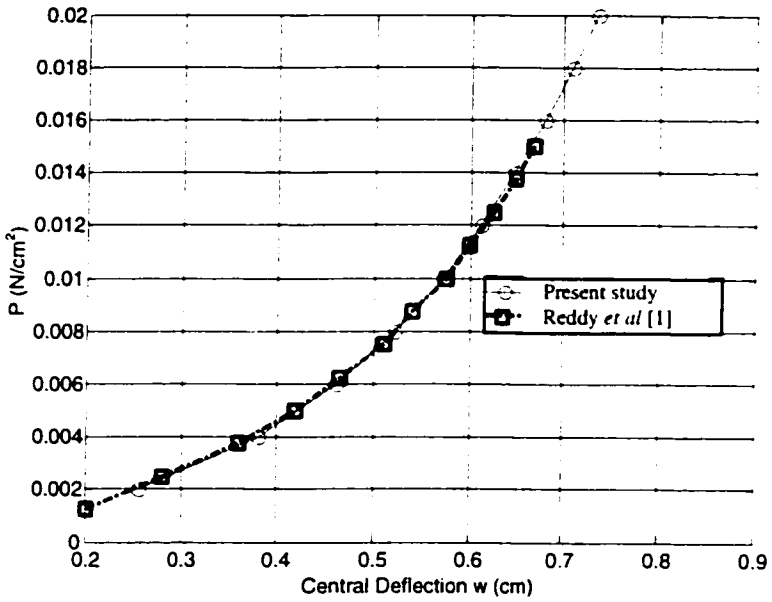

Figure 3-2 Bending of cross-ply (0/90) square laminate with simply-supported boundary condition subjected to a uniformly distributed loading

The mechanical properties of the material are:

$E_1 = 132.58$ GPa $\quad E_2 = 10.8$ GPa $\quad E_3 = 10.8$ GPa

$G_{13} = G_{12} = 5.7$ GPa $\quad \nu_{12} = \nu_{13} = 0.24$ $\quad \nu_{23} = 0.49$

The material strength properties are:

$X_t = 1.515$ GPa $\quad X_c = 1.697$ GPa

$Y_t = Z_t = 43.8$ MPa $\quad Y_c = Z_c = 43.8$ MPa

$R = 67.6$ MPa $\quad S = T = 86.9$ MPa

The boundary conditions are given below:

$u = w = \theta_y = 0$ $\quad$ at $x = 0$

$v = w = \theta_x = 0$ at $y = 0$

$w = \theta_y = 0$ at $x = a$

$u = \theta_x = 0$ at $y = b$

A 5 by 5 type finite element mesh is considered. Here, the first number refers to the number of elements in X direction (dimension of the plate in X direction is a) and the second number corresponds to Y direction (dimension of the plate in Y direction is b). The 5 by 5 type finite element mesh is shown in Figure 3-3.

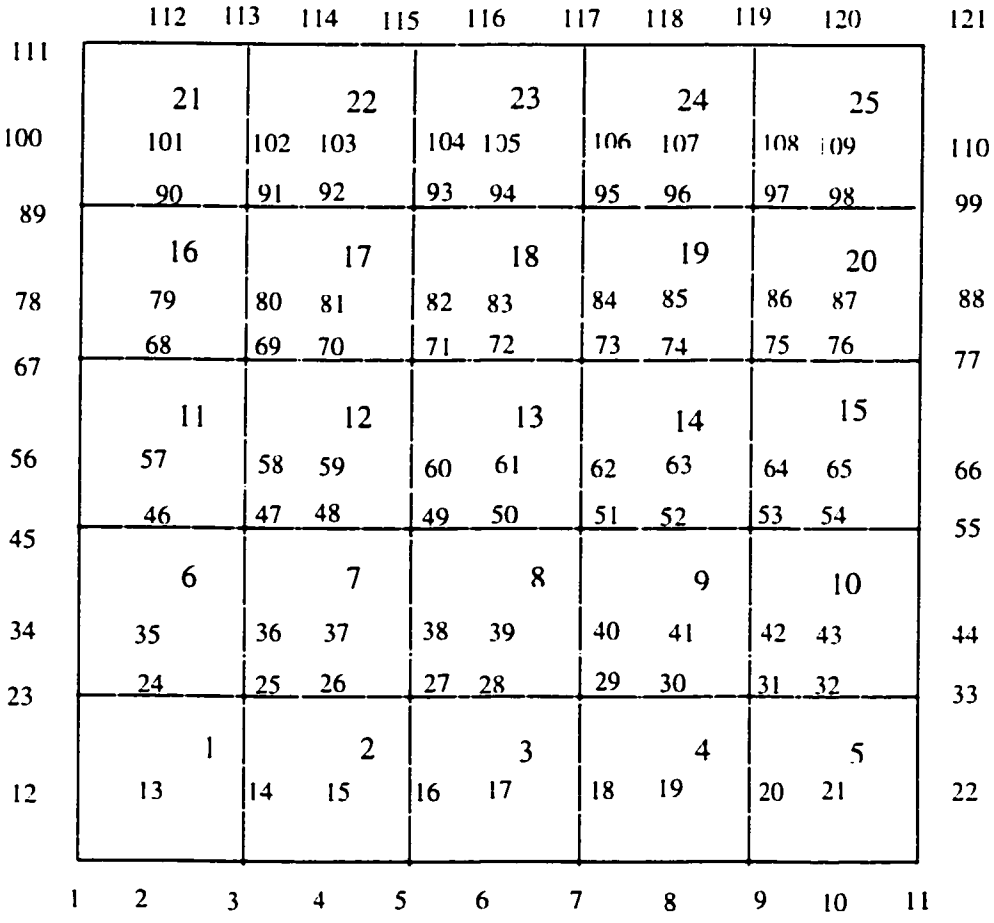

Figure 3-3 5 by 5 type finite element mesh for the plate

The first-ply failure load and the ultimate failure load for the $(\pm 45/0/90)_{2s}$ laminate under the action of uni-axial compression are given in Table 3-1. The first-ply failure load and the ultimate failure load for the $(\pm 45)_{4s}$ laminate under the action of uni-axial compression are given in Table 3-2. The first-ply failure load and ultimate failure load for the $(0/90)_{4s}$ laminate under the action of uni-axial compression are given in Table 3-3.

Table 3-1 The first-ply failure load and the ultimate failure load for $(\pm 45/0/90)_{2s}$ laminate under the action of uni-axial compression

	First-ply failure load ($N_x b^2/E_2 h^3$)	Ultimate failure load ($N_x b^2/E_2 h^3$)	Mode of first-ply failure
Singh *et al* [18]	58.09	77.45	Transverse*
Present study	55.78	81.53	Transverse

* Transverse mode of failure refers to the matrix failure

Table 3-2 The first-ply failure load and the ultimate failure load for $(\pm 45)_{4s}$ laminate under the action of uni-axial compression

	First-ply failure load ($N_x b^2/E_2 h^3$)	Ultimate failure load ($N_x b^2/E_2 h^3$)	Mode of first-ply failure
Singh *et al* [18]	49.06	65.83	Transverse *
Present study	47.92	67.94	Transverse

* Transverse mode of failure refers to the matrix failure

Table 3-3 The first-ply failure load and the ultimate failure load for $(0/90)_{4s}$ laminate under the action of uni-axial compression

	First-ply failure load ($N_x b^2/E_2 h^3$)	Ultimate failure load ($N_x b^2/E_2 h^3$)	Mode of first-ply failure
Singh *et al* [18]	60.24	71.86	Transverse*
Present study	61.50	75.81	Transverse

* Transverse mode of failure refers to the matrix failure

Figure 3-4 (a) and (b) show the load versus the central deflection response of $(\pm 45/0/90)_{2s}$ laminate under the action of uni-axial compression. In Figure 3-4, w_c is the central deflection of the plate. It is seen from these figures and Table 3-1 that the difference between the present results and the results obtained by Singh *et al* [18] are small.

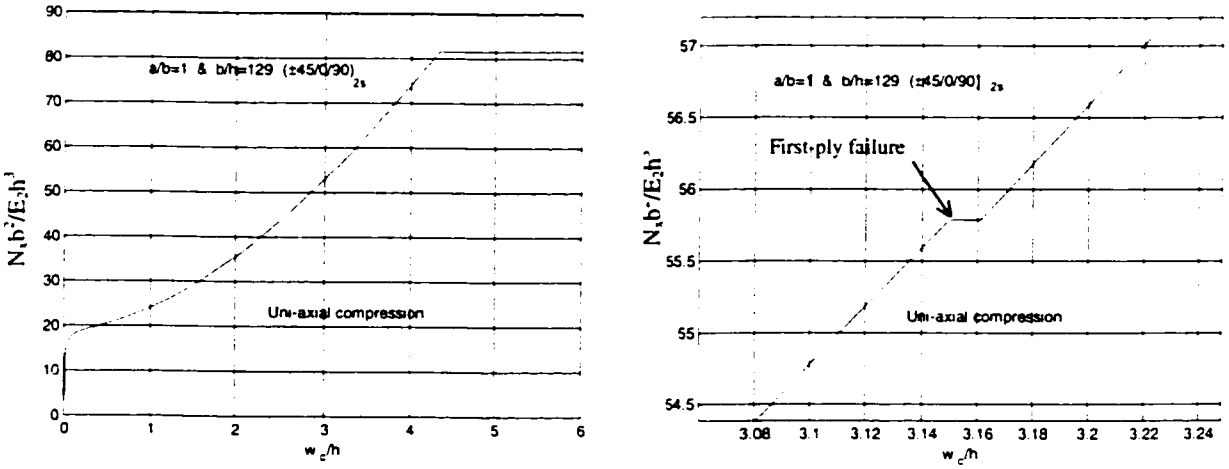

(a) (b)

Figure 3-4 Load versus the central deflection response of $(\pm 45/0/90)_{2s}$ laminate under the action of uni-axial compression

A $(\pm 45/0/90)_{2s}$ laminate with simply-supported boundary condition under the action of positive shear loading is now analyzed and the results are compared with results given in the work of Singh *et al* [19].

Dimensions of the plate, the material properties of the laminates and boundary conditions are same as that of the previous example. A 5 by 5 type finite element mesh is considered. See Figure 3-3. The first-ply failure load and the ultimate failure load for $(\pm 45/0/90)_{2s}$ laminate under the action of positive shear loading are given in Table 3-4.

Table 3-4 The first-ply failure load and the ultimate failure load for $(\pm 45/0/90)_{2s}$ Laminate under the action of positive shear loading

	First-ply failure load ($N_x b^2/E_2 h^3$)	Ultimate failure load ($N_x b^2/E_2 h^3$)
Singh *et al* [19]	59.38	116.18
Present study	61.68	115.32

Figure 3-5 (a) and (b) show the load versus the maximum deflection response of $(\pm 45/0/90)_{2s}$ laminate under the action of positive shear loading. In Figure 3-5, w_{max} is the maximum deflection of the plate. It is seen from Figure 3-5 and Table 3-4 that the difference between the present results and the results obtained by Singh *et al* [19] are small.

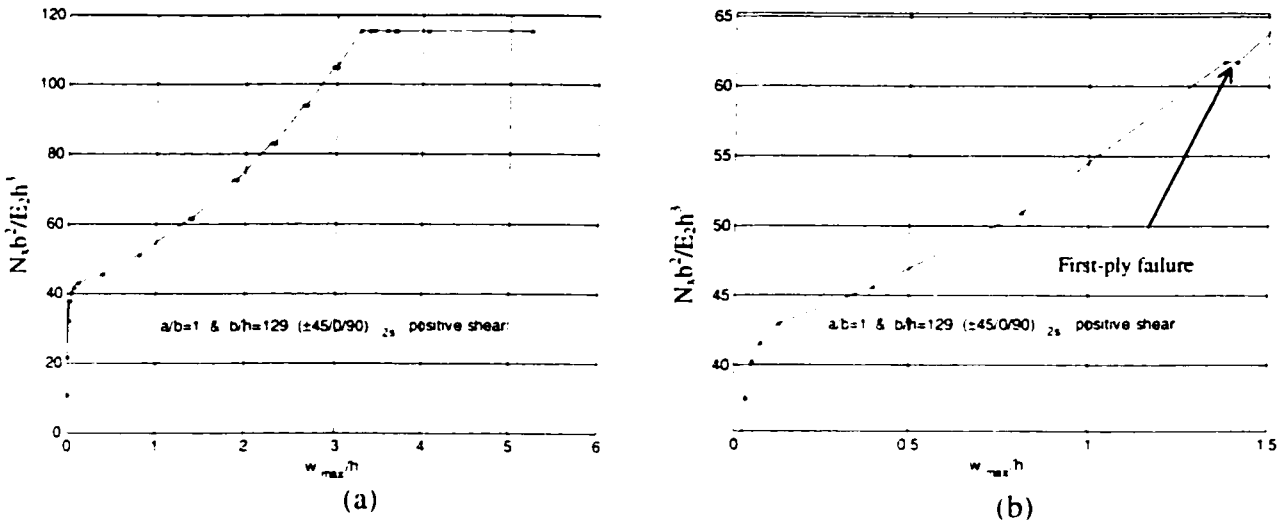

Figure 3-5 Load versus the maximum deflection response of $(\pm 45/0/90)_{2s}$ laminate under the action of positive shear

A $(\pm 45/0/90)_{2s}$ laminate with simply-supported boundary condition under the action of negative shear loading is now analyzed and the results are compared with the results given in the work of Singh *et al* [19].

Dimensions of the plate, the material properties of the laminates and boundary conditions are the same as that of the previous example. A 5 by 5 type finite element mesh is considered. See Figure 3-3. The first-ply failure load and the ultimate failure load for $(\pm 45/0/90)_{2s}$ laminate under the action of negative shear loading are given in Table 3-5.

Table 3-5 The first-ply failure load and the ultimate failure load for $(\pm 45/0/90)_{2s}$ laminate under the action of negative shear loading

	First-ply failure load ($N_x b^2/E_2 h^3$)	Ultimate failure load ($N_x b^2/E_2 h^3$)
Singh *et al* [20]	82.76	126.94
Present study	78.67	121.58

Figure 3-6 (a) and (b) show the load versus the maximum deflection response of a square $(\pm 45/0/90)_{2s}$ laminate under the action of negative shear loading. In Figure 3-5, w_{max} is the maximum deflection of the plate. It is seen from Figure 3-6 and Table 3-5 that the difference between the present results and the results obtained by Singh *et al* [20] are small.

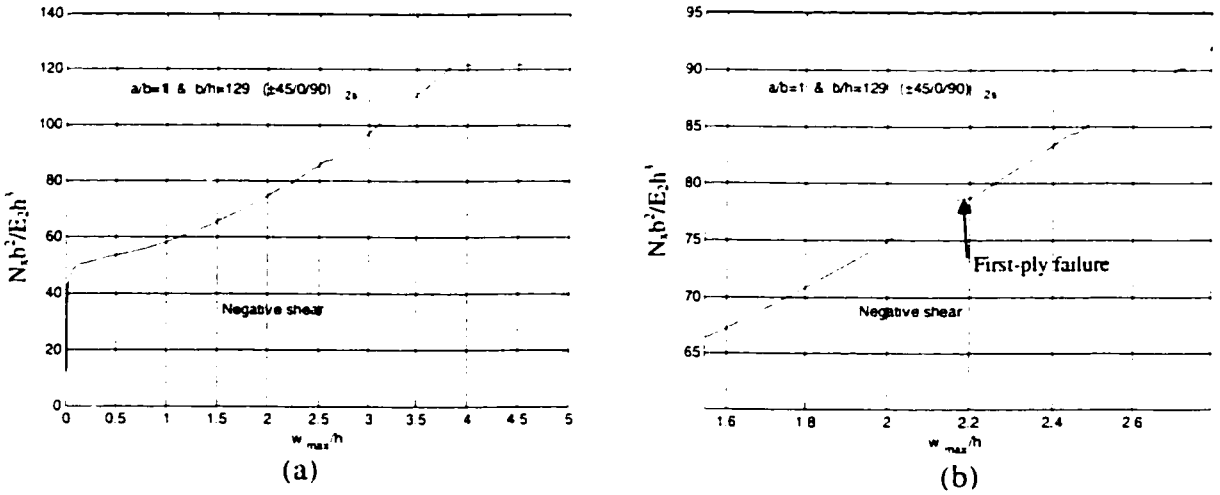

Figure 3-6 Load versus the maximum deflection response of $(\pm 45/0/90)_{2s}$ laminate under the action of negative shear

No results are available in the literature on the first-ply failure load and the ultimate failure load of laminates under the action of bi-axial compression as well as under the action of bi-axial compression combined with in-plane positive (or negative) shear loading, and therefore the comparison can not be made. However, a good comparison of the first-ply failure loads and ultimate failure loads for the cases of uni-axial compression and positive (or negative) shear loading with the results given in the work of Singh *et al* [18], [19] and [20], are indicative of the fact that the present results for the first-ply failure load and the ultimate failure load under the action of bi-axial compressive loading as well as bi-axial compression combined with in-plane positive (or negative) shear loading are reasonably accurate.

Chapter 4

Parametric Study

4.1 Introduction

Three symmetric laminate lay-up configurations, $(\pm 45/0/90)_{2s}$, $(\pm 45)_{4s}$ and $(0/90)_{4s}$ and three unsymmetric laminate lay-up configurations, $(\pm 45/0/90)_4$, $(\pm 45)_8$ and $(0/90)_8$ are considered in the present study to understand the progressive failure characteristics under the action of uni-axial compression, bi-axial compression, and bi-axial compression combined with in-plane positive (or negative) shear loading. In addition, $(\pm\theta)_{4s}$ laminates are also considered to understand the effect of fiber orientation on the failure strength of laminates. The boundary conditions that have been considered in this study are shown in Figure 4-1. Properties of the material (Reddy and Reddy [5]) used in the present study are presented in Table 4-1.

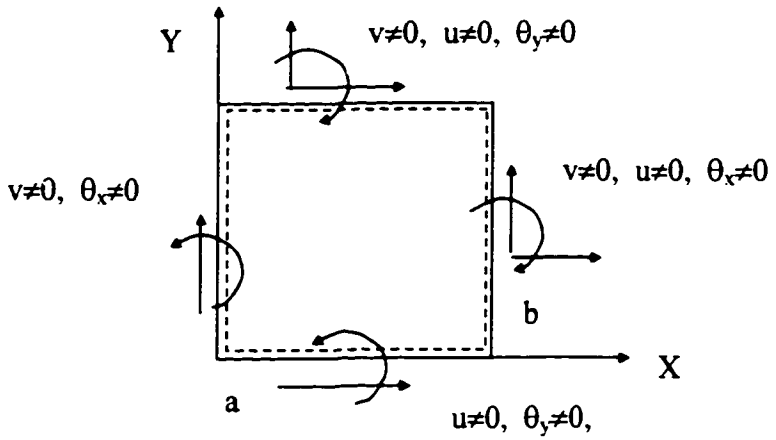

Figure 4-1 Details of boundary conditions for the laminated plate

In the Table 4-1, ν_{12}, ν_{13} and ν_{23} are the Poisson's ratios in the planes 1-2, 1-3 and 2-3, respectively. E_1, E_2 and E_3 are principal Young's modulus in fiber direction and in the direction transverse to it, respectively. G_{12}, G_{13} and G_{23} are shear modulus values associated with planes 1-2, 1-3 and 2-3, respectively. X_t is the tensile strength of lamina in fiber direction. X_c is the compressive strength of lamina in fiber direction. Y_t is the tensile strength of lamina in the direction (in plane 1-2) transverse to fiber direction. Y_c is the compressive strength of lamina in the same direction. Z_t is the tensile strength of lamina in principal material direction 3. Z_c is the compressive strength of lamina in principal material direction 3. R, S and T are shear strengths of lamina in planes 2-3, 1-3 and 1-2, respectively.

Table 4-1 Material properties of T300/5208 graphite-epoxy [5]

Mechanical properties	Values	Strength properties	Values
E_1	132.58 GPa	X_t	1.515 GPa
E_2	10.8 GPa	X_c	1.697 GPa
E_3	10.8GPa	$Y_t = Z_t$	43.8 MPa
$G_{12} = G_{13}$	5.7 GPa	$Y_c = Z_c$	43.8 MPa
$\nu_{12} = \nu_{13}$	0.24	R	67.6 MPa
ν_{23}	0.49	S=T	86.9 MPa

In the Figure 4-1, a and b are dimensions of the full plate in X and Y directions. Dimensions of the plate are: a = 279 mm and b = 279 mm. Ply thickness is 0.135 mm.

A 5 by 5 type finite element mesh is used in the present analysis. Here, the first number refers to the number of elements in X direction (dimension of the plate in X direction is a) and the second number corresponds to Y direction (dimension of the plate in Y direction is b). Figure 4-2 shows the finite element mesh for a square plate. Figure 4-3

and Figure 4-4 show the direction of the applied shear loading along with the fiber direction.

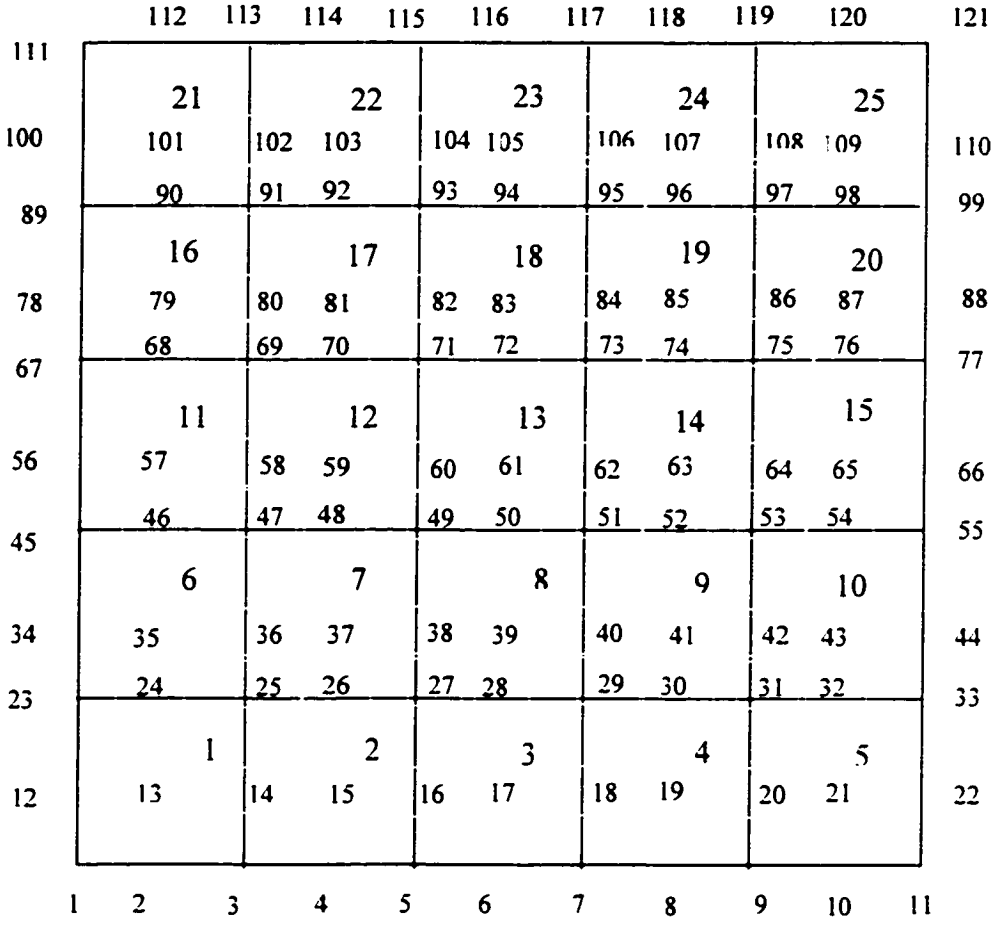

Figure 4-2 Finite element mesh for the plate

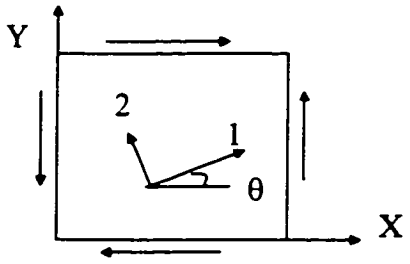

Figure 5-2 Notation for the positive shear

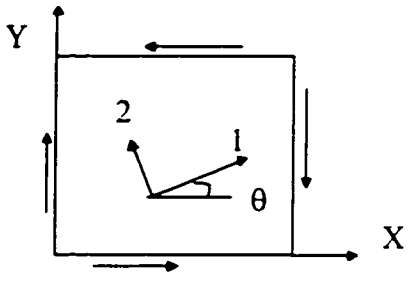

Figure 5-3 Notation for the negative shear

It is to be noted that in-plane shear loading is applied on all four edges of the plate, uni-axial compressive loading is applied at the edge x = a, and bi-axial compressive loadings are applied on the edges x = a and y = b.

Bi-axial compressive loadings N_x and N_y and in-plane shear loading N_{xy} are expressed in figures in non-dimensionalized forms as N_xb^2/E_2h^3, N_yb^2/E_2h^3 and $N_{xy}b^2/E_2h^3$, respectively. N_x is the applied X-direction axial compressive loading per unit length. N_y is the applied Y-direction axial compressive loading per unit length. N_{xy} is the applied in-plane shear loading per unit length. The corresponding central (transverse) deflection is also expressed in non-dimensionalized form as w_c/h and the maximum deflection is also expressed in non-dimensionalized form as w_{max}/h, where h is the total thickness of the laminate.

4.2 Failure Under Uni-axial Compression

Figure 4-5 shows the load versus the central deflection response of various laminates under the action of uni-axial compression. It is observed that the largest strength is exhibited by $(\pm45)_{4s}$ laminate within the deflection range $w_c/h \leq 1.0$ and by $(\pm45/0/90)_{2s}$ laminate within the deflection range $w_c/h > 1.0$. It is also observed that $(0/90)_{4s}$ laminate shows the least strength for a fixed value of the central deflection within the range $w_c/h < 2.4$. However, there is a drastic increase in strength for this laminate in the deflection range $w_c/h > 2.4$, and there is also a drastic increase in strength for $(\pm45/0/90)_{2s}$ laminate

in the deflection range $w_c/h > 1.0$. This is attributed to a substantial increase in the axial stiffness.

It is noted that the first-ply failure of all laminates occur at the loaded edge of the plate primarily.

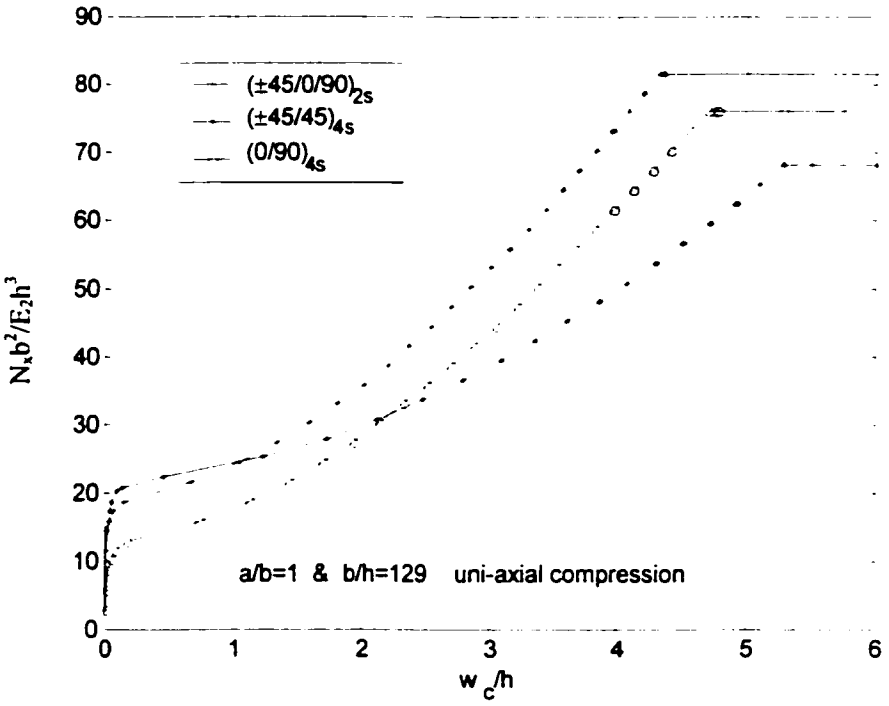

Figure 4-5 Load versus the central deflection response of different lay-up configurations under uni-axial compression

Figure 4-6 shows the progressive failure load versus the central deflection response of $(\pm 45/0/90)_{2s}$ laminate for various aspect ratio values under the action of uni-axial compression. For a fixed value of the central deflection, the highest strength is observed for the aspect ratio of 0.8 while the lowest for the aspect ratio of 2. The failure loads decrease with an increase of aspect ratio. The first-ply failure and the ultimate failure of

all laminates occur at the loaded edge. The first-ply failure is matrix failure while the ultimate failure is caused primarily by the fiber failure.

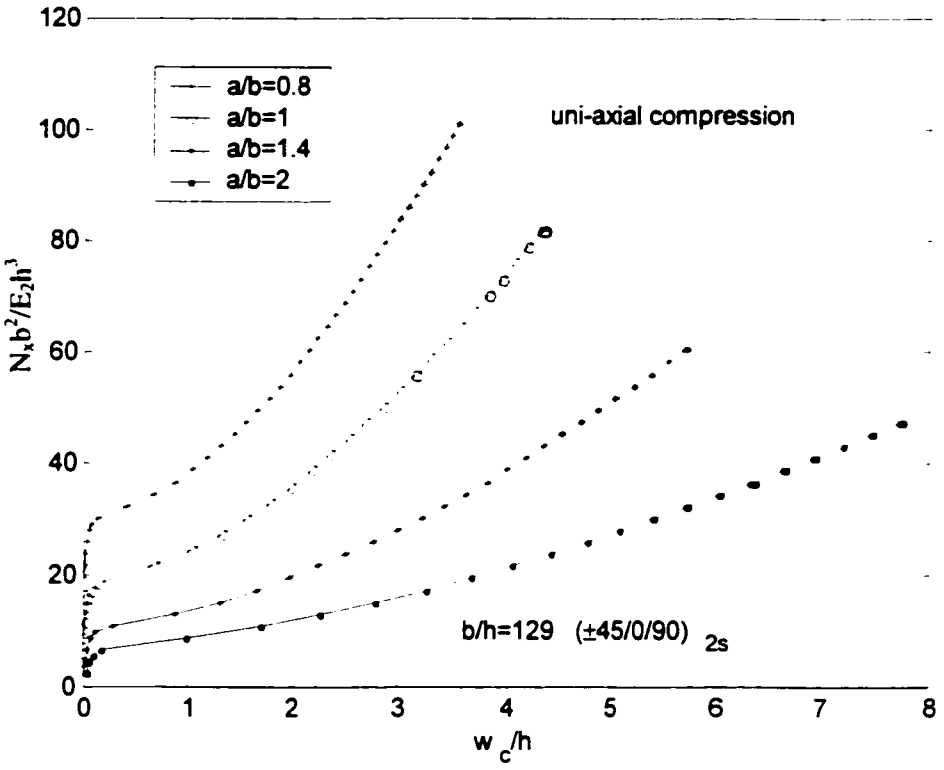

Figure 4-6 Load versus the central deflection response of $(\pm 45/0/90)_{2s}$ laminate under uni-axial compression for various aspect ratio values

Figure 4-7 shows the progressive failure load versus the central deflection response of various symmetric laminates $(\pm 45/0/90)_{2s}$, $(\pm 45)_{4s}$ and $(0/90)_{4s}$, and unsymmetric laminates $(\pm 45/0/90)_4$, $(\pm 45)_8$ and $(0/90)_8$ under the action of uni-axial compression. It is observed that for the symmetric laminate $(\pm 45)_{4s}$, the load-central deflection curve almost coincides with the load-central deflection curve of the unsymmetric laminate $(\pm 45)_8$. However, the central deflections of $(\pm 45/0/90)_{2s}$ laminate and $(0/90)_{4s}$ laminate are

positive while the central deflections of $(\pm 45/0/90)_4$ laminate and $(0/90)_8$ laminate are negative.

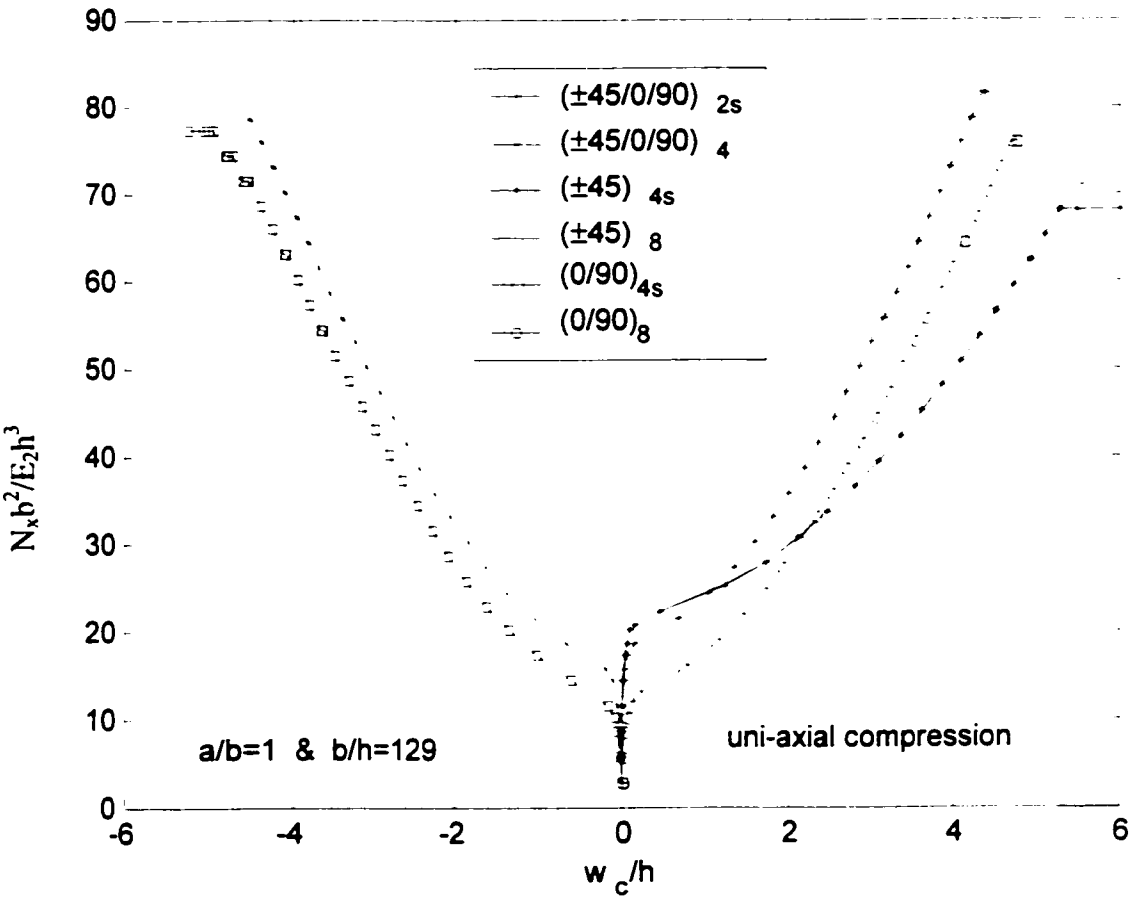

Figure 4-7 Progressive failure of symmetric and unsymmetric laminates under uni-axial compression

Figure 4-8 shows the deformed configuration of $(\pm 45/0/90)_{2s}$ laminate under the action of uni-axial compression and Figure 4-9 shows that of $(\pm 45/0/90)_4$ laminate.

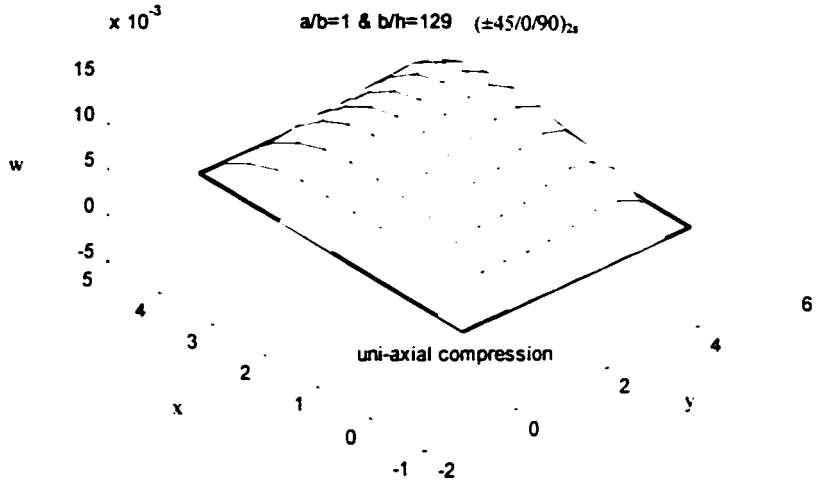

Figure 4-8 The deformed configuration of $(\pm 45/0/90)_{2s}$ laminate under uni-axial compression

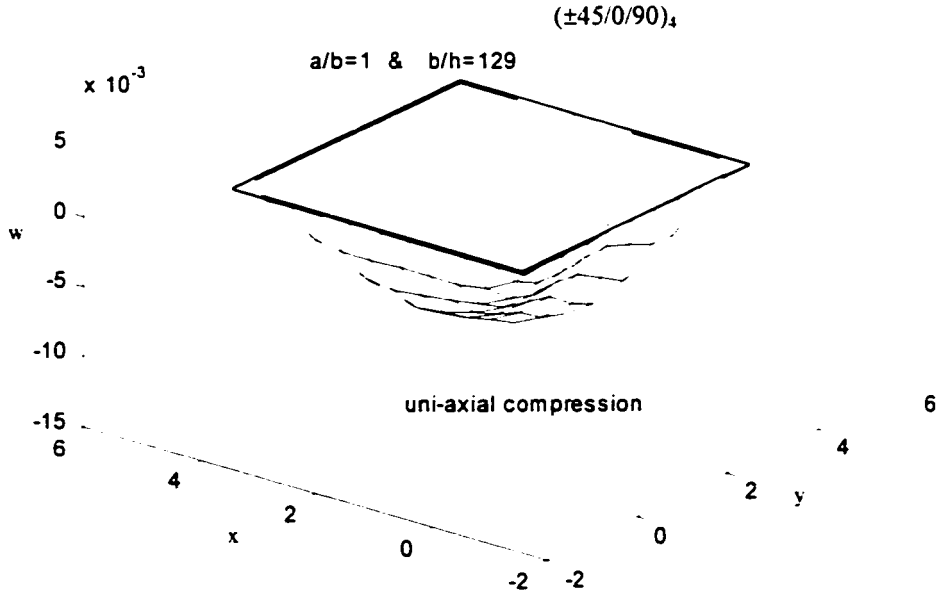

Figure 4-9 The deformed configuration of $(\pm 45/0/90)_4$ laminate under uni-axial compression

The first-ply failure loads and the ultimate failure loads of symmetric laminates $(\pm 45/0/90)_{2s}$, $(\pm 45)_{4s}$ and $(0/90)_{4s}$ and unsymmetric laminates $(\pm 45/0/90)_4$, $(\pm 45)_8$ and $(0/90)_8$ under the action of uni-axial compression are presented in Table 4-2.

Table 4-2 The first-ply failure loads and the ultimate failure loads of symmetric and unsymmetric laminates under uni-axial compression

Lay-up	First-ply failure load ($N_x b^2/E_2 h^3$)	Ultimate failure load ($N_x b^2/E_2 h^3$)	(w_c/h)*	Failure location (FL, FE)♣	First-ply failure mode
$(\pm 45/0/90)_{2s}$	55.79	81.53	3.16	1,25	Transverse ♠
$(\pm 45/0/90)_4$	55.78	78.67	-3.39	16,10	Transverse
$(\pm 45)_{4s}$	47.92	67.94	3.86	1,25	Transverse
$(\pm 45)_8$	47.92	70.80	3.87	1,20	Transverse
$(0/90)_{4s}$	61.51	75.81	3.97	1,25	Transverse
$(0/90)_8$	54.36	77.24	-3.64	16,10	Transverse

* Non-dimensionalized central deflection at first-ply failure

♣ FL and FE are the failed layer number and failed element number at first-ply failure

♠ Transverse mode of failure refers to the matrix failure

In order to get an idea of the sequence of modes of failure under the action of uni-axial compression, the sequence of the first occurrence of failure modes is shown in Figure 4-10 for $(\pm 45/0/90)_{2s}$ laminate under the action of uni-axial compression. The terms within the parenthesis (for all failure modes except the onset of delamination) represent the failed ply number and the location of the failed element, respectively. It is observed that the transverse shear mode of failure, in-plane shear mode of failure and the fiber failure mode occur at the same load level.

Figure 4-11 shows the variation of the first-ply failure load and the ultimate failure load of $(\pm\theta)_{4s}$ laminates with fiber orientation (θ) under the action of uni-axial compression. The results show that the variations in the response are symmetric with respect to 45^0 fiber orientation. Peak values of the first-ply failure load and the ultimate failure load are predicted to occur for 45^0 orientation. For $(0/0)_{4s}$ and $(\pm 15)_{4s}$ laminates the first-ply failure load is also the ultimate failure load.

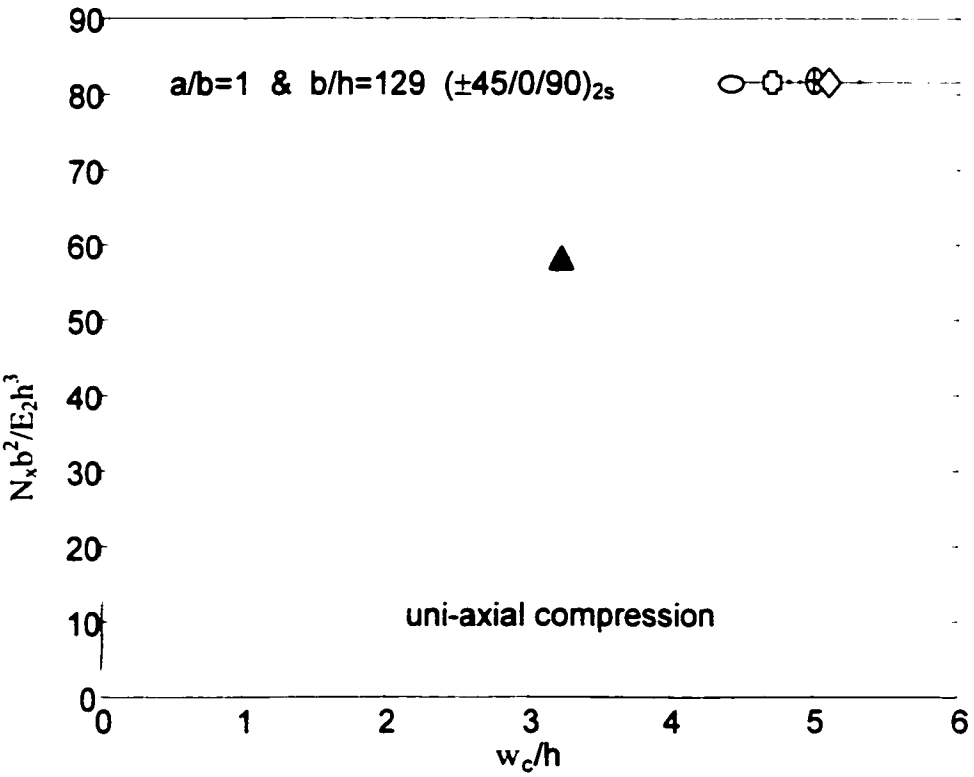

Figure 4-10 Modes of failure: (Δ) Transverse (in-plane) mode of failure (matrix failure) (1,25); (O) Transverse shear (τ_{xz}) mode of failure (1,25); (⌬) Fiber failure (1,25); (⊕) Transverse shear (τ_{yz}) mode of failure (1,25);
(◇) In–plane shear (τ_{xy}) mode of failure (1,25)

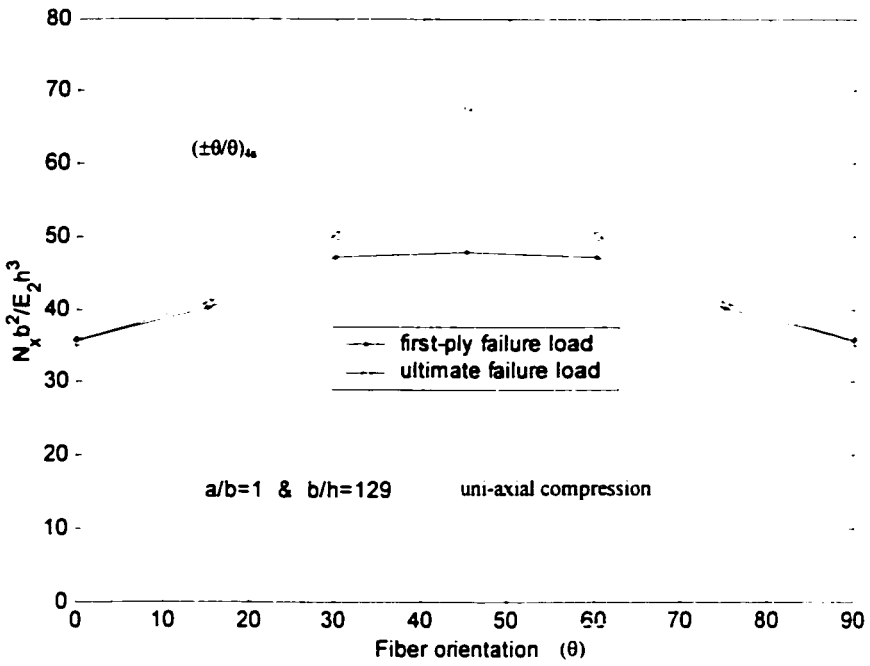

Figure 4-11 Variation of the first-ply failure load and the ultimate failure load of $(\pm\theta)_{4s}$ laminate with fiber orientation under uni-axial compression

Figure 4-12 shows the variation of the central deflection associated with the first-ply failure and that just before the ultimate failure for $(\pm\theta)_{4s}$ laminate. The results predict that the variations in the central deflection are symmetrical about the 45^0 fiber orientation. Peak values corresponding to the first-ply failure load and the ultimate failure load occur for 45^0 fiber orientation.

Figure 4-13 shows the variation of these loads with aspect ratio values for $(\pm 45/0/90)_{2s}$ laminates. It is seen that the first-ply failure load and the ultimate failure load decrease with an increase in the values of aspect ratio.

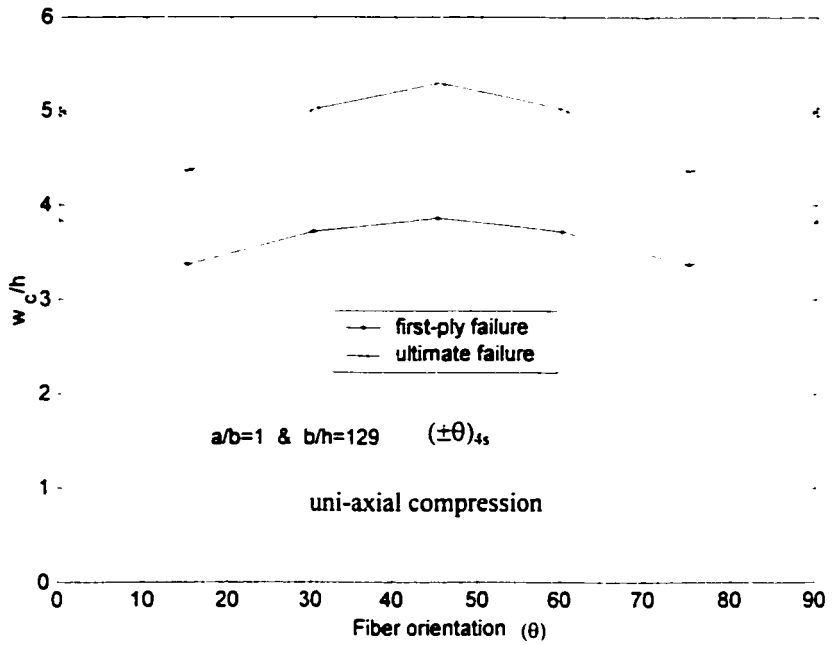

Figure 4-12 Variation of the central deflection associated with the first-ply failure and the ultimate failure of $(\pm\theta)_{4s}$ laminate with fiber orientation under uni-axial compression

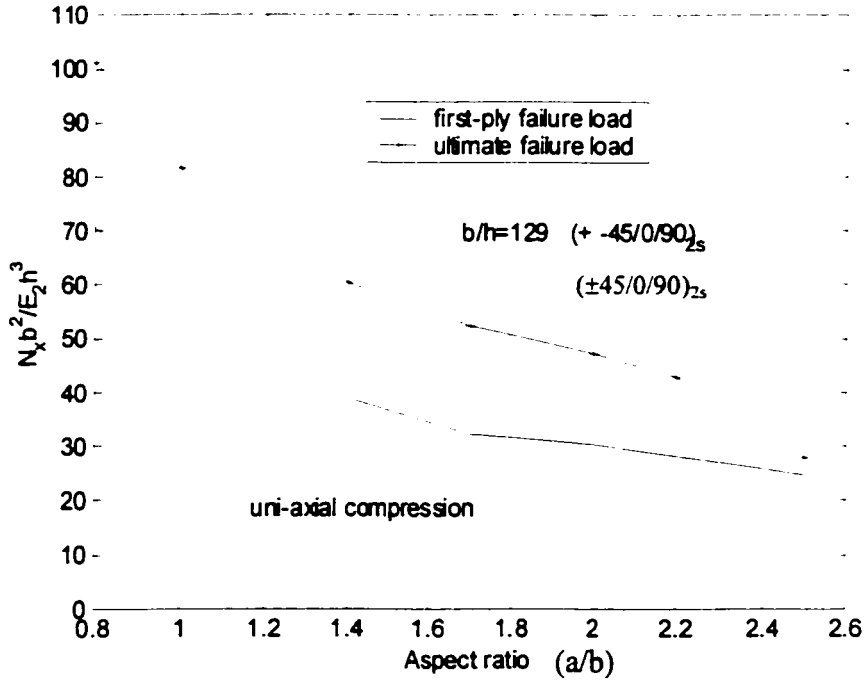

Figure 4-13 Variation of the first-ply failure load and the ultimate failure load of $(\pm45/0/90)_{2s}$ laminate with aspect ratio values under uni-axial compression

Figure 4-14 shows the variation of the central deflection associated with the first-ply failure and the ultimate failure, with aspect ratio values for $(\pm 45/0/90)_{2s}$ laminate. It is seen that the central deflections at the first-ply failure and the ultimate failure increase with increasing values of aspect ratio.

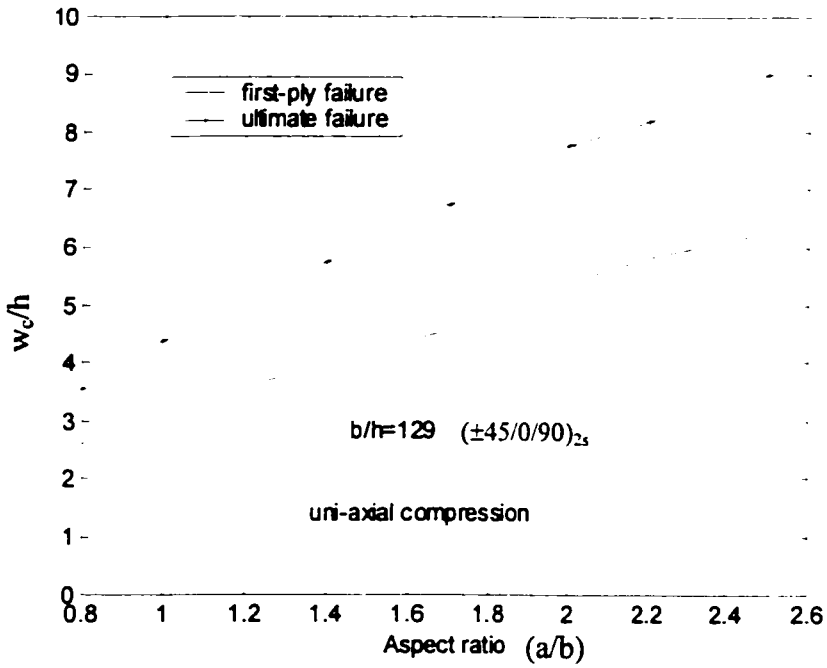

Figure 4-14 Variation of the central deflection of $(\pm 45/0/90)_{2s}$ laminate with aspect ratio values under uni-axial compression

4.3 Failure Under Bi-axial Compression

Figure 4-15 shows the load versus the central deflection response of various laminates under the action of bi-axial compression. It is observed that the largest strength is exhibited by $(\pm 45)_{4s}$ laminate within the deflection range $w_c/h \leq 1.1$ and by $(\pm 45/0/90)_{2s}$ laminate within the deflection range $w_c/h > 1.1$. It is also observed that $(0/90)_{4s}$ laminate shows the least strength for a fixed value of the central deflection within the range $w_c/h < 2.3$.

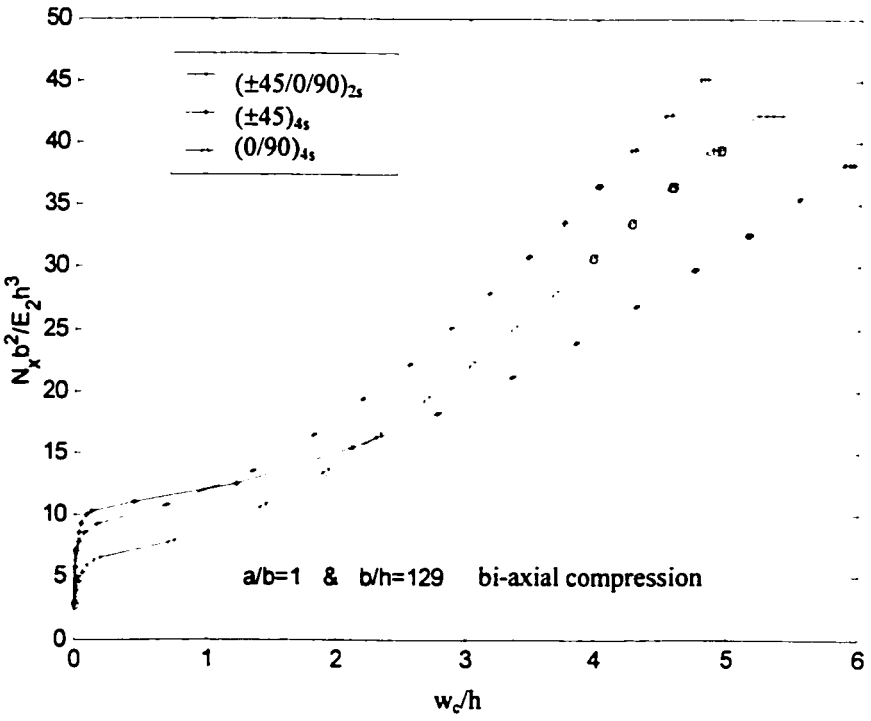

Figure 4-15 Load versus the central deflection response of different lay-up configurations under bi-axial compression

The progressive failure load versus the central deflection response of $(\pm 45/0/90)_{2s}$ laminate for various aspect ratio values under the action of bi-axial compression is shown

in Figure 4-16. For a fixed value of the central deflection, the highest strength is observed for the aspect ratio of 0.8 while the lowest for the aspect ratio 3. The failure loads decrease with an increase of aspect ratio. The first-ply failure and the ultimate failure of all laminates occur at the loaded edge. The first-ply failure is matrix failure while the ultimate failure is caused primarily by the transverse shear stress τ_{yz}. When a/b=2, the ultimate failure is caused by the transverse shear stress τ_{xz}. When a/b=3, ultimate failure is caused by the delamination.

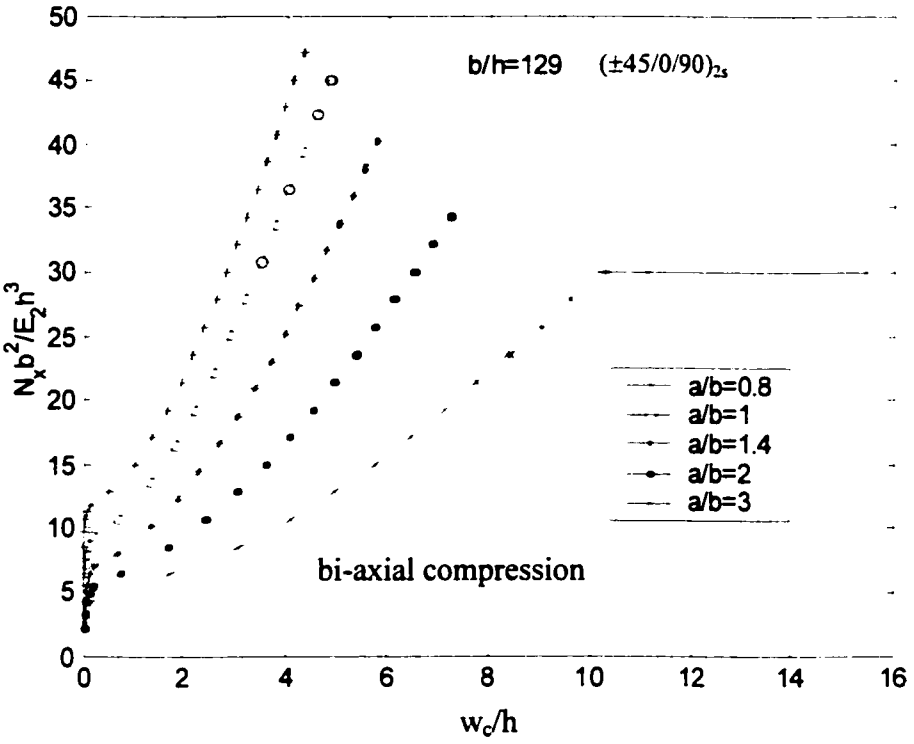

Figure 4-16 Load versus the central deflection response of $(\pm 45/0/90)_{2s}$ laminate for various aspect ratio values under bi-axial compression

Table 4-3 gives the values of the first-ply failure load and the ultimate failure load of symmetric laminates $(\pm 45/0/90)_{2s}$, $(\pm 45)_{4s}$ and $(0/90)_{4s}$ and unsymmetric laminates $(\pm 45/0/90)_4$, $(\pm 45)_8$ and $(0/90)_8$ under bi-axial compression. It is seen that for symmetric $(\pm 45/0/90)_{2s}$ and unsymmetric $(\pm 45/0/90)_4$ lay-up configurations, the first-ply failure loads are almost the same, and the ultimate failure loads are a little different. For symmetric laminate $(\pm 45)_{4s}$ and unsymmetric laminate $(\pm 45)_8$ lay-up configurations, the values of the first-ply failure load and the ultimate failure load are very close. For symmetric laminate $(0/90)_{4s}$ and unsymmetric laminate $(0/90)_8$ lay-up configurations, the values of the first-ply failure load and the ultimate failure load have some difference.

Table 4-3 The first-ply failure loads and the ultimate failure loads for symmetric and unsymmetric laminates under bi-axial compression

Lay-up	First-ply failure Load ($N_x b^2/E_2 h^3$)	Ultimate failure load ($N_x b^2/E_2 h^3$)	(w_c/h)*	Failure location (FL, FE) ♣	First-ply failure mode
$(\pm 45/0/90)_{2s}$	30.75	45.06	3.461	1,25	Transverse♠
$(\pm 45/0/90)_4$	30.04	41.48	3.389	1,25	Transverse
$(\pm 45)_{4s}$	27.89	40.45	4.313	1,20	Transverse
$(\pm 45)_8$	26.82	38.26	4.329	1,25	Transverse
$(0/90)_{4s}$	34.33	45.77	3.995	1,24	Transverse
$(0/90)_8$	30.75	42.20	3.989	1,25	Transverse

* Non–dimensionalized central deflection at first-ply failure

♠Transverse mode of failure refers to the matrix failure

♣ FL and FE are the failed layer number and the failed element number at first-ply failure

Table 4-4 gives the progressive failure loads and failure modes of $(\pm 45/0/90)_{2s}$ laminate for various load ratio values (N_x : N_y : N_{xy}) in terms of non-dimensionalized first–ply failure load, ultimate failure load and central deflection under the action of bi-axial compression. In addition, the first-ply failure locations (i.e. the failed ply number and the failed element number) and failure modes related to the first-ply failure and the ultimate failure are also shown in this table. It is observed that with increasing proportion of N_y (Y-direction axial compression) in the bi-axial compression, the first-ply failure load and the ultimate failure load decrease monotonically. At N_x : N_y : N_{xy} = 1:1:0, the percentage loss in the first-ply failure and the ultimate failure load are respectively, 44.9 and 44.7. It is observed that the first-ply failure is matrix failure.

Table 4-4 Progressive failure of the $(\pm 45/0/90)_{2s}$ laminate at various load ratio values under bi-axial compression

Load ratio N_x:N_y:N_{xy}	First-ply failure load ($N_x b^2/E_2 h^3$)	Ultimate failure load ($N_x b^2/E_2 h^3$)	(w_c/h)*	Failure location (FL,FE)♣	First-ply failure mode	Ultimate failure modes
1:0:0	55.78	81.53	3.161	1,25	Transverse♠	Shear stress τ_{yz}
1:0.2:0	47.20	70.80	3.228	1,25	Transverse	Shear stress τ_{yz}
1:0.4:0	40.77	60.08	3.253	1,25	Transverse	Shear stress τ_{yz}
1:0.6:0	35.94	53.10	3.274	1,25	Transverse	Shear stress τ_{yz}
1:0.8:0	34.33	48.63	3.484	1,25	Transverse	Shear stress τ_{yz}
1:1:0	30.75	45.06	3.470	1,25	Transverse	Delamination

* Non–dimensionalized center deflection at first-ply failure

♣FL and FE are the failed layer number and failed element number at first-ply failure

♠Transverse mode of failure refers to the matrix failure

Figure 4-17 shows the load versus the central deflection response of $(\pm 45/0/90)_{2s}$ laminate for different load ratio values ($N_x : N_y : N_{xy}$) under the action of bi-axial compression. It is seen that the first-ply failure load and the ultimate failure load decrease with increasing load ratio values (increasing N_y).

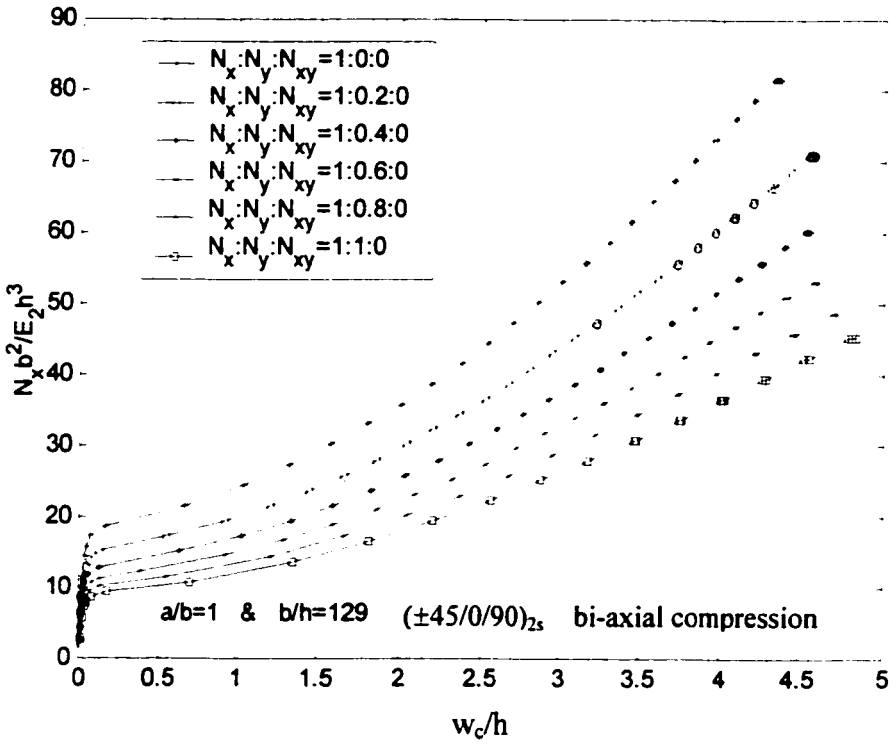

Figure 4-17 Load versus the central deflection response of $(\pm 45/0/90)_{2s}$ laminate for different load ratio values under bi-axial compression

Table 4-5 gives the results of the progressive failure analysis of $(\pm 45)_{4s}$ laminate at various load ratio values ($N_x : N_y : N_{xy}$) in terms of the non-dimensionalized first-ply failure load, ultimate failure load and central deflection under the action of bi-axial

compression. In addition, the first-ply failure locations (i.e. the failed ply number and the failed element number) and failure modes related to the first-ply failure and the ultimate failure are also shown in this table. It is observed that with increasing proportion of N_y (Y-direction axial compression) in the bi-axial compression, the first-ply failure load and the ultimate failure load decrease monotonically. At $N_x : N_y : N_{xy} = 1:1:0$, the percentage loss in the first-ply failure and the ultimate failure load are respectively, 44 and 43.67. It is observed that the first-ply failure is matrix failure.

Table 4-5 Progressive failure of $(\pm 45)_{4s}$ laminate at various load ratio values under bi-axial compression

Load ratio $N_x:N_y:N_{xy}$	First-ply failure load $(N_x b^2/E_2 h^3)$	Ultimate failure load $(N_x b^2/E_2 h^3)$	$(w_c/h)^*$	Failure location (FL,FE)$^\clubsuit$	First-ply failure mode	Ultimate failure mode
1:0:0	47.92	67.94	3.859	1,25	Transverse$^\spadesuit$	Transverse
1:0.2:0	41.48	61.51	4.016	1,25	Transverse	Delamination
1:0.4:0	36.47	53.64	4.113	1,25	Transverse	Transverse
1:0.6:0	32.18	46.49	4.147	1,25	Transverse	Transverse τ_{yz}
1:0.8:0	27.89	42.20	4.045	1,25	Transverse	Delamination
1:1:0	26.82	38.27	4.313	1,25	Transverse	Delamination

*Non–dimensionalized central deflection at first-ply failure

$^\clubsuit$FL and FE are the failed layer number and the failed element number at first-ply failure

$^\spadesuit$Transverse mode of failure refers to the matrix failure

Figure 4-18 shows the load versus the central deflection response of $(\pm 45)_{4s}$ laminate for different load ratio values ($N_x : N_y : N_y$) under the action of bi-axial compression. It is

seen that the first-ply failure load and the ultimate failure load decrease with increasing load ratio values (increasing N_y).

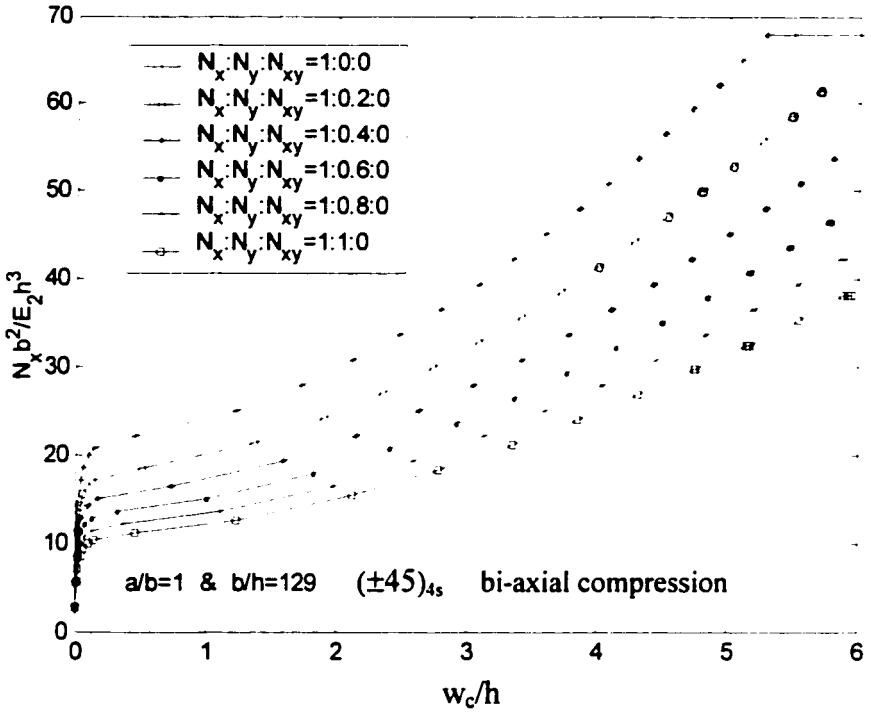

Figure 4-18 Load versus the center deflection response of $(\pm 45)_{4s}$ laminate for different load ratio values under bi-axial compression

Table 4-6 gives the results of the progressive failure analysis of $(0/90)_{4s}$ laminate at various load ratio values (N_x : N_y : N_{xy}) in terms of the non-dimensionalized first–ply failure load, ultimate failure load and central deflection under the action of bi-axial compression. In addition, the first-ply failure locations (i.e. the failed ply number and the failed element number) and failure mode related to the first-ply failure and the ultimate

failure are also shown in this table. It is observed that with increasing proportion of N_y (Y-direction axial compression) in the bi-axial compression, the first-ply failure load and the ultimate failure load decrease monotonically. At $N_x : N_y : N_{xy} = 1 : 1 : 0$, the percentage loss in the first-ply failure and the ultimate failure load are respectively, 50 and 44.33. It is observed that the first-ply failure is matrix failure.

Table 4-6 Progressive failure of $(0/90)_{4s}$ laminate at various load ratio values under bi-axial compression

Load ratio $N_x:N_y:N_{xy}$	First-ply failure load $(N_x b^2/E_2h^3)$	Ultimate failure load $(N_x b^2/E_2h^3)$	$(w_c/h)^*$	Failure location (FL,FE)$^\clubsuit$	First-ply failure mode	Ultimate failure modes
1:0:0	61.51	75.81	3.973	1,25	Transverse$^\clubsuit$	Fiber failure
1:0.2:0	51.49	68.66	3.991	1,25	Transverse	Delamination
1:0.4:0	45.06	59.36	4.062	1,25	Transverse	Delamination
1:0.6:0	37.91	52.21	3.974	1,25	Transverse	Delamination
1:0.8:0	34.33	45.77	3.995	1,25	Transverse	Delamination
1:1:0	30.75	42.20	3.975	1,25	Transverse	Delamination

*Non–dimensionalized central deflection at first-ply failure

$^\clubsuit$FL and FE are the failed layer number and the failed element number at first-ply failure

$^\clubsuit$Transverse mode of failure refers to the matrix failure

Figure 4-19 shows the load versus the central deflection response of $(0/90)_{4s}$ laminate for different load ratio values ($N_x : N_y : N_{xy}$) under the action of bi-axial compression. It is seen that the first-ply failure load and ultimate failure load decrease with increasing load ratio values (increasing N_y).

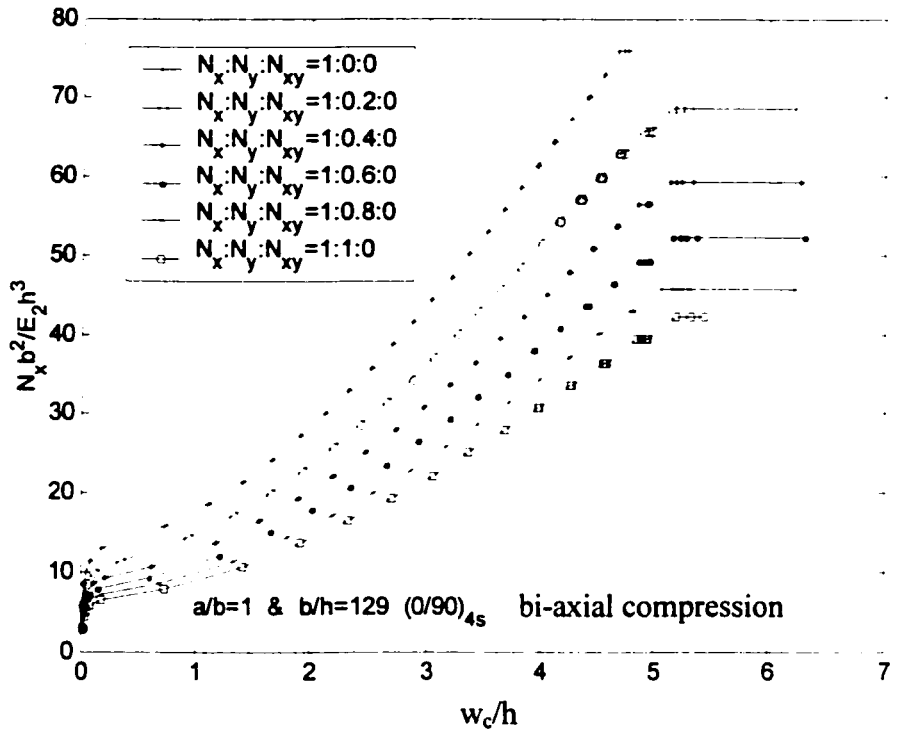

Figure 4-19 Load versus the central deflection response of $(0/90)_{4s}$ laminate for different load ratio values under bi-axial compression

In order to get an idea of the sequence of modes of failure under the action of uni-axial compression, the sequence of the first occurrence of failure modes are shown in Figure 4-20 for $(\pm 45/0/90)_{2s}$ laminate under the action of bi-axial compressive loadings. The terms within the parenthesis (for all failure modes except the onset of delamination) represent the failed ply number and the location of the failed element, respectively. It is observed that the transverse shear mode of failure, in-plane shear mode, the fiber failure and delamination occur at the same load level.

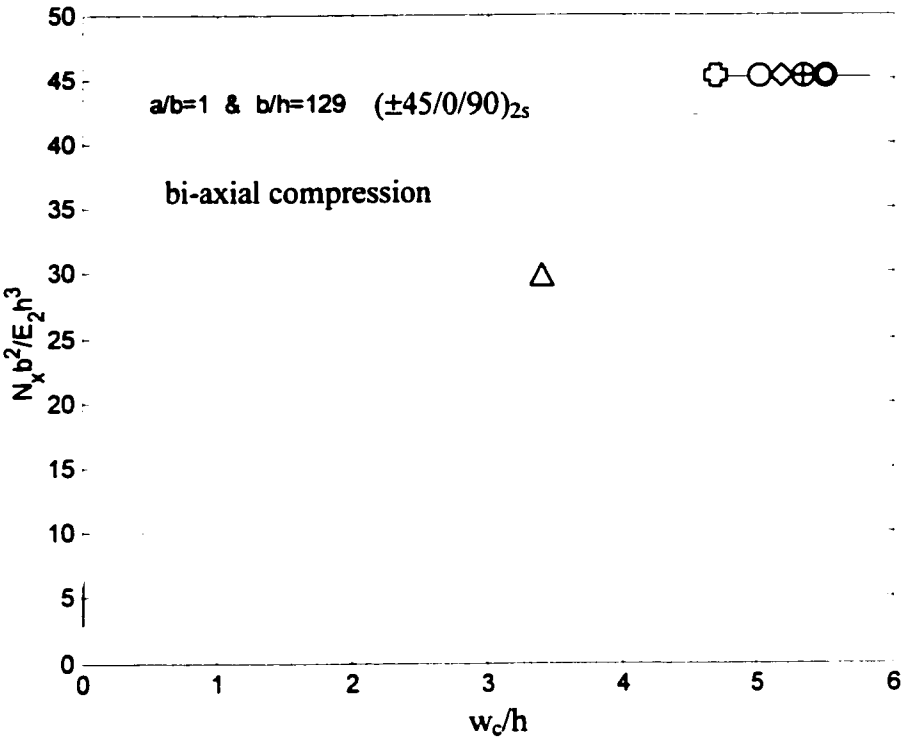

Figure 4-20 (Δ) Transverse (in -plane) mode of failure (matrix failure) (1,25). (⬡) fiber failure (1,25) (O) Transverse shear τ_{xz} mode of failure (1,25).(◇) Transverse shear τ_{yz} mode of failure (1,1). (⊕) In –plane shear mode of failure (1,25).(O) Delamination

Figure 4-21 shows the variation of first-ply failure load and ultimate load of $(\pm\theta)_{4s}$ laminates with fiber orientation (θ) under the action of bi-axial compression. The results show that the variations in the response are symmetric with respect to 45^0 fiber orientation. Peak values of the first-ply failure load and the ultimate failure load are predicted to occur for 45^0 orientation. For $(0/0)_{4s}$, $(\pm15)_{4s}$ and $(\pm30)_{4s}$ laminates the first-ply failure loads also are the ultimate failure loads.

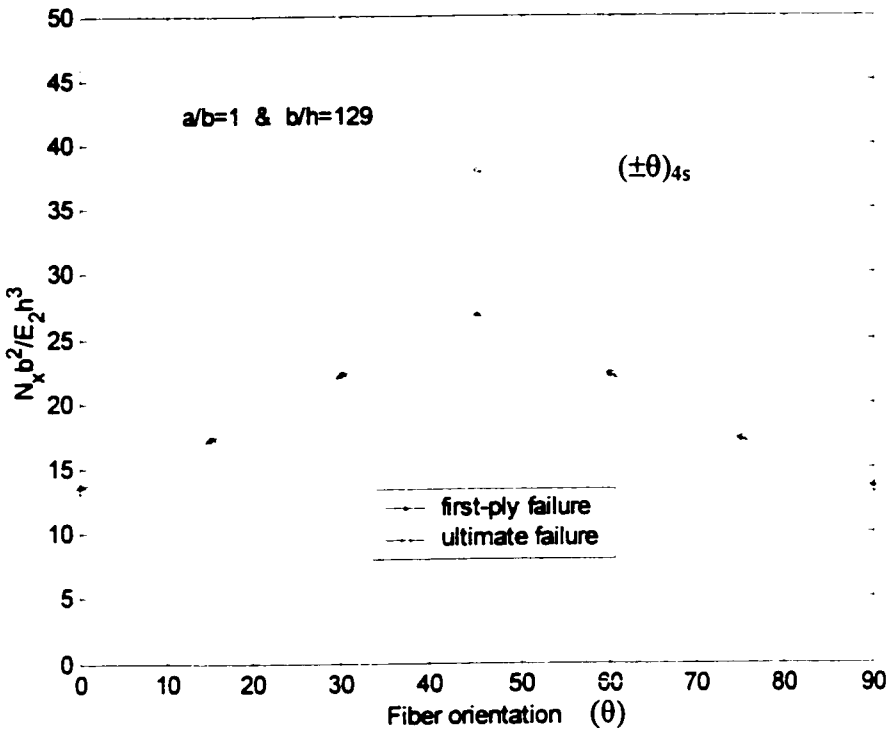

Figure 4-21 Variation of the first-ply failure load and the ultimate failure load of $(\pm\theta)_{4s}$ laminate with fiber orientation under bi-axial compression

Figure 4-22 shows the variation of the central deflection associated with the first-ply failure and that just before the ultimate failure for $(\pm\theta)_{4s}$ laminate. The results predict that the variations in the central deflection are symmetrical about the 45^0 fiber orientation. A peak value corresponding to the first-ply failure load occurs for 45^0 fiber orientation. It is observed that the central deflection associated with the ultimate failure load also has a symmetric pattern in the case of bi-axial compression.

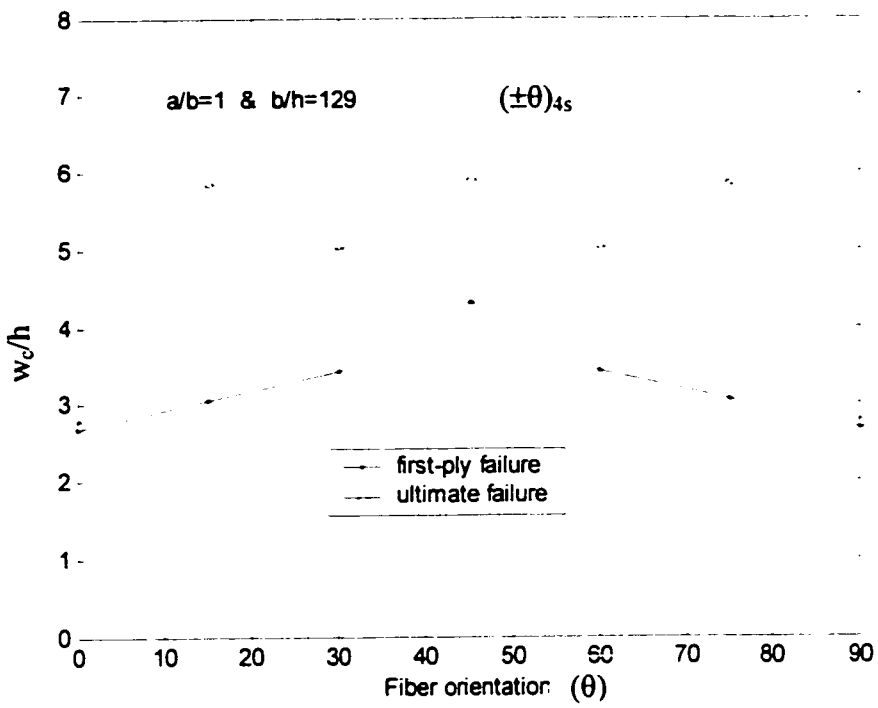

Figure 4-22 Variation of the central deflection associated with the first-ply failure and the ultimate failure of $(\pm\theta)_{4s}$ laminate with fiber orientation under bi-axial compression

Figure 4-23 shows the variation of these loads with aspect ratio values for $(\pm 45/0/90)_{2s}$ laminate. It is seen that the first-ply failure load and the ultimate failure load decrease with an increase in the values of aspect ratio.

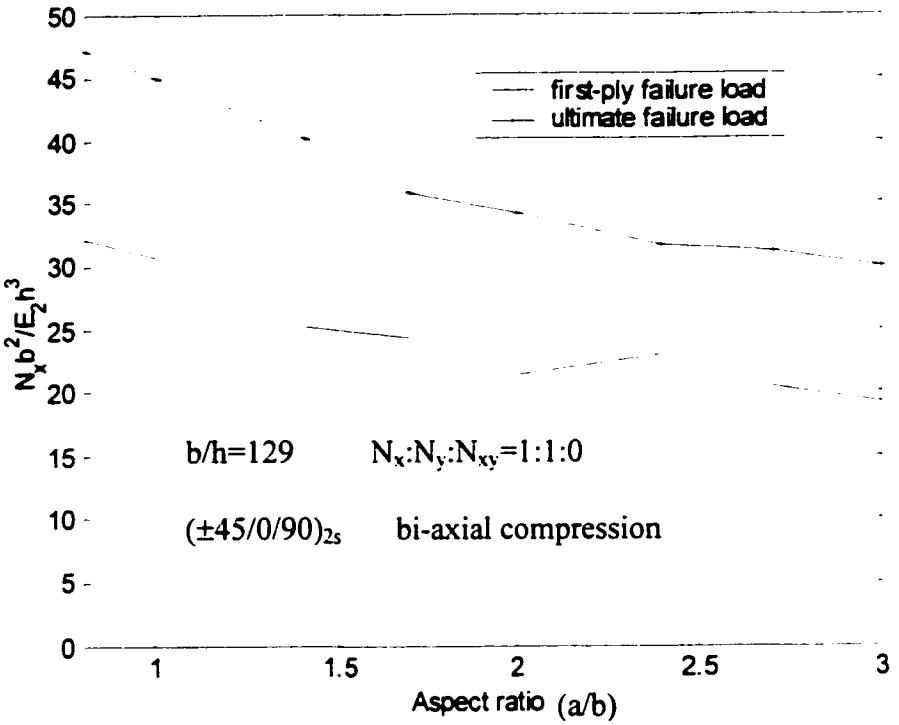

Figure 4-23 Variation of the first-ply failure load and the ultimate failure load of the $(\pm 45/0/90)_{2s}$ laminate with aspect ratio values under bi-axial compression

Figure 4-24 shows the variation of the central deflection associated with the first-ply failure and the ultimate failure, with aspect ratio values for $(\pm 45/0/90)_{2s}$ laminate. It is seen that the central deflection at the first-ply failure and the ultimate failure increase with increasing values of aspect ratio.

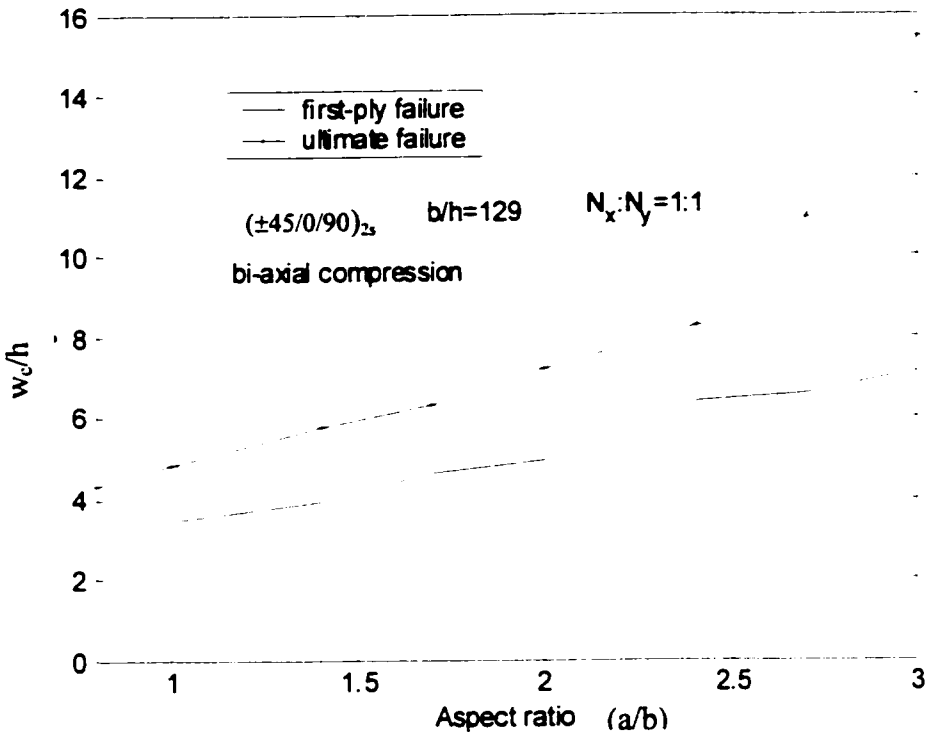

Figure 4-24 Variation of the central deflection of $(\pm 45/0/90)_{2s}$ laminate with aspect ratio values under bi-axial compression

4.4 Failure Under Bi-axial Compression Combined with In-plane Positive Shear

Figure 4-25 shows the load versus the maximum deflection response of various laminates under the action of bi-axial compression combined with in-plane positive shear loading. It is observed that the largest strength is exhibited by $(\pm 45)_{4s}$ laminate within the deflection range $w_{max}/h \leq 0.6$ and by $(\pm 45/0/90)_{2s}$ laminate within the deflection range $w_{max}/h > 0.6$. It is also observed that $(0/90)_{4s}$ laminate shows the least strength for a fixed value of the maximum deflection within the range $w_{max}/h < 1.9$.

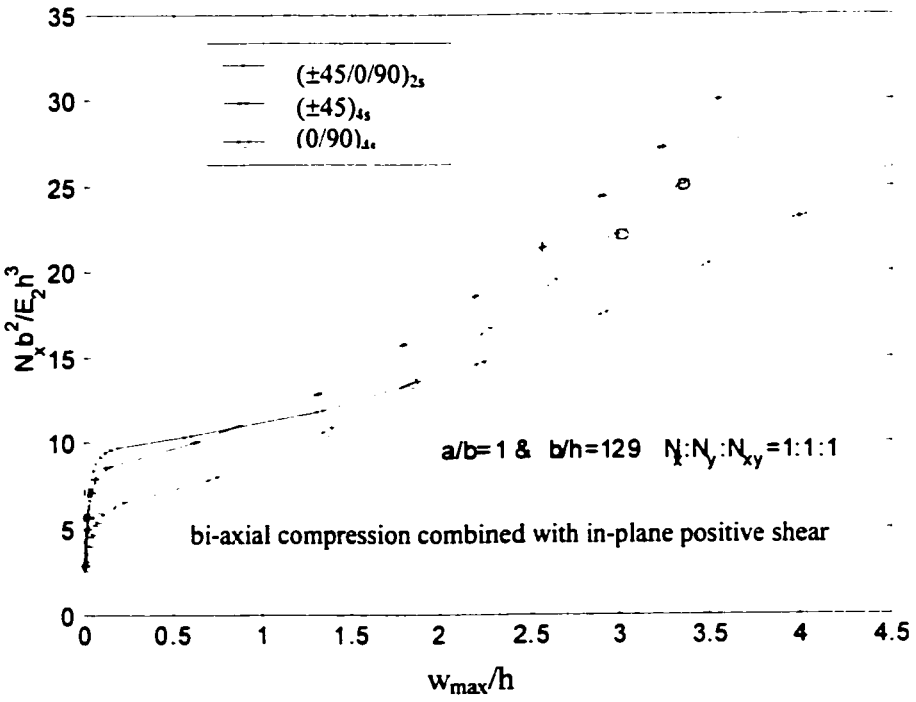

Figure 4-25 Load versus the maximum deflection response of different laminates under bi-axial compression combined with in-plane positive shear

Figure 4-26 shows the load versus the maximum deflection response of $(\pm 45/0/90)_{2s}$ laminate for various aspect ratio values under the action of bi-axial compression combined with in-plane positive shear loading. For a fixed value of the maximum deflection, the highest strength is observed for the aspect ratio of 0.8 while the lowest for the aspect ratio of 3. The failure loads decrease with an increase in the aspect ratio values. The first-ply failure and the ultimate failure of laminates occur at loaded edge primarily (when a/b=3 the first-ply failure occurs in element 24). The first-ply failure is matrix failure while the ultimate failure is caused by the delamination.

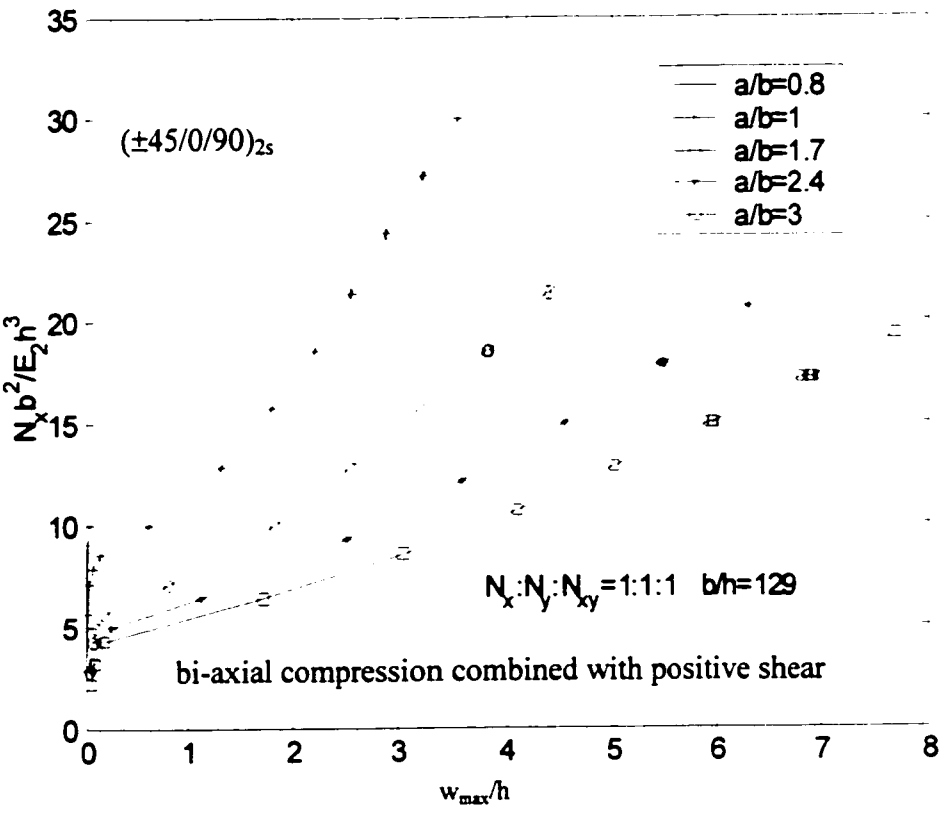

Figure 4-26 Load versus the maximum deflection response of $(\pm 45/0/90)_{2s}$ laminate for various aspect ratio values under bi-axial compression combined with in-plane positive shear

Table 4-7 gives the results for the first-ply failure load and the ultimate failure load of symmetric laminates $(\pm 45/0/90)_{2s}$, $(\pm 45)_{4s}$ and $(0/90)_{4s}$ and unsymmetric laminates $(\pm 45/0/90)_4$, $(\pm 45)_8$ and $(0/90)_8$ under the action of bi-axial compression combined with in-plane positive shear loading. It is seen that for symmetric $(\pm 45/0/90)_{2s}$ and unsymmetric $(\pm 45/0/90)_4$ laminates the ultimate failure loads are almost the same, and the first-ply failure loads are a little different. For the symmetric laminate $(0/90)_{4s}$ and unsymmetric laminate $(0/90)_8$, the first-ply failure load and the ultimate failure load are very close. The first-ply failure mode for all symmetric laminates and unsymmetric laminates is transverse (matrix) failure. Ultimate failure mode for all symmetric laminates and unsymmetric laminates is delamination.

Table 4-7 The first-ply failure loads and the ultimate failure loads for symmetric and unsymmetric laminates under bi-axial compression combined with in-plane positive shear

Lay-up	First-ply failure load ($N_x b^2/E_2 h^3$)	Ultimate failure load ($N_x b^2/E_2 h^3$)	w_{max}/h*	Failure location (FL,FE)♣	First-ply failure mode	Ultimate failure mode
$(\pm 45/0/90)_{2s}$	21.46	30.04	2.562	1,1	Transverse♠	delamination
$(\pm 45/0/90)_{4s}$	24.32	30.04	2.929	1,1	Transverse	delamination
$(\pm 45)_{4s}$	20.38	26.11	3.478	16,25	Transverse	delamination
$(\pm 45)_8$	22.89	25.75	3.900	1,20	Transverse	delamination
$(0/90)_{4s}$	22.17	27.89	3.005	1,1	Transverse	delamination
$(0/90)_8$	22.17	27.89	3.010	1,1	Transverse	delamination

*Non–dimensionalized maximum deflection at first-ply failure

♠Transverse mode of failure refers to the matrix failure

♣EL and FE are the failed layer number and the failed element number at first-ply failure

Table 4-8 gives the progressive failure analysis results for $(\pm 45/0/90)_{2s}$ laminate for various load ratio values ($N_x : N_y : N_{xy}$) in terms of the non-dimensionalized first-ply failure load, ultimate failure load and maximum deflection under the bi-axial compression combined with in-plane positive shear loading. The ratio of N_x and N_y is set to a value of 1, and the value of N_{xy} is changed. In addition, the first-ply failure locations (i.e. the failed ply number and the failed element number) and failure mode related to the first-ply failure and the ultimate failure are also shown in this table. It is observed that with increasing proportion of in-plane positive shear in the combined loading, the first-ply failure load and the ultimate failure load are not changed too much. It is observed that the first-ply failure is matrix failure and the ultimate failure is delamination in all cases.

Table 4-8 Progressive failure of $(\pm 45/0/90)_{2s}$ laminate at various load ratio values under bi-axial compression combined with in-plane positive shear

Load ratio $N_x:N_y:N_{xy}$	First-ply failure load $(N_x b^2/E_2 h^3)$	Ultimate failure load $(N_x b^2/E_2 h^3)$	w_{max}/h^*	Failure location (FL,FE)♣	First-ply failure mode	Ultimate failure mode
1:1:0.2	27.89	33.61	3.284	1,25	Transverse♠	Delamination
1:1:0.4	27.89	33.61	3.277	1,1	Transverse	Delamination
1:1:0.6	25.03	30.75	2.927	1,25	Transverse	Delamination
1:1:0.8	25.03	30.75	2.941	1,1	Transverse	Delamination
1:1:1	21.45	30.04	2.562	1,1	Transverse	Delamination

*Non–dimensionalized maximum deflection at first-ply failure

♣FL and FE are the failed layer number andthe failed element number at first-ply failure

♠Transverse mode of failure refers to the matrix failure

Figure 4-27 (a), (b) and (c) show the load versus the maximum deflection response of $(\pm 45/0/90)_{2s}$ laminate for different load ratio values $N_x : N_y : N_{xy}$ ($N_x : N_y = 1 : 1$, change N_{xy} values) under the action of bi-axial compression combined with in-plane positive shear loading.

Table 4-9 gives the progressive failure analysis results for $(\pm 45/0/90)_{2s}$ laminate for various load ratio values ($N_x : N_y : N_{xy}$) in terms of the non-dimensionalized first-ply failure load, ultimate failure load and maximum deflection under the action of bi-axial compression combined with in-plane positive shear loading. Here, the value of N_{xy} is fixed, and the values of N_x and N_y are changed with 1:1 ratio. In addition, the first-ply failure locations (i.e. the failed ply number and the failed element number) and failure modes related to the first-ply failure and the ultimate failure are also shown in this table. It is observed that with increasing proportion of bi-axial compression in the combined loading, the first-ply failure load and the ultimate failure load decrease monotonically. At $N_x : N_y : N_{xy} = 1 : 1 : 1$, the percentage loss (compared to the case $N_x : N_y : N_{xy} = 0.2 : 0.2 : 1$) in the first-ply failure and the ultimate failure loads are respectively, 48.2 and 53.3. It is observed that the first-ply failure is matrix failure and the ultimate failure is delamination in all cases.

Figure 4-28 shows the load versus the maximum deflection response of $(\pm 45/0/90)_{2s}$ laminate for different load ratio values $N_x : N_y : N_{xy}$ ($N_{xy} = 1$, change N_x and N_y values) under the action of bi-axial compression combined with in-plane positive shear loading. It is seen that the first-ply failure load and the ultimate failure load decrease with an increase of load ratio values (N_x, N_y).

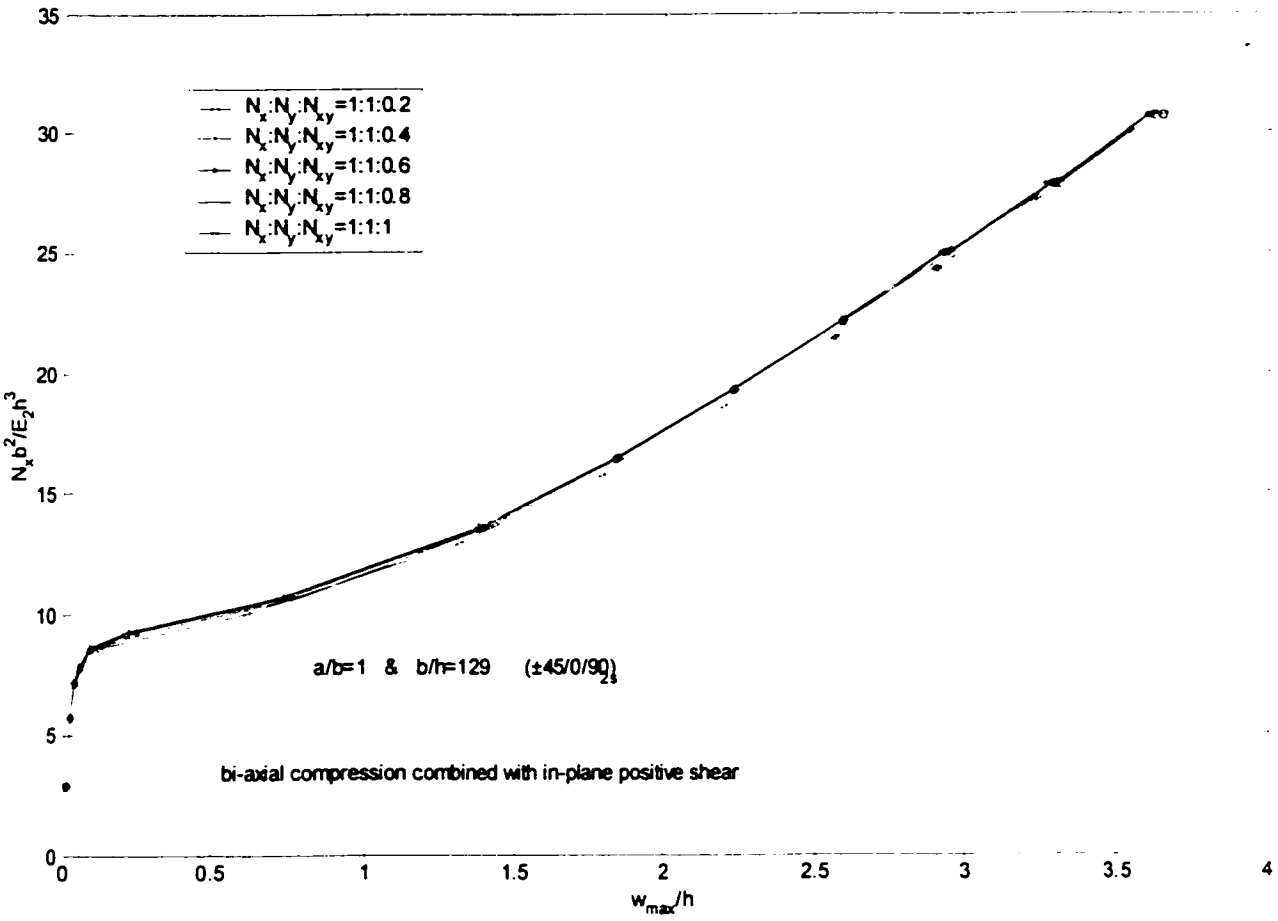

Figure 4-27 (a) Load versus the maximum deflection response of $(\pm 45/0/90)_{2s}$ laminate for different load ratio values of bi-axial compression combined with in-plane positive shear

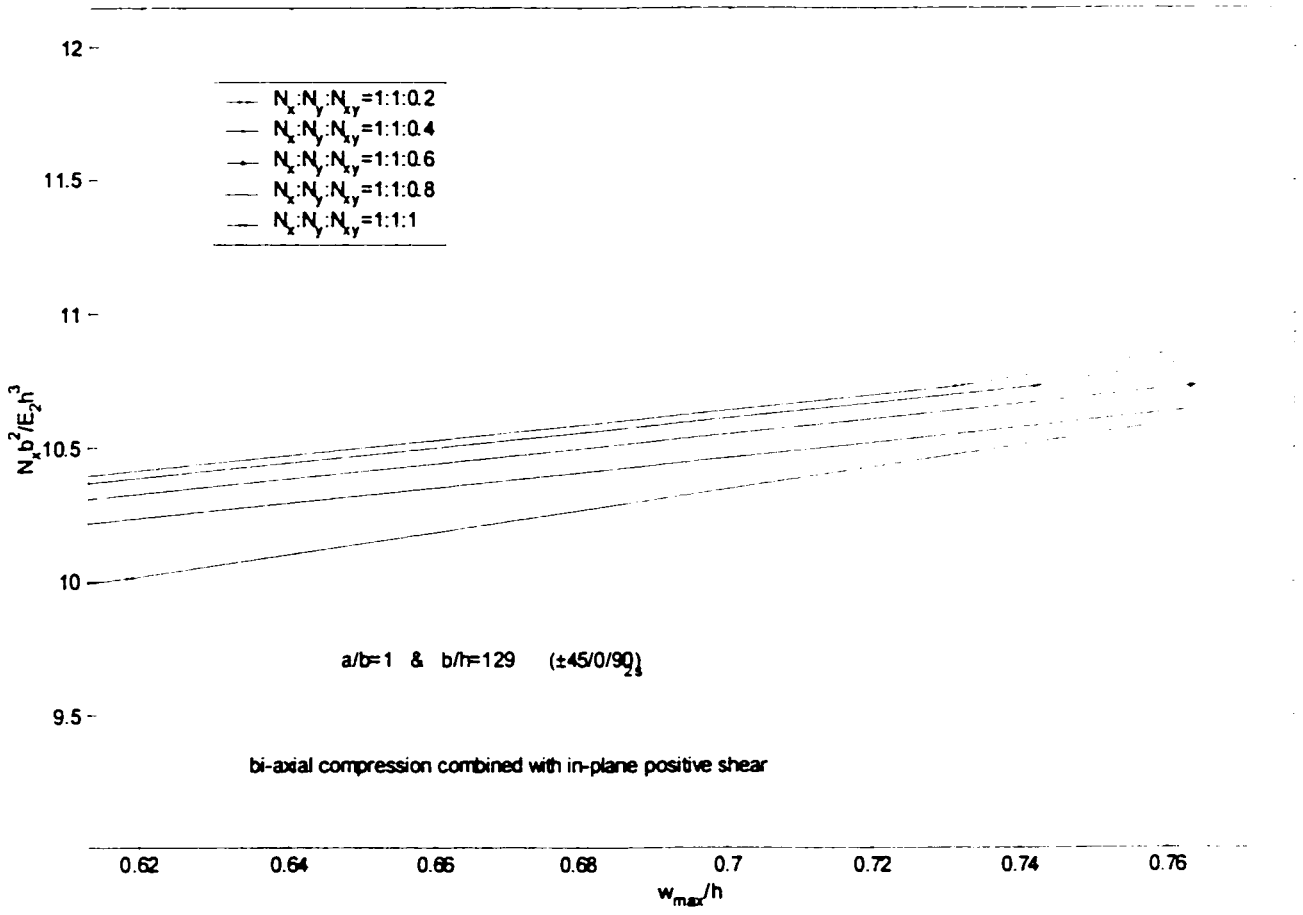

Figure 4-27 (b) Load versus the maximum deflection response of $(\pm 45/0/90)_{2s}$ laminate for different load ratio values of bi-axial compression combined with in-plane positive shear

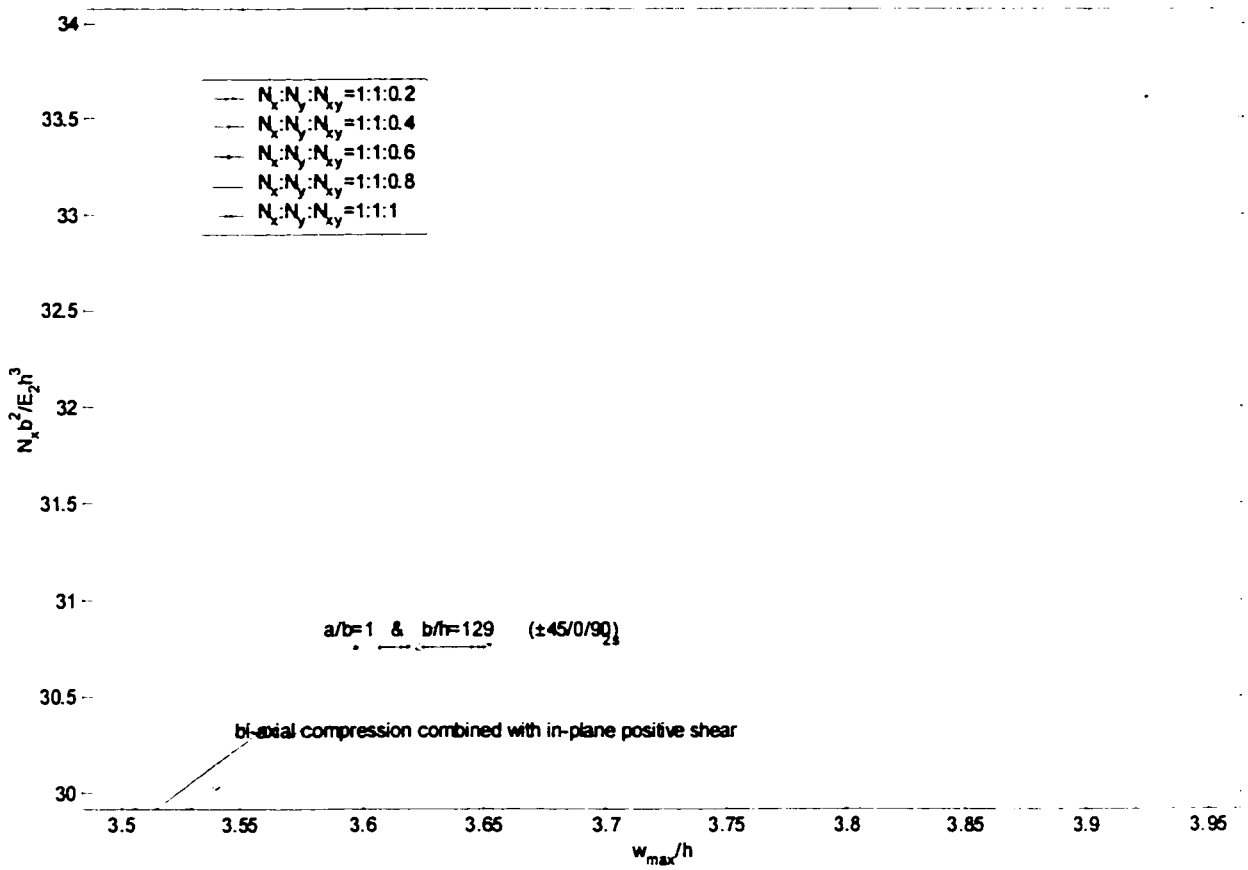

Figure 4-27 (c) Load versus the maximum deflection response of $(\pm 45/0/90)_{2s}$ laminate for different load ratio values of bi-axial compression combined with in-plane positive shear

Table 4-9 Progressive failure of $(\pm 45/0/90)_{2s}$ laminate at various load ratio values under bi-axial compression combined with in-plane positive shear

Load ratio N_x: N_y: N_{xy}	First-ply failure load ($N_x b^2/E_2 h^3$)	Ultimate failure load ($N_x b^2/E_2 h^3$)	(w_{max}/h)*	Failure location (FL,FE)♣	First-ply failure mode	Ultimate failure mode
0.2:0.2:1	41.48	64.37	1.4876	1,1	Transverse♠	Delamination
0.4:0.4:1	35.76	52.92	2.003	1,1	Transverse	Delamination
0.6:0.6:1	29.32	43.63	2.239	1,1	Transverse	Delamination
0.8:0.8:1	26.46	35.04	2.585	1,1	Transverse	Delamination
1:1:1	21.45	30.04	2.562	1,1	Transverse	Delamination

*Non–dimensionalized maximum deflection at first-ply failure

♣FL and FE are the failed layer number and the failed element number at first-ply failure

♠Transverse mode of failure refers to the matrix failure

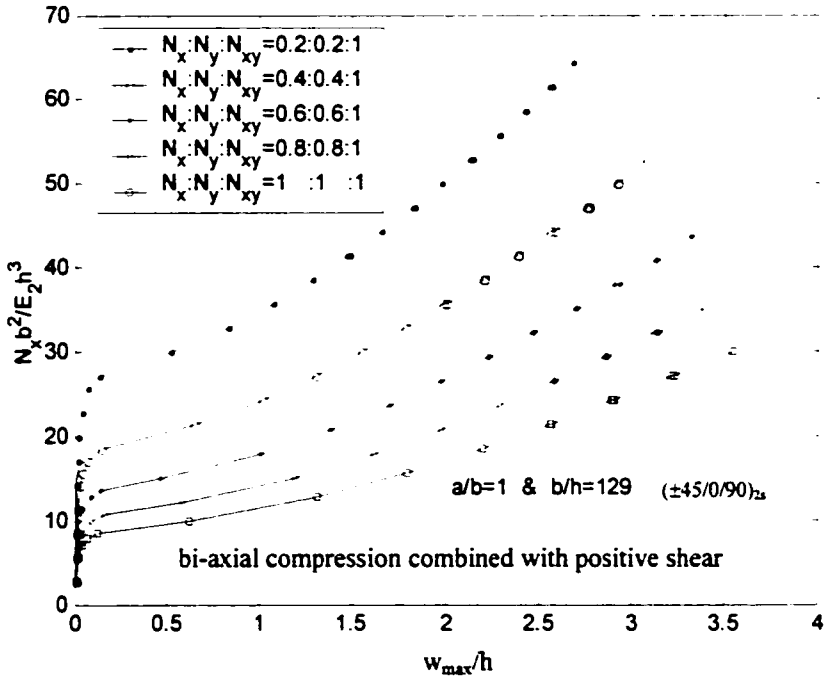

Figure 4-28 Load versus the maximum deflection response of $(\pm 45/0/90)_{2s}$ laminate for different load ratio values of bi-axial compression combined with in-plane positive shear

Table 4-10 gives the progressive failure analysis results for $(\pm 45/0/90)_{2s}$ laminate for various load ratio values ($N_x : N_y : N_{xy}$) in terms of non-dimensionalized first-ply failure load, ultimate failure load and maximum deflection under the action of bi-axial compression combined with in-plane positive shear loading. The ratio of N_{xy} and N_y is set to a value of 1, and the value of N_x is changed. In addition, the first-ply failure locations (i.e. the failed ply number and the failed element number) and the failure mode related to the first-ply failure and the ultimate failure are also shown in this table. It is observed that with increasing proportion of compression in the combined loading, the first-ply failure load and the ultimate failure load decrease monotonically. At $N_x : N_y : N_{xy} = 1 : 1 : 1$, the percentage loss (compared to the case $N_x : N_y : N_{xy} = 0.2 : 1 : 1$) in the first-ply failure load and the ultimate failure load are respectively, 26.8 and 31.2. It is observed that the first-ply failure is matrix failure and the ultimate failure is delamination in all cases.

Table 4-10 Progressive failure of $(\pm 45/0/90)_{2s}$ laminate at various load ratio values under bi-axial compression combined with in-plane positive shear

Load ratio N_x: N_y: N_{xy}	First-ply failure load ($N_x b^2/E_2 h^3$)	Ultimate failure load ($N_x b^2/E_2 h^3$)	(w_{max}/h)*	Failure location (FL,FE)♣	First-ply failure mode	Ultimate failure mode
0.2:1:1	29.32	43.63	2.242	1,1	Transverse♠	Delamination
0.4:1:1	27.89	39.34	2.431	1,1	Transverse	Delamination
0.6:1:1	26.46	35.04	2.586	1,1	Transverse	Delamination
0.8:1:1	22.88	31.47	2.483	1,1	Transverse	Delamination
1:1:1	21.45	30.03	2.562	1,1	Transverse	Delamination

*Non–dimensionalized maximum deflection at first-ply failure

♣FL and FE are the failed layer and the failed element number at first-ply failure

♠Transverse mode of failure refers to the matrix failure

Figure 4-29 shows the load versus the maximum deflection response of $(\pm 45/0/90)_{2s}$ laminate for different load ratio values $N_x : N_y : N_{xy}$ ($N_{xy} = N_y = 1$; change N_x values) under the action of bi-axial compression combined with in-plane positive shear loading. It is seen that the first-ply failure load and the ultimate failure load decrease with increase in the load ratio values (N_x).

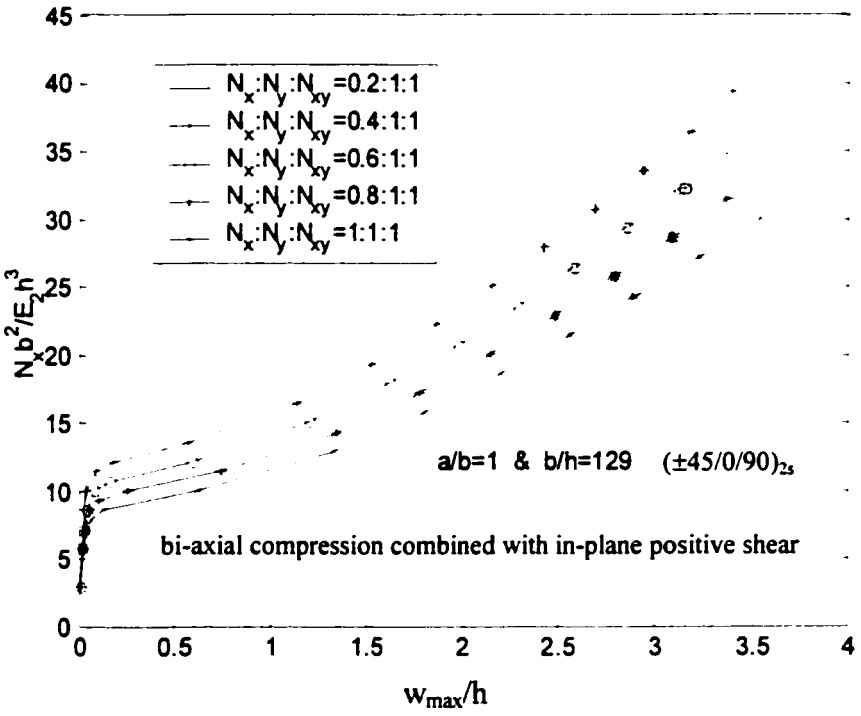

Figure 4-29 Load versus the maximum deflection response of $(\pm 45/0/90)_{2s}$ laminate for different load ratio values of bi-axial compression combined with in-plane positive shear

Figure 4-30 shows the variation of the first-ply failure load and the ultimate load of $(\pm\theta)_{4s}$ laminates with fiber orientation (θ) under the action of bi-axial compression combined with in-plane positive shear loading. The results show that the variation in response are

symmetric with respect to 45^0 fiber orientation. Peak values of the first-ply failure load and the ultimate failure load are predicted to occur for 45^0 orientation. For $(0/0)_{4s}$ and $(\pm 15)_{4s}$ laminates the first-ply failure loads also are the ultimate failure loads.

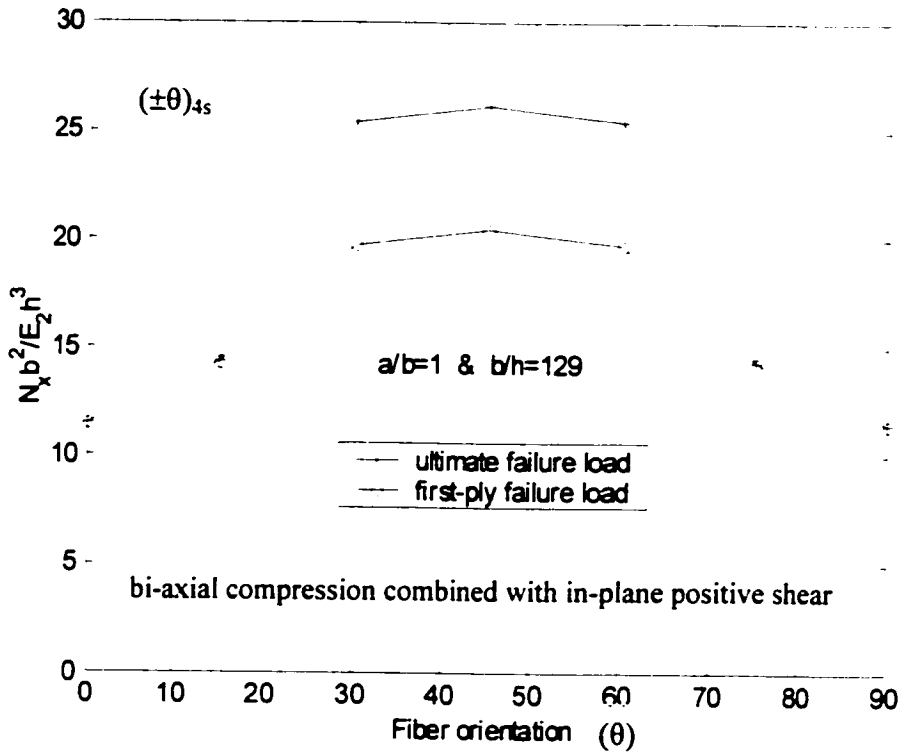

Figure 4-30 Variation of the first-ply failure load and the ultimate load of $(\pm\theta)_{4s}$ laminate with fiber orientation under bi-axial compression combined with in-plane positive shear

Figure 4-31 shows the variation of the maximum deflection associated with the first-ply failure and that just before the ultimate failure for $(\pm\theta)_{4s}$ laminate. The results predict that the variations in the maximum deflection are symmetrical about the 45^0 fiber orientation. A peak value corresponding to the first-ply failure load occurs for 45^0 fiber orientation. It

is observed that the maximum deflection associated with the ultimate load has symmetric pattern in the case of bi-axial compression combined with in-plane positive shear loading.

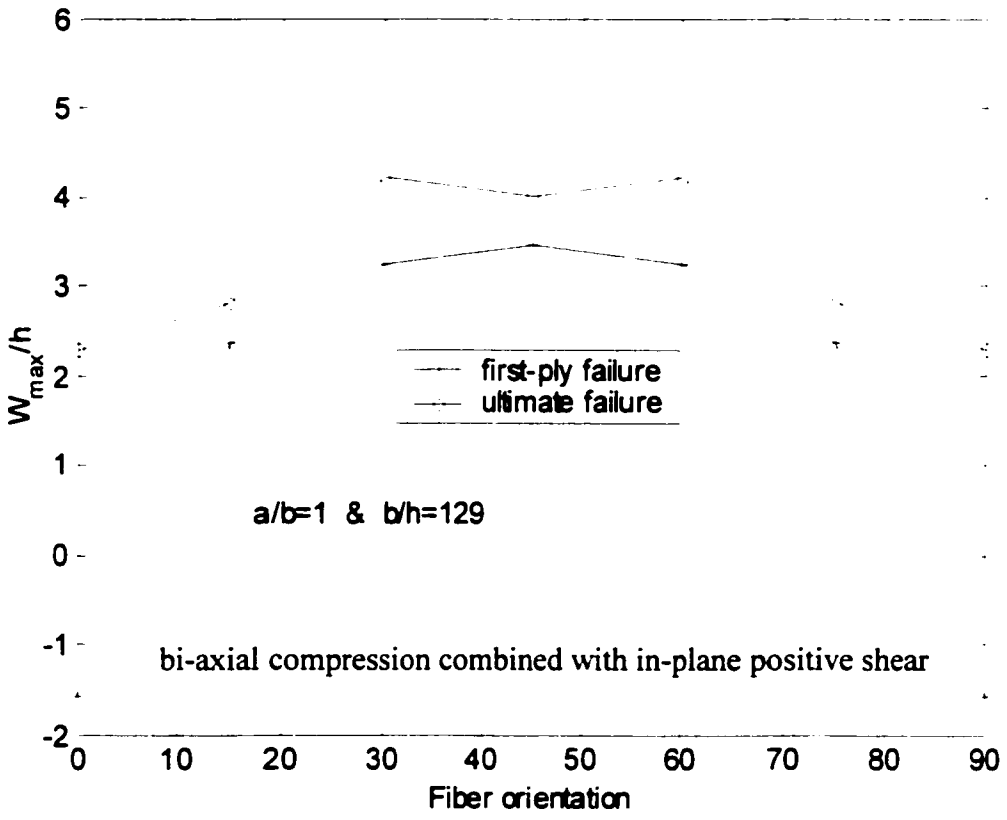

Figure 4-31 Variation of the maximum deflection associated with the first-ply failure load and the ultimate load of $(\pm\theta)_{4s}$ laminate with fiber orientation under bi-axial compression combined with in-plane positive shear

Figure 4-32 shows the variation of these loads with aspect ratio values for $(\pm 45/0/90)_{2s}$ laminate. It is seen that the first-ply failure load and the ultimate failure load decrease with an increase in the values of aspect ratio.

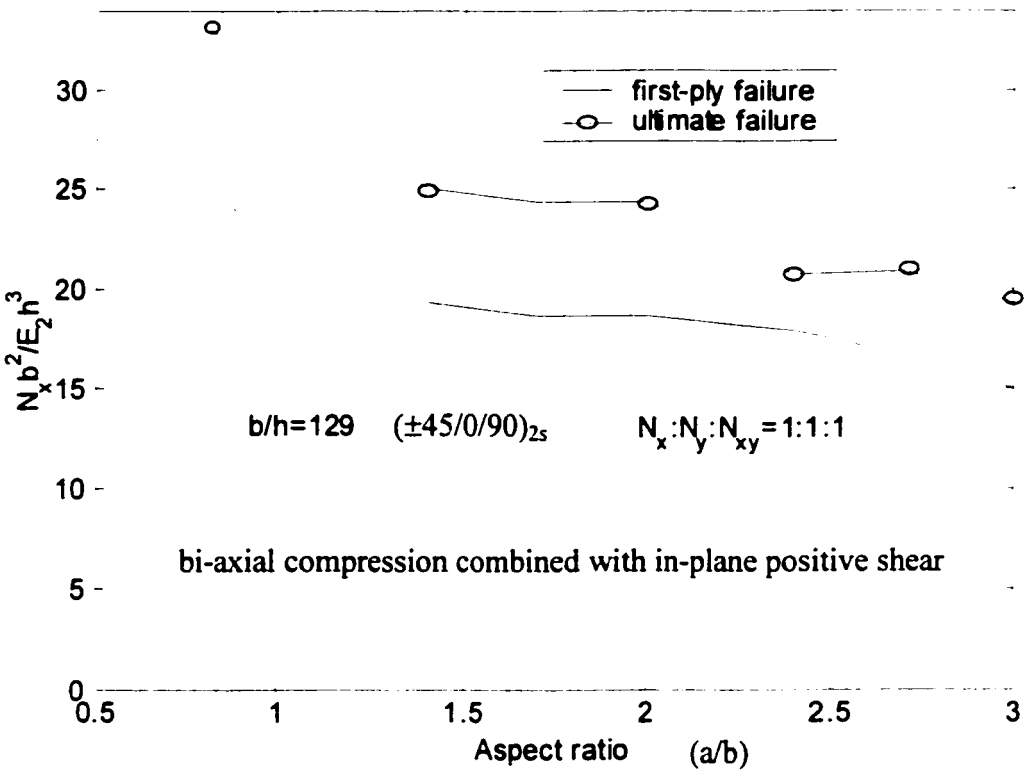

Figure 4-32 Variation of the first-ply failure load and the ultimate load of $(\pm 45/0/90)_{2s}$ laminate with aspect ratio values under bi-axial compression combined with in-plane positive shear

Figure 4-33 shows the variation of the maximum deflection associated with the first-ply failure and the ultimate failure, with aspect ratio values for $(\pm 45/0/90)_{2s}$ laminate under the action of bi-axial compression combined with in-plane positive shear loading.

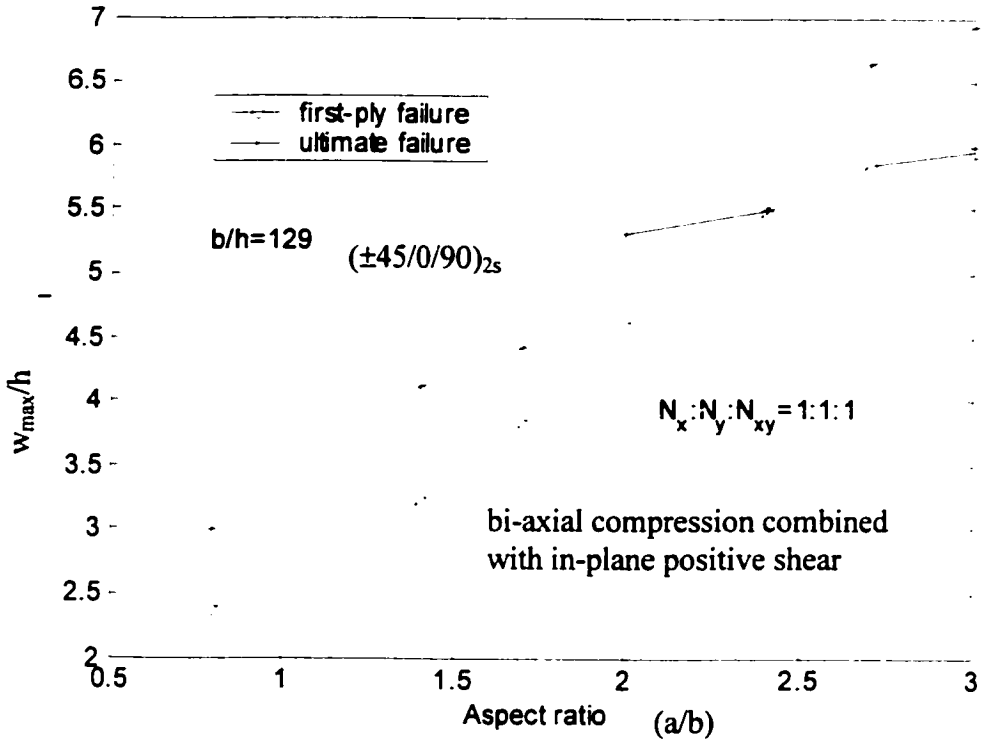

Figure 4-33 Variation of the maximum deflection of $(\pm 45/0/90)_{2s}$ laminate with aspect ratio values under bi-axial compression combined with in-plane positive shear

4.5 Failure Under Bi-axial Compression Combined with In-plane Negative Shear

Figure 4-34 shows load versus the maximum deflection response of various laminates under the action of bi-axial compression combined with in-plane negative shear loading. It is observed that the largest strength is exhibited by $(\pm 45)_{4s}$ laminate within the deflection range $w_{max}/h \leq 1.6$ and by $(\pm 45/0/90)_{2s}$ laminate within the deflection range $w_{max}/h > 1.6$. It is also observed that $(0/90)_{4s}$ laminate shows the least strength for a fixed value of the maximum deflection within the range $w_{max}/h < 3.7$.

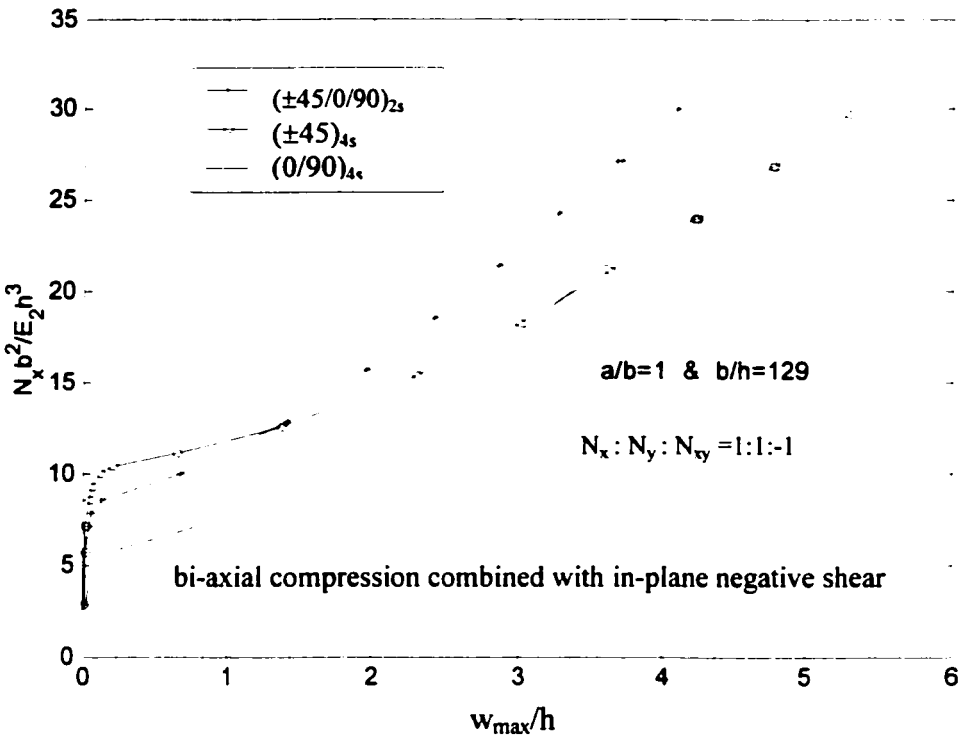

Figure 4-34 Load versus the maximum deflection response of different laminates under bi-axial compression combined with in-plane negative shear

Figure 4-35 shows the load versus the maximum deflection response of $(\pm 45/0/90)_{2s}$ laminate for various aspect ratio values under the action of bi-axial compression combined with in-plane negative shear loading. For a fixed value of the maximum deflection, the highest strength is observed for the aspect ratio of 0.8 while the lowest for aspect ratio of 3. The failure loads decrease with an increase in the aspect ratio values. The first-ply failure is matrix failure while the ultimate failure is caused by the delamination.

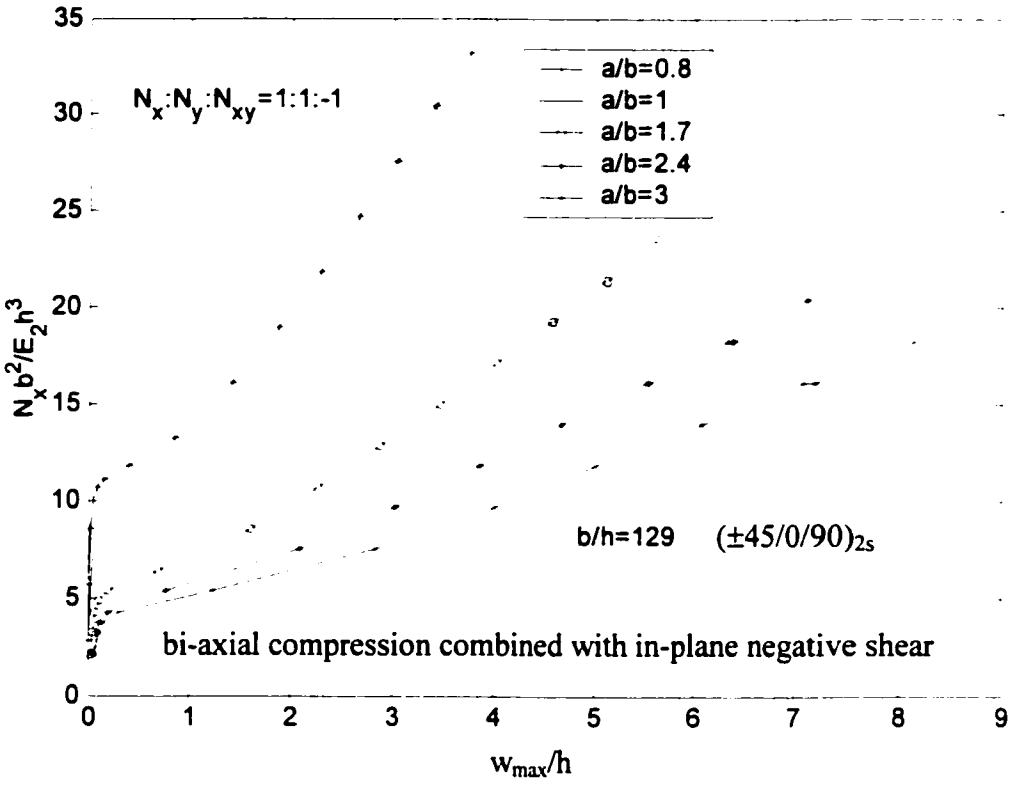

Figure 4-35 Load versus the maximum deflection response of $(\pm 45/0/90)_{2s}$ laminate for various aspect ratio values under bi-axial compression combined with in-plane negative shear

Table 4-11 gives the results for the first-ply failure load and the ultimate failure load of symmetic laminates $(\pm 45/0/90)_{2s}$, $(\pm 45)_{4s}$ and $(0/90)_{4s}$ and unsymmetric laminates $(\pm 45/0/90)_4$, $(\pm 45)_8$ and $(0/90)_8$ under the action of bi-axial compression combined with in-plane negative shear loading. It is seen that for symmetric and unsymmetric laminates, the first-ply failure load and the ultimate failure load are a little different. The first-ply failure mode for all symmetric laminates and unsymmetric laminates is transverse (matrix) failure. The ultimate failure mode for all symmetric laminates and unsymmetric

laminates is delamination. The first-ply failures in all cases occur at the loaded edge. For unsymmetric $(\pm 45/0/90)_4$ and $(\pm 45)_8$ laminates, the maximum deflection values are negative.

Table 4-11 The first-ply failure loads and the ultimate failure loads for symmetric and unsymmetric laminates under bi-axial compression combined with in-plane negative shear

Lay-up	First-ply failure load ($N_x b^2/E_2 h^3$)	Ultimate failure load ($N_x b^2/E_2 h^3$)	(w_{max}/h)*	Failure location (FL,FE)♣	First-ply failure mode	Ultimate failure mode
$(\pm 45/0/90)_{2s}$	24.32	30.04	3.288	2,21	Transverse♠	delamination
$(\pm 45/0/90)_4$	22.89	28.61	-3.410	1,5	Transverse	delamination
$(\pm 45)_{4s}$	23.96	29.68	4.218	2,5	Transverse	delamination
$(\pm 45)_8$	21.46	27.18	-3.889	2,5	Transverse	delamination
$(0/90)_{4s}$	18.59	24.32	3.143	16,21	Transverse	delamination
$(0/90)_8$	19.85	24.14	3.334	16,5	Transverse	delamination

*Non–dimensionalized maximum deflection at first-ply failure

♠Transverse mode of failure refers to the matrix failure

♣FL and FE are the failed layer and the failed element number at first-ply failure

Figure 4-36 shows the load versus the maximum deflection response of various symmetric laminates $(\pm 45/0/90)_{2s}$, $(\pm 45)_{4s}$ and $(0/90)_{4s}$ and unsymmetric laminates $(\pm 45/0/90)_4$, $(\pm 45)_8$ and $(0/90)_8$ under the action of bi-axial compression combined with in-plane negative shear loading. It is observed that for symmetric laminate $(0/90)_{4s}$, the load-maximum deflection curve almost coincides with the load-maximum deflection curve of unsymmetric laminate $(0/90)_8$. However, the maximum deflection of

$(\pm 45/0/90)_{2s}$ laminate and $(\pm 45)_{4s}$ laminate are positive while the maximum deflection of $(\pm 45/0/90)_4$ laminate and $(\pm 45)_8$ laminate are negative.

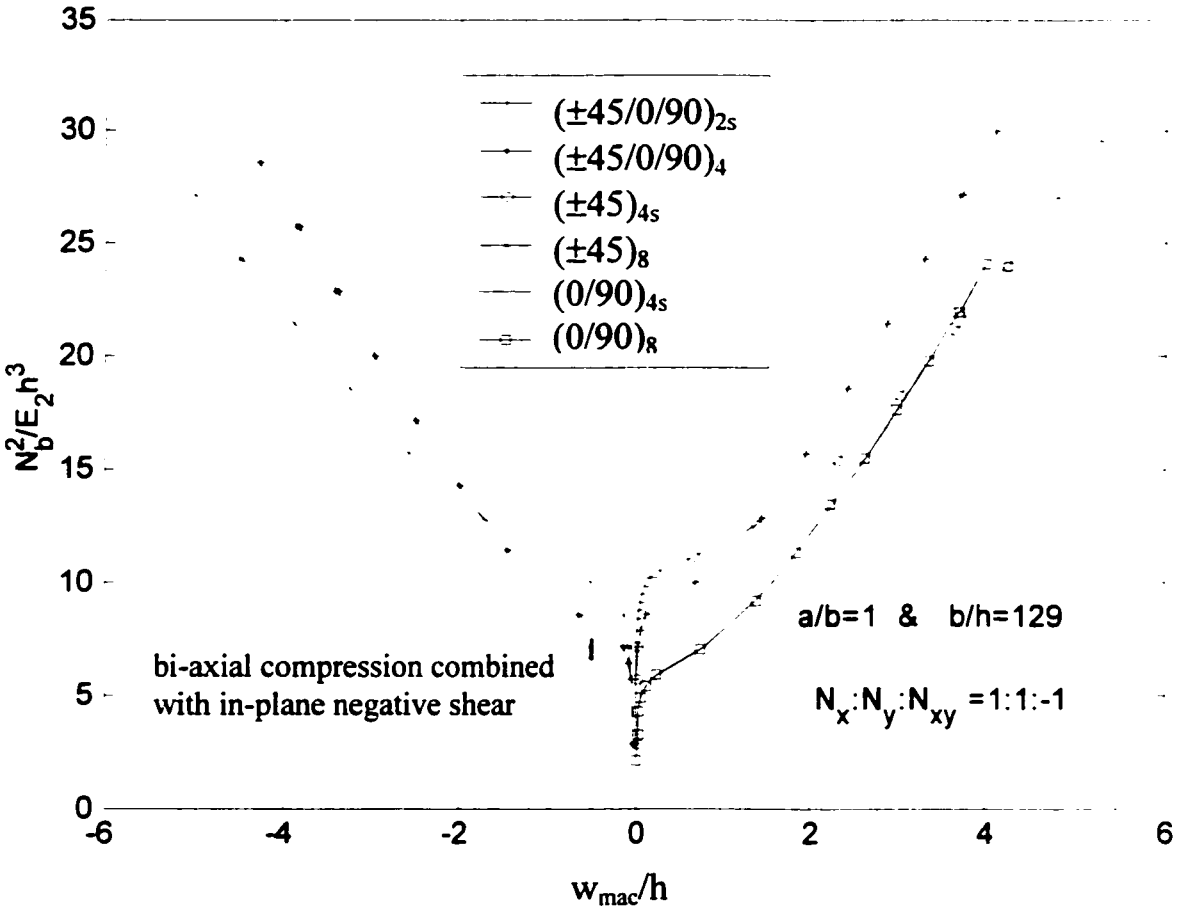

Figure 4-36 Progressive failure of symmetric and unsymmetric laminates under bi-axial compression combined with in-plane negative shear

Table 4-12 gives the progressive failure analysis results for $(\pm 45/0/90)_{2s}$ laminate for various load ratio values ($N_x : N_y : N_{xy}$) in terms of non-dimensionalized first-ply failure load, ultimate failure load and maximum deflection under the action of bi-axial

compression combined with in-plane negative shear loading. The ratio of N_x and N_y is set to a value of 1, and the value of N_{xy} is changed. In addition, the first-ply failure locations (i.e. the failed ply number and the failed element number) and the failure modes related to the first-ply failure and the ultimate failure are also shown in this table. It is observed that with increasing proportion of in-plane negative shear in the combined loading, the first-ply failure load and the ultimate failure load are not changed too much. It is observed that the first-ply failure is matrix failure and the ultimate failure is delamination in all cases.

Table 4-12 Progressive failure of $(\pm 45/0/90)_{2s}$ laminate at various load ratio values under bi-axial compression combined with in-plane negative shear

Load ratio N_x:N_y:N_{xy}	First-ply failur load ($N_x b^2/E_2 h^3$)	Ultimate failure load ($N_x b^2/E_2 h^3$)	(w_{max}/h)*	Failure location (FL,FE) ♣	First-ply failure mode	Ultimate failure mode
1:1:-0.2	27.89	33.61	3.399	1,25	Transverse♠	Delamination
1:1:-0.4	27.89	36.47	3.469	1,25	Transverse	Delamination
1:1:-0.6	27.36	33.79	3.493	2,21	Transverse	Delamination
1: 1:-0.8	27.89	33.62	3.684	2,5	Transverse	Delamination
1:1:-1	24.31	30.04	3.288	2,21	Transverse	Delamination

*Non–dimensionalized maximum deflection at first-ply failure

♣ FL and FE are the failed layer number and the failed element number at first-ply

♠Transverse mode of failure refers to the matrix failure

Figure 4-37 shows the load versus the maximum deflection response of $(\pm 45/0/90)_{2s}$ laminate for different load ratio values $N_x : N_y : N_{xy}$ ($N_x : N_y = 1$, change N_{xy} values) under the action of bi-axial compression combined with in-plane negative shear loading.

Table 4-13 gives the progressive failure analysis results for (+ -45/0/90)$_{2s}$ laminate for various load ratio values (N_x : N_y : N_{xy}) in terms of non-dimensionalized first-ply failure load, ultimate failure load and maximum deflection under the action of bi-axial compression combined with in-plane negative shear loading. Here, the value of N_{xy} is fixed, and the values N_x and N_y are changed with 1:1 ratio. In addition, the first-ply failure locations (i.e. the failed ply number and the failed element number) and the failure modes related to the first-ply failure and the ultimate failure are also shown in this table. It is observed that with increasing proportion of compressions in the combined loading, the first-ply failure load and the ultimate failure load decrease monotonically. At N_x : N_y : N_{xy} = 1 : 1 : -1, the percentage loss (compared to the case N_x : N_y : N_{xy} = 0.2 : 0.2 : -1) in

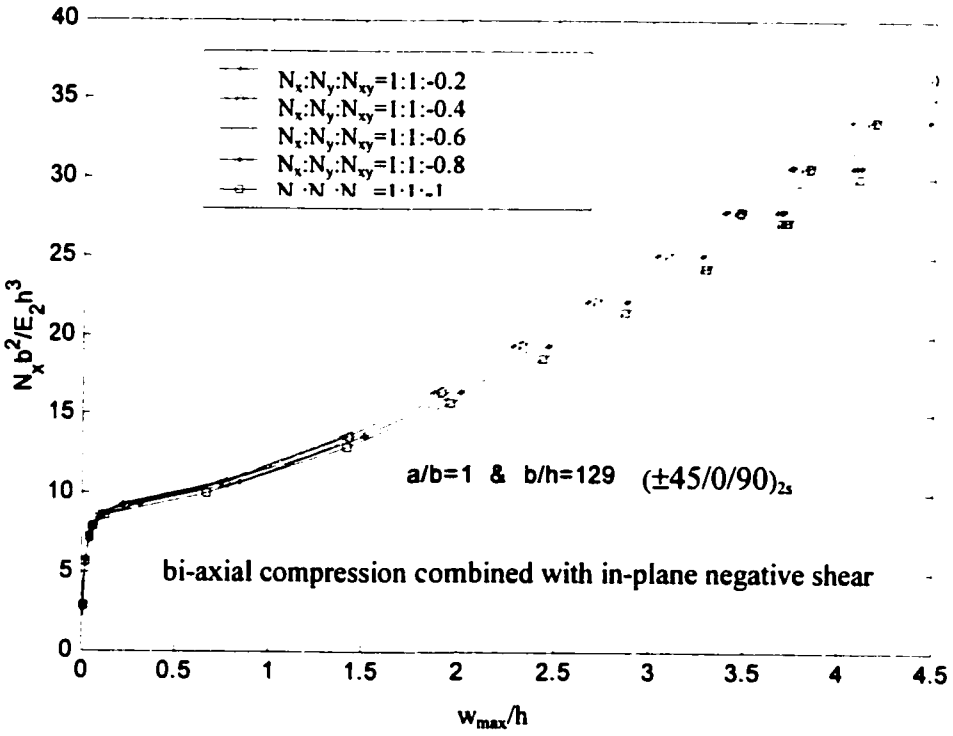

Figure 4-37 Load versus the maximum deflection response of (±45/0/90)$_{2s}$ laminate for different load ratio values of bi-axial compression combined with in-plane negative shear

the first-ply failure and the ultimate failure load are respectively, 57.5 and 43.75. It is observed that the first-ply failure is matrix failure and the ultimate failure is delamination in all cases.

Table 4-13 Progressive failure of the $(\pm 45/0/90)_{2s}$ laminate at various load ratio values under bi-axial compression combined with in-plane negative shear

Load ratio $N_x:N_y:N_{xy}$	First-ply failure load $(N_x b^2/E_2h^3)$	Ultimate failure load $(N_x b^2/E_2h^3)$	(w_{max}/h)*	Failure location (FL,FE)♣	First-ply failure mode	Ultimate failure mode
0.2:0.2:-1	57.22	68.66	3.844	2,5	Transverse♠	Delamination
0.4:0.4:-1	44.34	52.92	3.023	2,5	Transverse	Delamination
0.6:0.6:-1	35.04	43.63	3.161	2,5	Transverse	Delamination
0.8:0.8:-1	29.32	35.04	3.308	2,5	Transverse	Delamination
1:1:-1	24.32	30.04	3.288	2,21	Transverse	Delamination

*Non–dimensionalized maximum deflection at first-ply failure

♣FL and FE are the failed layer number and the failed element number at first-ply failure

♠Transverse mode of failure refers to the matrix failure

Figure 4-38 shows the load versus the maximum deflection response of $(\pm 45/0/90)_{2s}$ laminate for different load ratio values $N_x : N_y : N_{xy}$ (N_{xy} = -1, change N_x and N_y values) under the action of bi-axial compression combined with in-plane negative shear loading. It is seen that the first-ply failure load and the ultimate failure load decrease with increasing load ratio values (N_x, N_y).

Table 4-14 gives the progressive failure analysis results for $(\pm 45/0/90)_{2s}$ laminate for various load ratio values ($N_x : N_y : N_{xy}$) in terms of non-dimensionalized first-ply failure

load, ultimate failure load and maximum deflection under the bi-axial compression combined with in-plane negative shear loading. The ratio of N_{xy} and N_y is set to a value of 1, and the value of N_x is changed. In addition, the first-ply failure locations (i.e. the failed ply number and the failed element number) and the failure modes related to the first-ply failure and the ultimate failure are also shown in this table. It is observed that with increasing proportion of compressions in the combined loading, the first-ply failure load and the ultimate failure load decrease monotonically. At N_x: N_y : N_{xy} = 1 : 1 : -1, the percentage loss (compared to the case N_x : N_y : N_{xy} = 0.2 : 1 : -1) in the first-ply failure and the ultimate failure loads is respectively, 24.4 and 26.3.

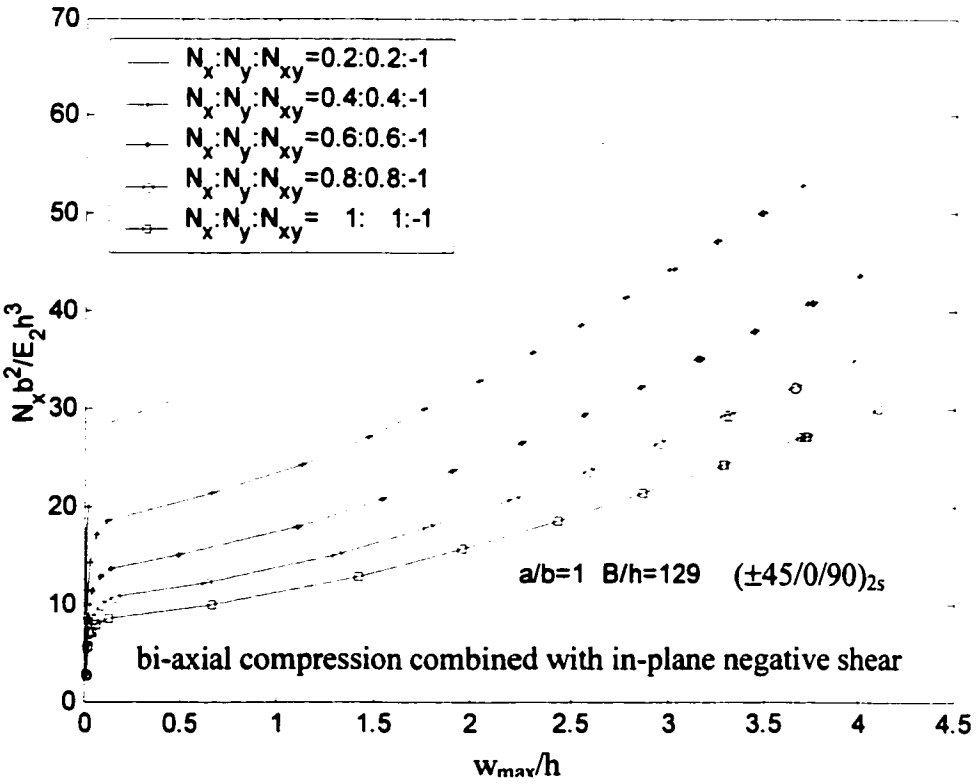

Figure 4-38 Load versus the maximum deflection response of $(\pm 45/0/90)_{2s}$ laminate for different load ratio values of bi-axial compression combined with in-plane negative shear

Table 4-14 Progressive failure of $(\pm 45/0/90)_{2s}$ laminate at various load ratio values under bi-axial compression combined with in-plane negative shear

Load ratio $N_x:N_y:N_{xy}$	First-ply failure load $(N_x b^2/E_2 h^3)$	Ultimate Failure load $(N_x b^2/E_2 h^3)$	$(w_{max}/h)^*$	Failure location (FL,FE)$^\clubsuit$	First-ply failure mode	Ultimate failure mode
0.2:1:-1	32.18	40.77	2.923	2,21	Transverse$^\clubsuit$	Delamination
0.4:1:-1	30.75	36.47	3.144	2,21	Transverse	Delamination
0.6:1:-1	29.32	35.04	3.333	2,5	Transverse	Delamination
0.8:1:-1	25.75	31.47	3.193	2,21	Transverse	Delamination
1:1:-1	24.32	30.04	3.288	2,21	Transverse	Delamination

*Non–dimensionalized maximum deflection at first-ply failure

$^\clubsuit$FL and FE are the failed layer number and the failed element number at first-ply failure

$^\clubsuit$Transverse mode of failure refers to the matrix failure

Figure 4-39 shows the load versus the maximum deflection response of $(\pm 45/0/90)_{2s}$ laminate for different load ratio values $N_x : N_y : N_{xy}$ ($N_{xy} = -1$, $N_y = 1$, change N_x values) under the action of bi-axial compression combined with in-plane negative shear loading. It is seen that the first-ply failure load and the ultimate failure load decrease with increase in the load ratio values (N_x).

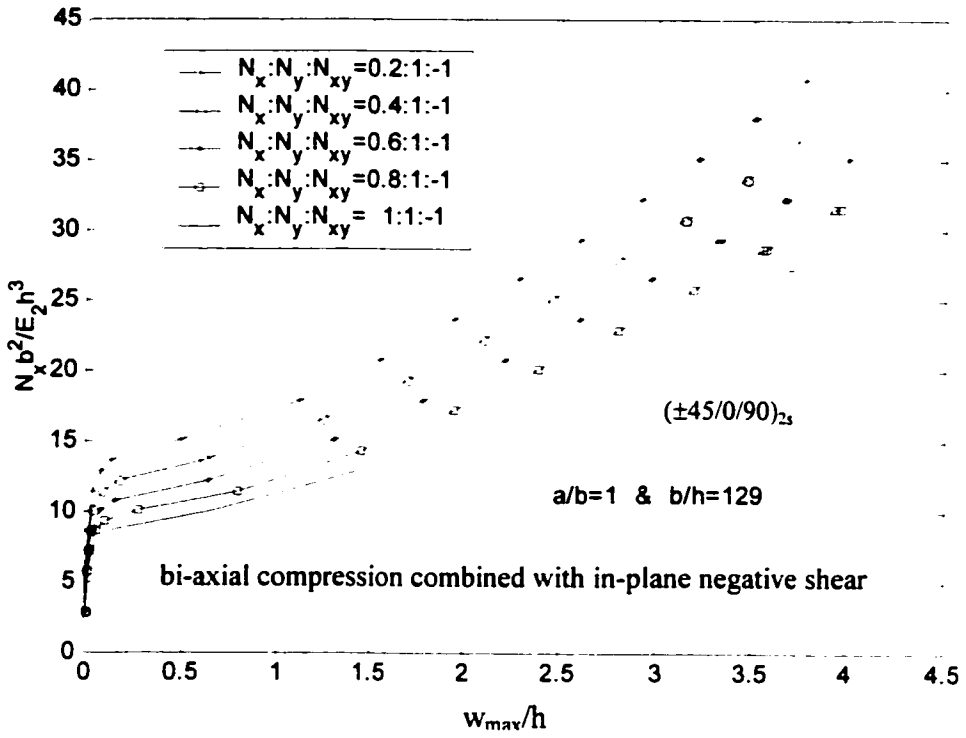

Figure 4-39 Load versus the maximum deflection response of $(\pm 45/0/90)_{2s}$ laminate for different load ratio values of bi-axial compression combined with in-plane negative shear

Figure 4-40 shows the variation of the first-ply failure load and the ultimate load of $(\pm\theta)_{4s}$ laminates with fiber orientation (θ) under the action of bi-axial compression combined with in-plane negative shear loading. The results show that the variations in response are symmetric with respect to 45^0 fiber orientation. Peak values of the first-ply failure load and the ultimate failure load are predicted to occur for 45^0 orientation. For $(0/0)_{4s}$ and $(\pm 15)_{4s}$ laminates, the first-ply failure loads also are the ultimate failure loads.

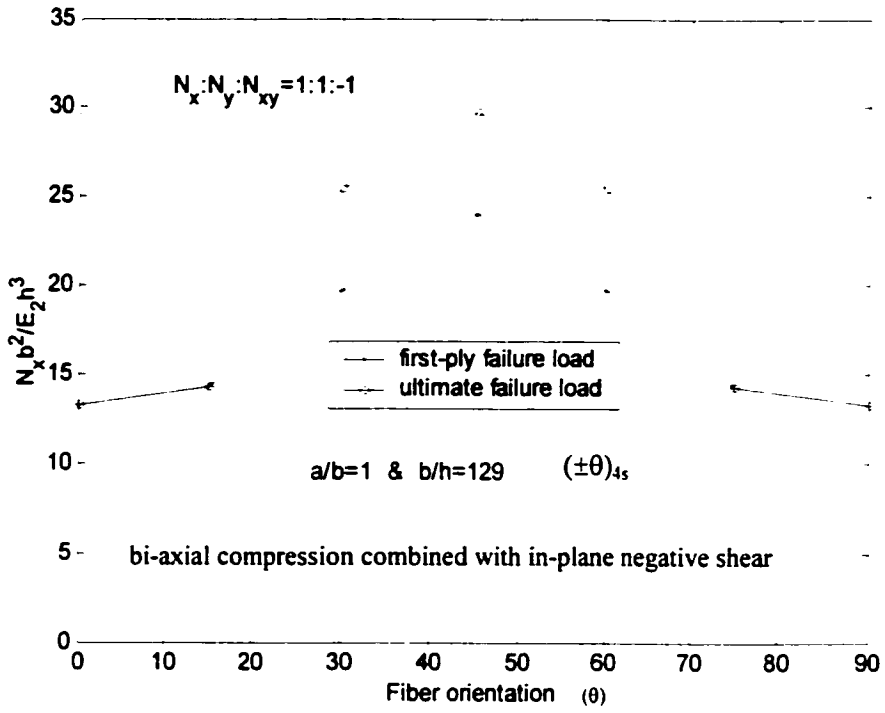

Figure 4-40 Variation of the first-ply failure load and the ultimate load of $(\pm\theta)_{4s}$ laminate with fiber orientation under bi-axial compression combined with in-plane negative shear

Figure 4-41 shows the variation of the maximum deflection associated with the first-ply failure and that just before the ultimate failure for $(\pm\theta)_{4s}$ laminate. The results predict that the variations in the maximum deflection are symmetrical about the 45^0 fiber orientation. A peak value corresponding to the first-ply failure load occurs for 45^0 fiber orientation. It is observed that the maximum deflection associated with the ultimate load has a symmetric pattern in the case of bi-axial compression combined with in-plane negative shear loading.

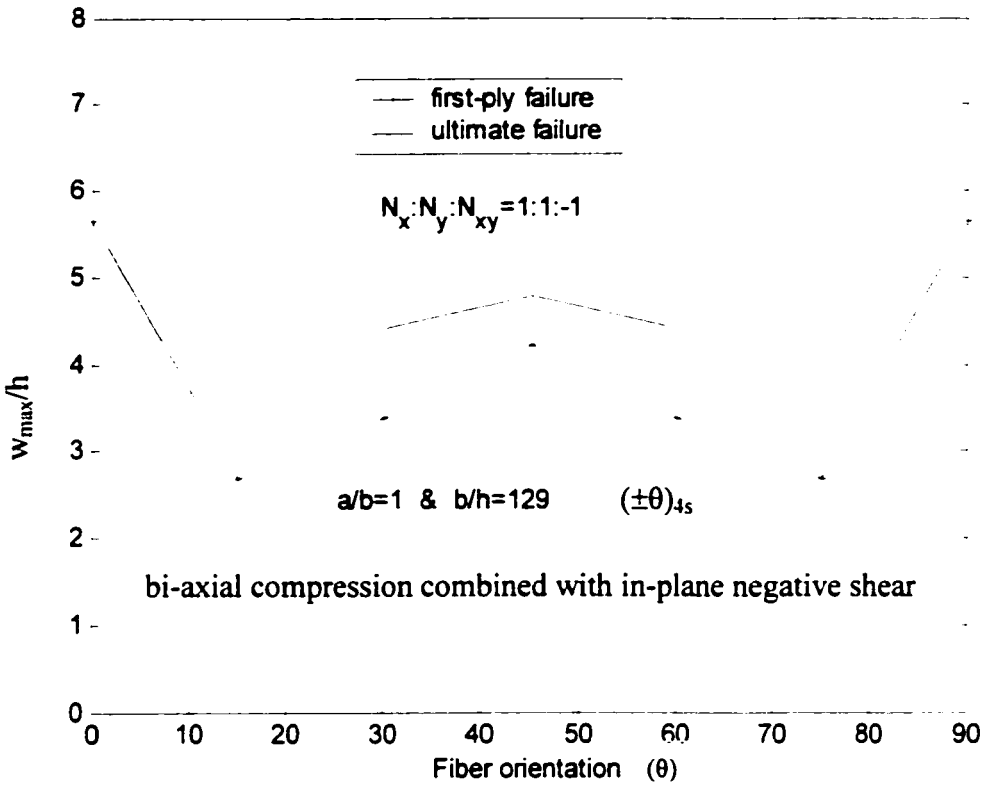

Figure 4-41 Variation of the maximum deflection associated with the first-ply failure and the ultimate load of $(\pm\theta)_{4s}$ laminate with fiber orientation under bi-axial compression combined with in-plane negative shear

Figure 4-42 shows the variation of these loads with aspect ratio values for $(\pm 45/0/90)_{2s}$ laminates under the action of bi-axial compression combined with in-plane negative shear.

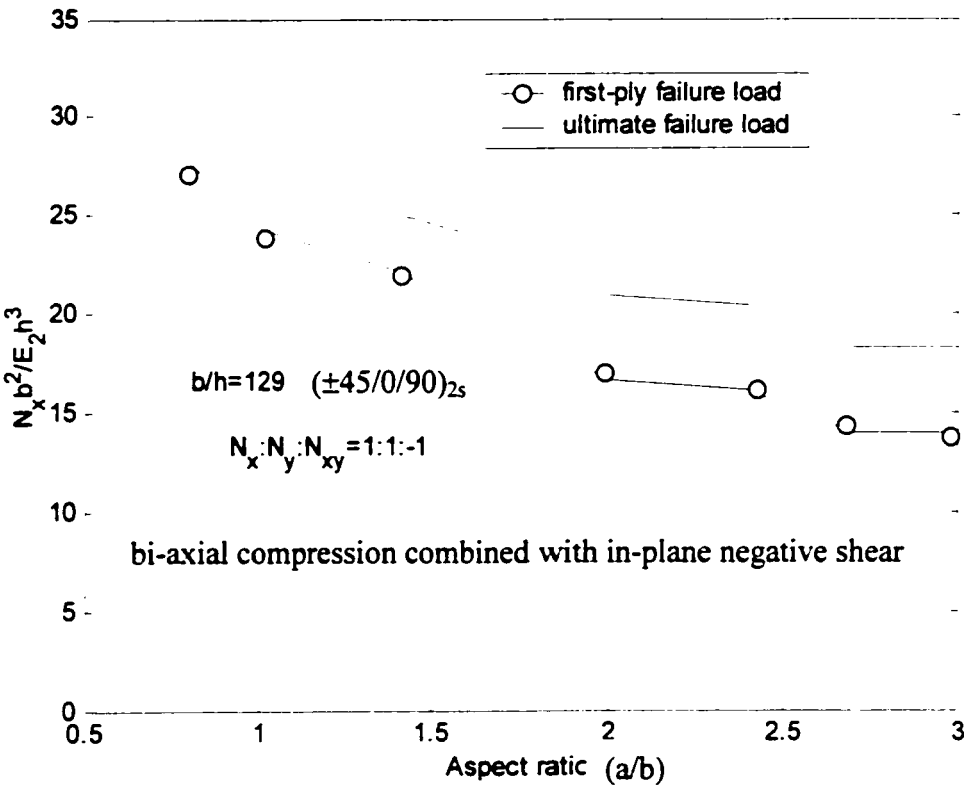

Figure 4-42 Variation of the first-ply failure load and the ultimate failure load of $(\pm 45/0/90)_{2s}$ laminate with aspect ratio values under bi-axial compression combined with in-plane negative shear

Figure 4-43 shows the variation of the maximum deflection associated with the first-ply failure and the ultimate failure with aspect ratio values for $(\pm 45/0/90)_{2s}$ laminate under the action of bi-axial compression combined with in-plane negative shear loading.

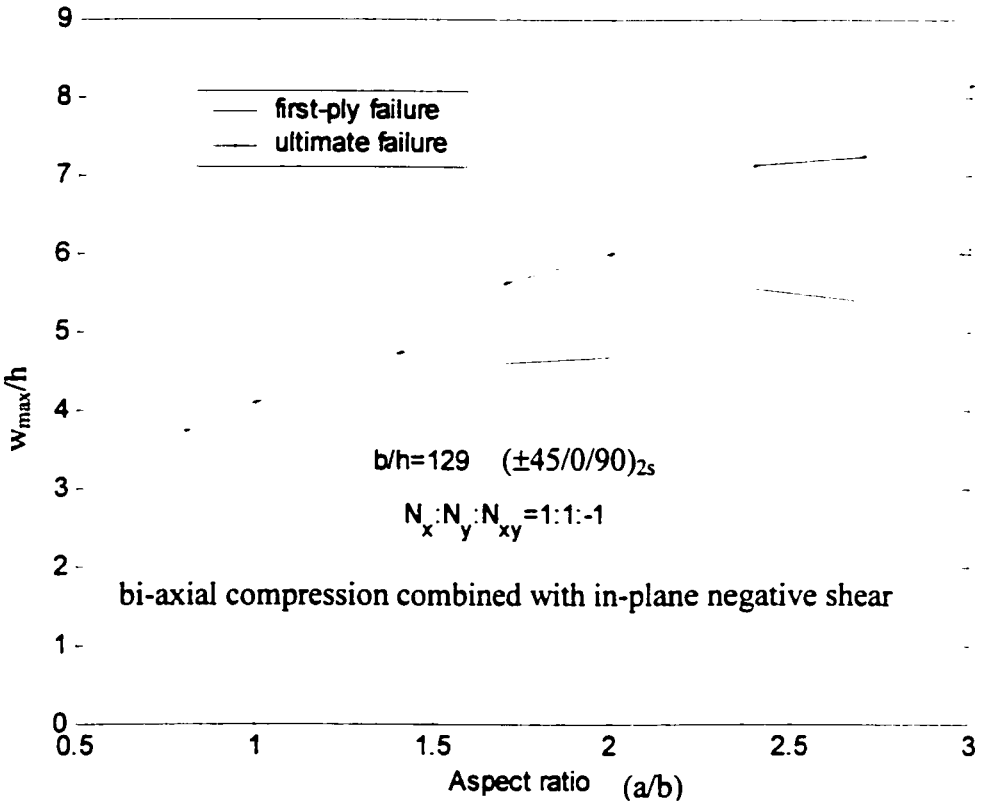

Figure 4-43 Variation of the maximum deflection of $(\pm 45/0/90)_{2s}$ laminate with aspect ratio values under bi-axial compression combined with in-plane negative shear

4.6 Conclusion

For the case of uni-axial compression or bi-axial compression, the tensor polynomial form of the maximum stress criterion is used to predict the failure of the lamina. For the case of bi-axial compression combined with in-plane positive or negative shear loadings,

the tensor polynomial form of the 3-D Tsai-Hill criterion is used to predict the failure of the lamina. The maximum stress criterion is used to predict the onset of delamination at the interface between two adjacent layers.

The influences of plate aspect ratio, symmetric and unsymmetric lay-ups, and fiber orientations on the deflection response, first-ply failure load, ultimate failure load, failure mode and the maximum deflection associated with failure loads are determined. The results of the present study predict that the maximum difference in the first-ply failure loads and the ultimate failure loads are strongly dependent on the type of laminate lay-up and aspect ratio value. Failure mode of the first-ply failure is associated with the localized matrix cracking and occurs primarily due to in-plane normal stresses acting in the direction transverse to the fiber direction irrespective of the laminate lay-up and aspect ratio value. The first-ply failure locations are found to be the most critical points of failure and they lie near the loaded edges of the plate. In $(\pm 45/0/90)_{2s}$ laminate (for all aspect ratio values) under the action of bi-axial compression combined with in-plane shear loading, the ultimate failure mode is delamination. The failure loads of laminates under the action of bi-axial compression are lesser than that for the laminates under the action of uni-axial compression. However, there is a small change in the first-ply and ultimate failure loads when the bi-axial compression is applied together with the shear load.

Chapter 5

Stochastic Failure Analysis

5.1 Introduction

The reliability of many engineering structures in the presence of uncertainty has been a crucial factor in their analysis and design. Primary and secondary systems related to aerospace structures are quite sensitive to small imperfertions in pertinent design variables. Several of these variables are inherently random and can be most appropriately modeled as random processes. They may include quantities such as modulus of elasticity, Poisson ratio, shear strength, and a variety of other physical and mathematical parameters. Clearly, the complexity of these modern structures requires the use of versatile numerical techniques such as the finite element method to obtain accurate mathematical approximations to their physical behavior.

Significant randomness is displayed in the spatial variations in the properties of fibers and of matrix materials, in the properties at interfaces, in the fiber orientation angles of various piles, in the thickness of lamina, and so on. Tests on a single material specimen provide a specific value for each material parameter and mechanical property. However, different randomly distributed values are obtained for the same mechanical property or the material parameter after a number of specimens are tested. Most of the existing techniques are limited to dealing with deterministic loadings and environmental conditions despite the fact that they intrinsically involve randomness and uncertainty to a

considerable degree. Therefore, the analysis of laminates should be performed based on a probabilistic approach. In light of this, this thesis applies tools such as the Markov Model and Stochastic Finite Element Analysis, which is basically Finite Element Analysis performed on the basis of a stochastic approach.

We begin in the following section with a description of the analytical modeling of material properties as stochastic processes. MATLAB program developed in Chapter 3 and Chapter 4 is extended so as to incorporate stochastic description of material properties and stochastic finite element analysis.

5.2 Stochastic Field Modeling of Material Properties

Such spatial variations of material properties as Young's modulus, Poisson's ratio and the shear modulus, are each considered to constitute a two-dimensional homogeneous stochastic field. The fluctuating components of a material property have a zero mean. For illustrative purposes, first the stochastic field of Young's modulus in the fiber direction (E_1) is described below. A similar procedure is applicable to E_2, E_3, G_{12}, G_{13}, G_{23}, ν_{12}, ν_{23} and ν_{13}, ply orientation angle and ply thickness.

$$E_1 = \overline{E}_1[1 + a(X)] \tag{5.1}$$

$$E[a(X)] = 0 \tag{5.2}$$

The auto-correlation function is given by

$$R_{aa}(\xi) = E[a(X)a(X+\xi)] \tag{5.3}$$

In the equations (5.1-5.3), $X = [x, y]^T$ indicates the position vector and $\xi = [\xi_1, \xi_2]^T$ represents the separation vector between two points X and $(X + \xi)$. In the present thesis, it is assumed that each material property varies at each Gauss point of all the finite elements. Thus, if there are a total of n finite elements present in the structure, and m represents the order of Gauss quadrature, then there are N (equal to n*m) material property values associated with the n elements. Consider only the fluctuating component of the homogeneous stochastic field, which models the material property variations around the expected value. These N values $a_i = a(X_i)$, $(i = 1,2,3,\ldots,N)$, are random variables with mean zero, but correlated. Here, X_i corresponds to the location of each Gauss point. Their correlation characteristics can be specified in terms of the covariance matrix C_{aa} of order N*N, whose ij^{th} component is given by:

$$c_{ij} = Cov[a_i a_j] = E[[a_i a_j]] = R_{aa}(\xi_{ij}) \qquad i, j = 1,\ldots,N \tag{5.4}$$

in which $\xi_{ij} = (X_j - X_i)$ represents the separation distance between the Gauss points i and j. Then, a vector $a = [a_1 \quad a_2 \quad a_3 \ldots \quad a_N]^T$ can be obtained as

$$a = LZ \tag{5.5}$$

where $Z = [Z_1 \quad Z_2 \quad Z_3 \ldots \quad Z_N]^T$ is a matrix consisting of N independent Gaussian random variables with zero mean and unit standard deviation, and L is a lower triangular matrix obtained by the Cholesky decomposition of the covariance matrix C_{aa}. Thus,

$$LL^T = C_{aa} \tag{5.6}$$

Once the Cholesky decomposition is accomplished, different sample vectors of a are easily obtained by generating different samples for the Gaussian random vectors Z.

The correlation properties of the stochastic field representing the fluctuating components of material properties are expressed using the Markov correlation model, also known as the First-order autoregressive model. The choice of this model in this work is due to its familiarity and wide use.

5.3 Markov Model

The Markov correlation model is given by [25]

$$R_{aa}(\xi) = \sigma_0^2 \exp\left[-\left(\frac{|\xi|}{d}\right)\right] \tag{5.6}$$

in which the correlation length d is a positive parameter such that when it is large the correlation disappears more slowly, and σ_0 is the standard deviation of the stochastic field $a(X)$.

The process $a(X)$ is defined as the stochastic field which represents the deviatoric components of the material property with autocorrelation function as given in the Markov model. The basic material properties such as the elastic modulus and Poisson's ratio are assumed to have a Gaussian distribution and are given by:

$$E_{1e} = E_{1m}(1 + a_e)$$ 1-directional Young's modulus (5.6)

$$E_{2e} = E_{2m}(1 + b_e)$$ 2-directional Young's modulus (5.7)

$$E_{3e} = E_{3m}(1 + c_e)$$ 3-directional Young's modulus (5.8)

$$v_{12e} = v_{12m}(1 + d_e)$$ 1-2 directional Poisson's ratio (5.9)

$$v_{13e} = v_{13m}(1 + e_e)$$ 1-3 directional Poisson's ratio (5.10)

$$v_{23e} = v_{23m}(1 + f_e)$$ 2-3 directional Poisson's ratio (5.11)

$$G_{12e} = G_{12m}(1 + g_e)$$ 1-2 directional Shear modulus (5.12)

$$G_{13e} = G_{13m}(1 + h_e)$$ 1-3 directional Shear modulus (5.13)

$$G_{23e} = G_{23m}(1 + j_e)$$ 2-3 directional Shear modulus (5.14)

in which a_e, b_e, c_e, d_e, e_e, f_e, g_e, h_e and j_e are the values of the stochastic field $a(X)$, $b(X)$, $c(X)$, $d(X)$, $e(X)$, $f(X)$, $g(X)$, $h(X)$ and $j(X)$, respectively, at each Gauss point in the structure. These values also represent the variations in the material properties

E_1, E_2, E_3, v_{12}, v_{13}, v_{23}, G_{12}, G_{13} and G_{23}. E_{1m}, E_{2m} and E_{3m} are the mean values of the Young's modulus in directions 1, 2 and 3, respectively, and, v_{12m}, v_{13m}, and v_{23m} are the mean values of the 1-2 direction Poisson's ratio, 1-3 direction Poisson's ratio and 2-3

direction Poisson's ratio. G_{12m}, G_{13m} and G_{23m} are the mean values of the 1-2 direction Shear modulus, 1-3 direction Shear modulus and 2-3 direction Shear modulus.

Variations of fiber orientation angle θ_ε and thickness of plies t_ε are expressed in a similar manner given by:

$$\theta_\varepsilon = \theta_m(1 + k_\varepsilon) \tag{5.15}$$

$$t_\varepsilon = t_m(1 + l_\varepsilon) \tag{5.16}$$

in which θ_m and t_m are the mean values of the fiber orientation angle and ply thickness respectively.

The assumption of Gaussian distribution implies the possibility of generating negative values for the material properties. In order to avoid this difficulty, the values of the random variable a_ε in the case of Monte-Carlo simulation are confined to the range

$$-1 + \varepsilon \le a_\varepsilon \le 1 - \varepsilon \tag{5.17}$$

in which ε is a positive constant introduced to avoid the mathematical complications that would arise if the sum $(1+a_\varepsilon)$ becomes negative or zero. The other material property values are confined in a similar manner.

5.4 Stochastic Elasticity Matrix

The boundary conditions that have been considered in this study are shown in Figure 5-1. Properties of NCT-301 graphite/epoxy material (Ganesan and Haque [66]) used in the present study are presented in Table 5-1.

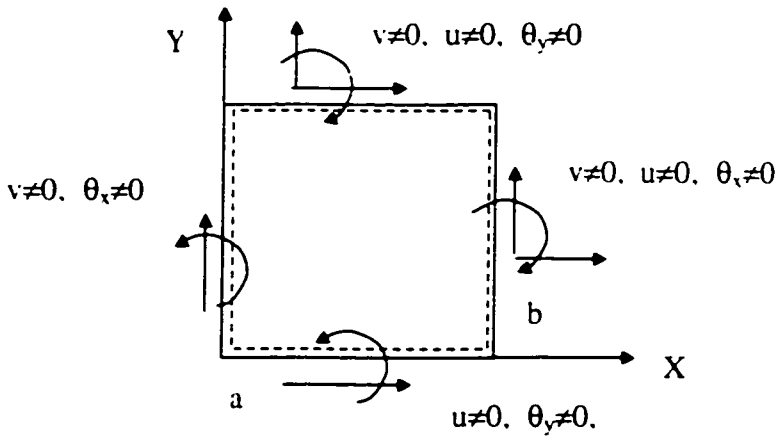

Figure 5-1 Details of boundary conditions for the laminated plate

Table 5-1 Material properties of NCT-301 graphite-epoxy [64]

Mechanical properties	Mean values	Standard deviation	Strength properties	Values
E_1	129.43 GPa	2.8719	X_t	1584.8 MPa
E_2	7.99 GPa	0.3298	X_c	1033.5 MPa
E_3	7.99 GPa	0.3298	$Y_t = Z_t$	48.28 MPa
$G_{12} = G_{13}$	4.28 GPa	0.2366	$Y_c = Z_c$	48.28 MPa
$\nu_{12} = \nu_{13}$	0.33	0.0317	R	25.90 MPa
ν_{23}	0.4	0.0317	S=T	33.3 MPa

In the Table 5-1, ν_{12}, ν_{13} and ν_{23} are the Poisson's ratios in the planes 1-2, 1-3 and 2-3, respectively. E_1, and E_2 and E_3 are principal Young's modulus in the fiber direction and in the directions transverse to it, respectively. G_{12}, G_{13} and G_{23} are shear modulus

associated with planes 1-2, 1-3 and 2-3, respectively. X_t is the tensile strength of lamina in fiber direction. X_c is the compressive strength of lamina in the fiber direction. Y_t is the tensile strength of lamina in the direction (in plane 1-2) transverse to the fiber direction. Y_c is the compressive strength of lamina in the same direction. Z_t is the tensile strength of lamina in principal material direction 3. Z_c is the compressive strength of lamina in principal material direction 3. R, S and T are shear strengths of lamina in planes 2-3, 1-3 and 1-2, respectively.

In the Figure 5-1, a and b are dimensions of the full plate in X and Y directions. Dimensions of the plate are: a = 279 mm and b = 279 mm. Ply thickness is 0.135 mm.

A 5×5 finite element mesh is used in the present analysis. Figure 4-2 shows the finite element mesh for 5×5 type. Figure 5-2 and Figure 5-3 show the direction of the applied shear loading along with the fiber direction.

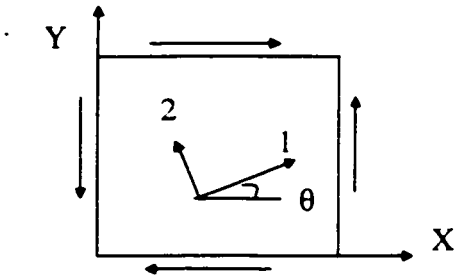

Figure 5-2 Notation for the positive shear

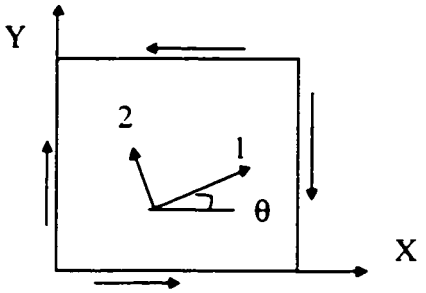

Figure 5-3 Notation for the negative shear

It is to be noted that in-plane shear loading is applied on all four edges of the plate, while uni-axial compressive loading is applied at the edge x = a, and bi-axial compressive loadings are applied on the edges x = a and y = b.

Bi-axial compressive loadings N_x and N_y are expressed in figures in non-dimensionalized forms by $N_x b^2/E_2 h^3$ and $N_y b^2/E_2 h^3$ respectively. N_x is the applied X-direction axial compressive loading per unit length. N_y is the applied Y-direction axial compressive loading per unit length. The corresponding central (transverse) deflection is also expressed in non-dimensionalized form by w_c/h where h is the total thickness of the laminate.

Using the test data on elastic constants of the composite material (given in Table 5-1) and the generated sample realizations of elastic constants at each Gauss point, the stochastic Young's modulus, Poisson's ratio, and shear modulus are determined according to the equations (5.3-5.17). Further, the stochastic laminate elasticity matrix [E] at the corresponding Gauss point is obtained in the same way. In practice, a three-point Gauss quadrature is employed as it gives the most accurate results for 9-node element. Sample realizations of Young's moduli, Poisson's ratios, Shear moduli and the stochastic elasticity matrix [E] calculated for element 1 and 13 in the structure of laminate $(\pm 45/0/90)_{2s}$ are shown in Figure 5-4.

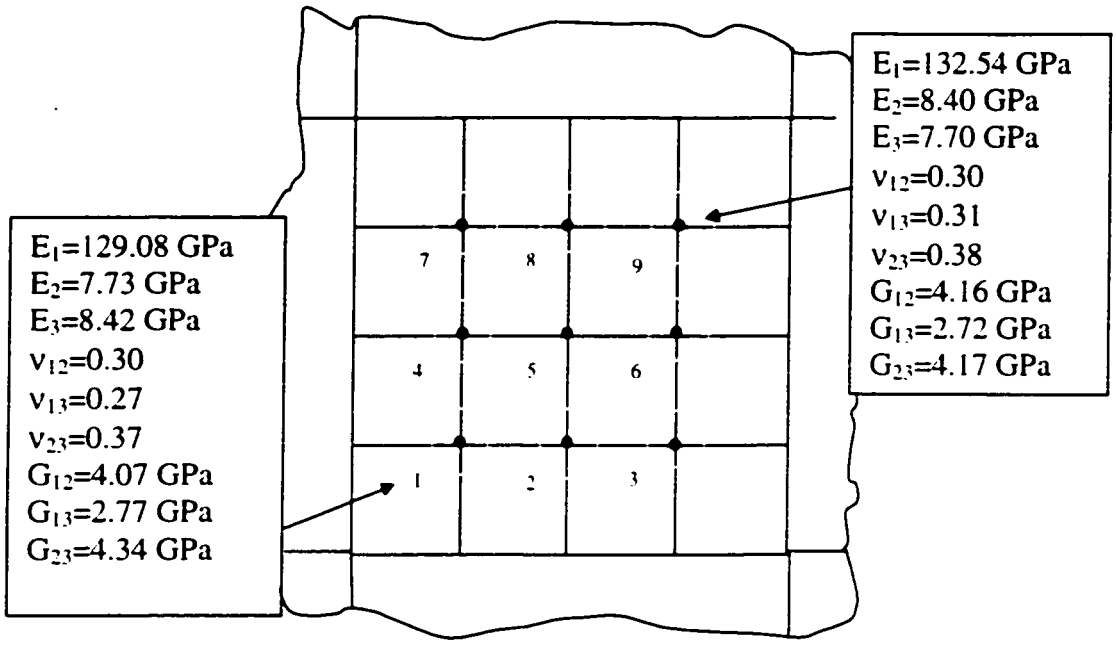

Element 1

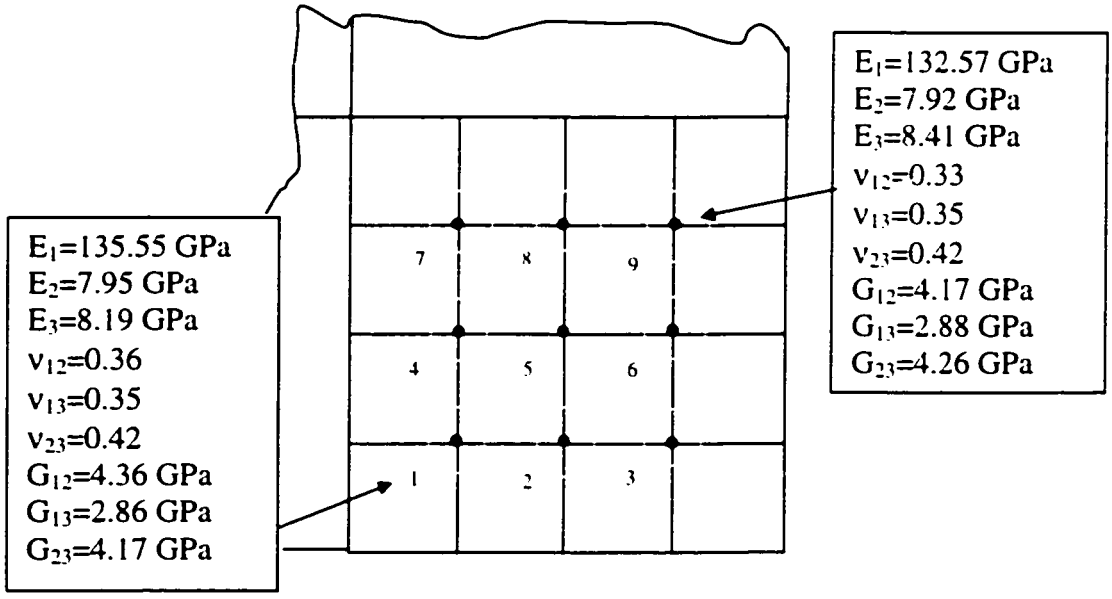

Element 13

Figure 5-4 A set of sample realizations of elastic constants at different Gauss points in element 1 (at the loaded edge) and element 13 (the central element)

5.5 Stochastic Analysis Results

In the stochastic analysis, the number of simulations is kept at 150 considering the computational time taken for the entire stochastic analysis. The mean values and the standard deviation values of both the first-ply failure load and the ultimate failure load for the $(\pm 45/0/90)_{2s}$ laminate that is subjected to uni-axial compressive loading are determined.

The mean values of the first-ply failure load and the corresponding maximum deflection are presented in Figure 5-5. The mean values of the first-ply failure load and the maximum deflection are both influenced by the number of simulations. Within the range of 1-30 simulations, the mean value of the first-ply failure load decreases. Within the range of 30-150 simulations the mean value increases. It can be observed that between the range of 10-150 simulations, the mean values of the first-ply failure load and mean values of the maximum deflection at the first-ply failure have the same trend of variation.

The variations of the standard deviation values of the first-ply failure load and the maximum deflection with the number of simulations are presented below in Figure 5-6. The standard deviation values of the first-ply failure load and the maximum deflection are both influenced by the number of simulations. It can be observed that between the range of 60-150 simulations, the standard deviation values of the first-ply failure load and the standard deviation values of the maximum deflection at the first-ply failure have the same trend of variation. The standard deviation values of the first-ply failure load and the

standard deviation values of the maximum deflection at the first-ply failure decrease in the range of 60-150.

The mean values of the ultimate failure load and the corresponding maximum deflection are presented in Figure 5-7. The mean values of the ultimate failure load and the mean values of the maximum deflection are influenced by the number of simulations. The mean values of the ultimate failure load and the mean values of the maximum deflection have the same trend of variation between 60-140 simulations.

The ratio of the mean value of the ultimate failure load to the mean value of the first-ply failure load corresponding to each simulation is calculated. It has been observed that the minimum value of this ratio is 1.060 and the maximum value is 1.065.

The variations of the standard deviation values with the number of simulations are presented below in Figure 5-8. The standard deviation values of the ultimate failure load and the maximum deflection are both influenced by the number of simulations.

The ratio of the standard deviation of the ultimate failure load to the standard deviation of the first-ply failure load corresponding to each simulation is calculated. It has been observed that the minimum value of this ratio is 0.866 and the maximum value is 0.909. This indicates that the degree of randomness in the ultimate failure is lesser than that in the first-ply failure.

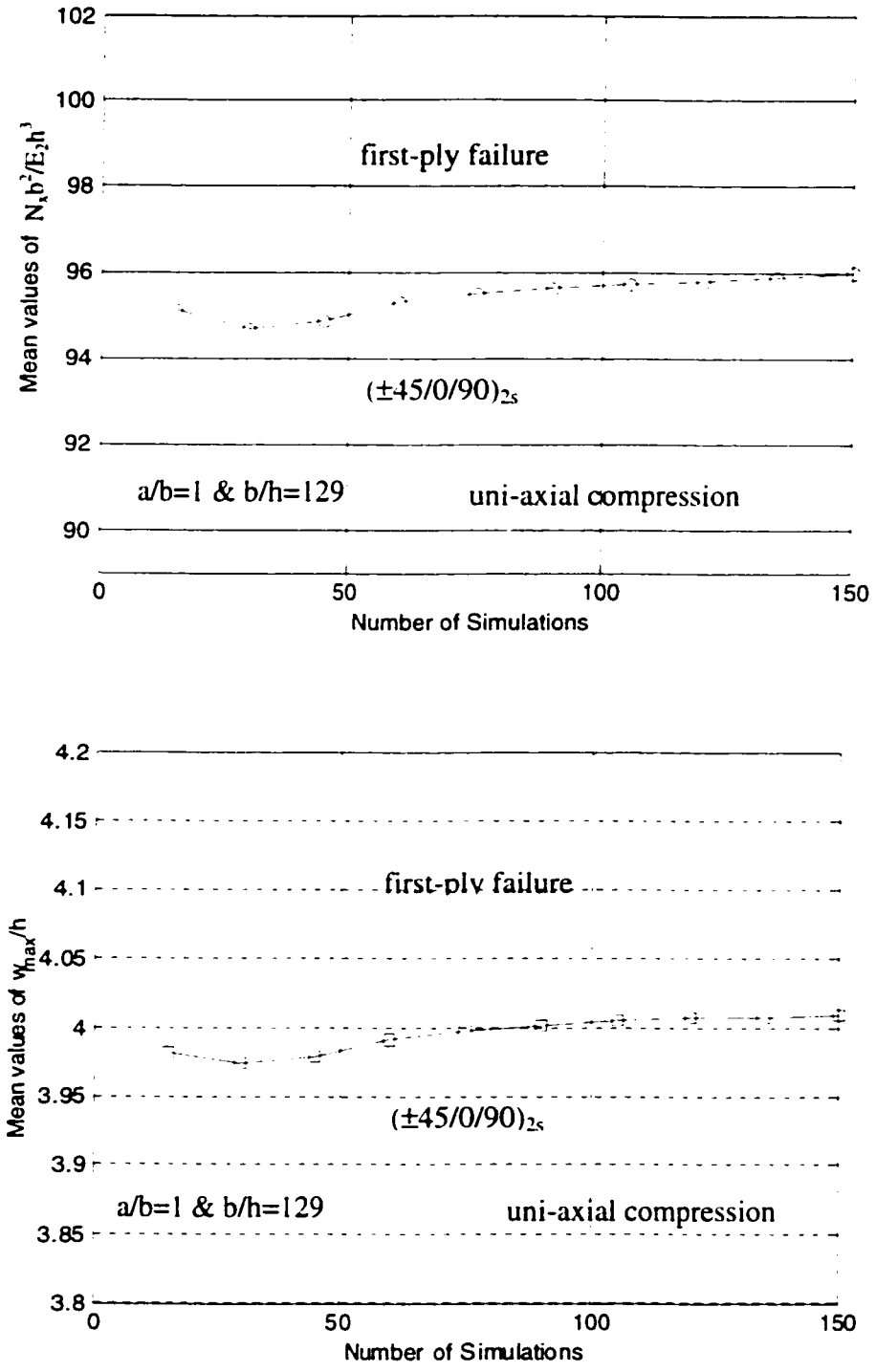

Figure 5-5 The mean values of the first-ply failure load and the maximum deflection for $(\pm 45/0/90)_{2s}$ laminate under uni-axial compression

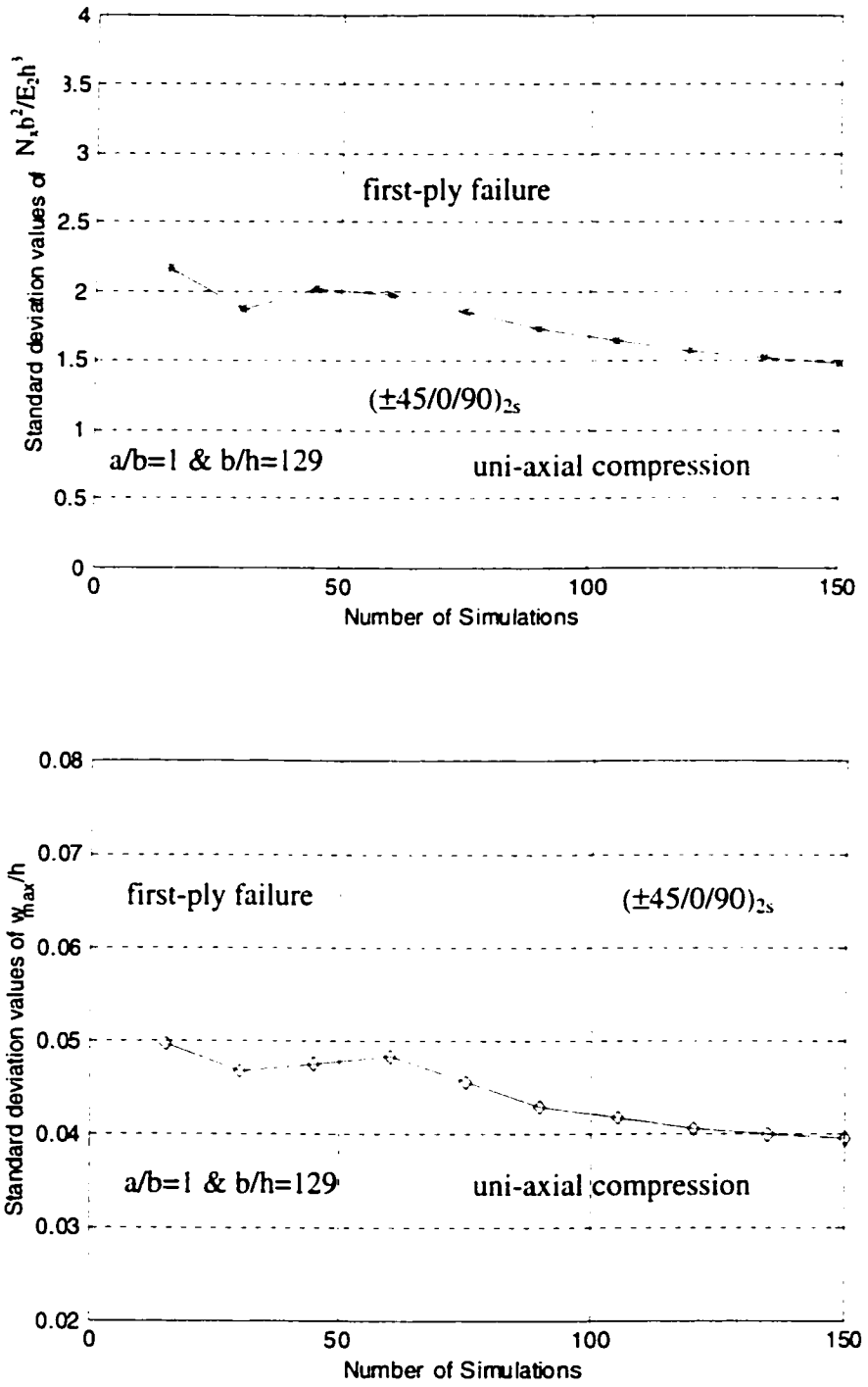

Figure 5-6 The standard deviation values of the first-ply failure load and the maximum deflection for $(\pm 45/0/90)_{2s}$ laminate under uni-axial compression

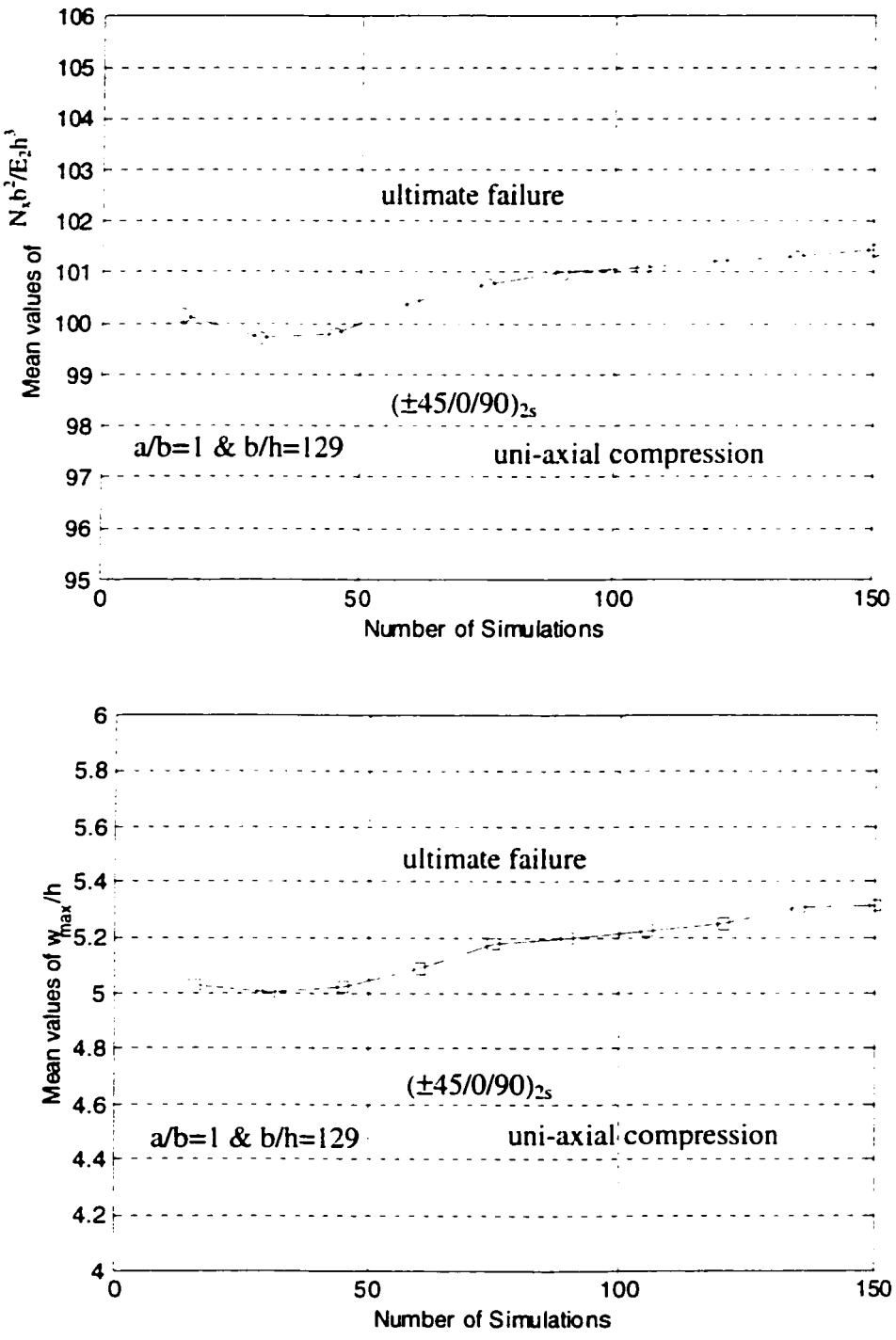

Figure 5-7 The mean values of the ultimate failure load and the maximum deflection for $(\pm 45/0/90)_{2s}$ laminate under uni-axial compression

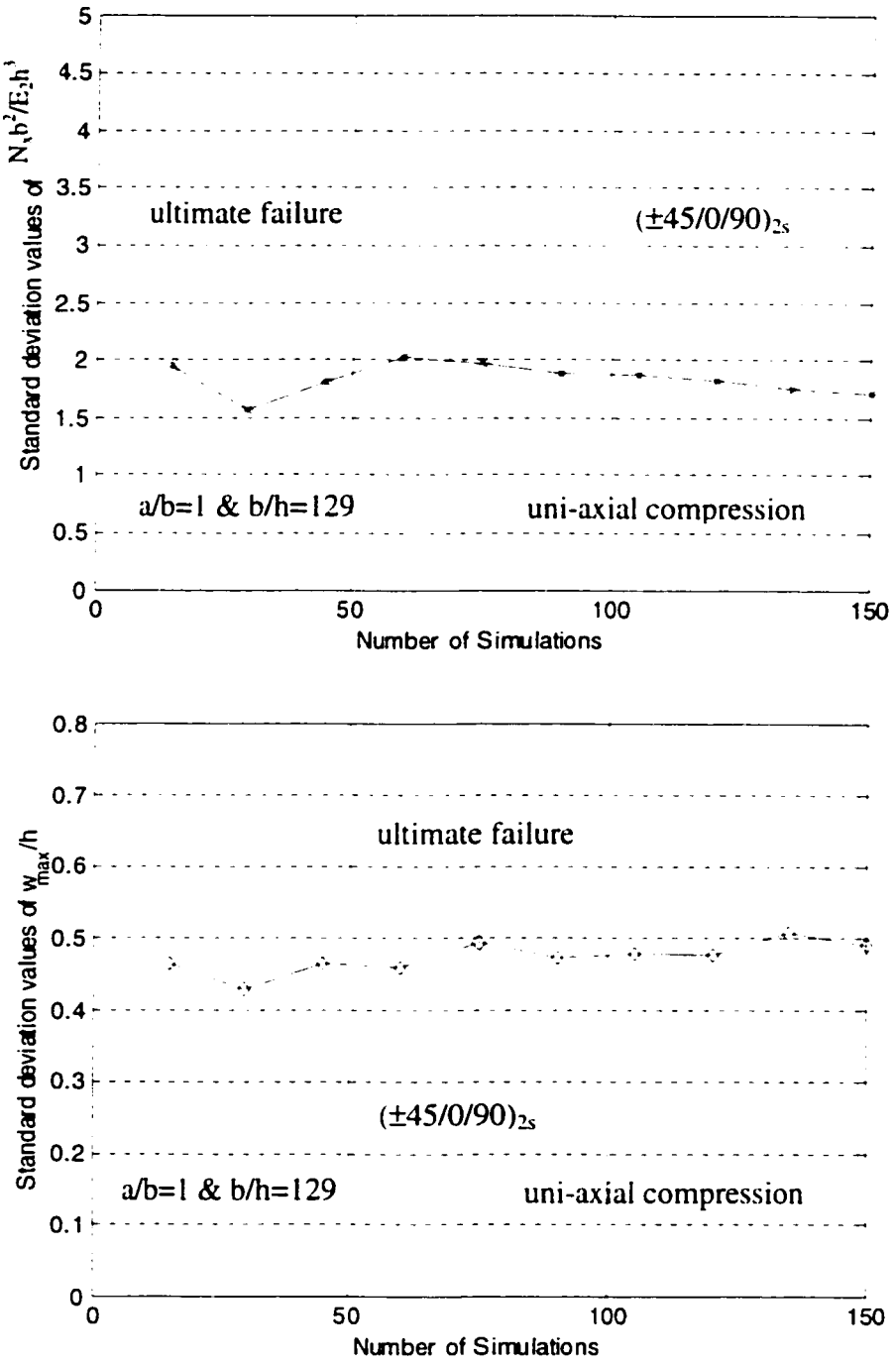

Figure 5-8 The standard deviation values of the ultimate failure load and the maximum deflection for $(\pm 45/0/90)_{2s}$ laminate under uni-axial compression

Now the case of bi-axial compression is considered. The ratio of N_x : N_y is set to be equal to (1 : 1). The variations of the mean values of the first-ply failure load and the maximum deflection are shown in Figure 5-9. The mean values of the first-ply failure load and the maximum deflection are both influenced by the number of simulations. It can be observed that between the range of 45-150 simulations, the mean values of the first-ply failure load and mean values of the maximum deflection at the first-ply failure have the same trend of variation.

The variations of the standard deviation values of the first-ply failure load and the maximum deflection with the number of simulations are presented below in Figure 5-10. The standard deviation values of the first-ply failure load and the maximum deflection are both influenced by the number of simulations. It can be observed that in the range of 30-150 simulations, the standard deviation values of the first-ply failure load and the standard deviation values of the maximum deflection at the first-ply failure have the same trend of variation.

The mean values of the ultimate failure load and the corresponding maximum deflection are presented in Figure 5-11. The mean values of the ultimate failure load and the mean values of the maximum deflection are influenced by the number of simulations. The mean values of the ultimate failure load and the mean values of the maximum deflection have the same trend of variation between 10-140 simulations.

The ratio of the mean value of the ultimate failure load to the mean value of the first-ply failure load corresponding to each simulation is calculated. The minimum value of this ratio is found to be 1.056 and the maximum value is 1.057.

The variations of the standard deviation values with the number of simulations are presented below in Figure 5-12. The standard deviation values of the ultimate failure load and the maximum deflection are both influenced by the number of simulations.

The ratio of the standard deviation of the ultimate failure load to the standard deviation of the first-ply failure load corresponding to each simulation is calculated. It is observed that the minimum value of this ratio is 0.979 and the maximum value is 0.98. This indicates that the degree of randomness in the ultimate failure and that in the first-ply failure are almost the same, in the case of bi-axial loading. It has previously been pointed out that this is not the case when the loading is uni-axial.

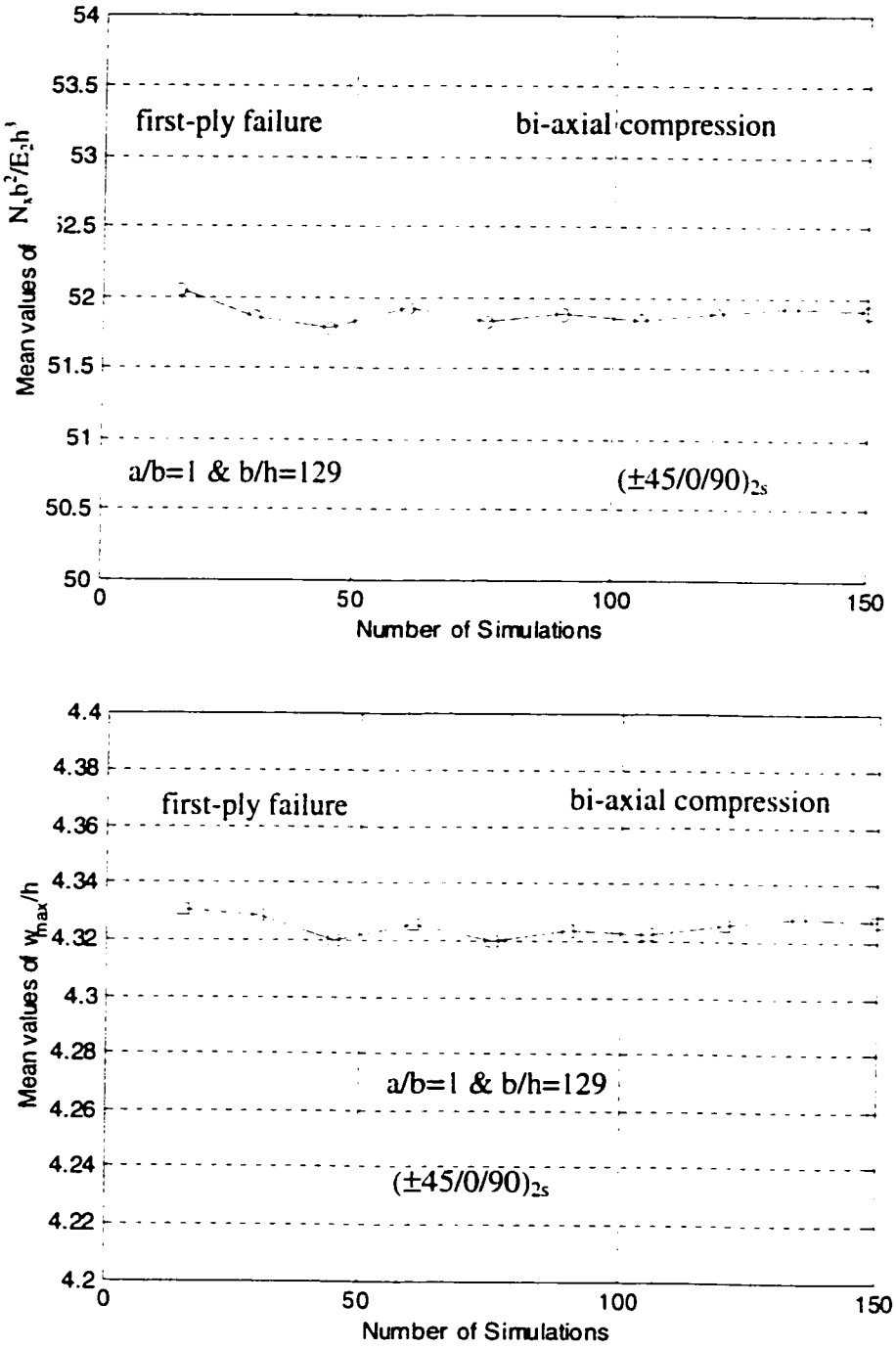

Figure 5-9 The mean values of the first-ply failure load and the maximum deflection for $(\pm 45/0/90)_{2s}$ laminate under bi-axial compression

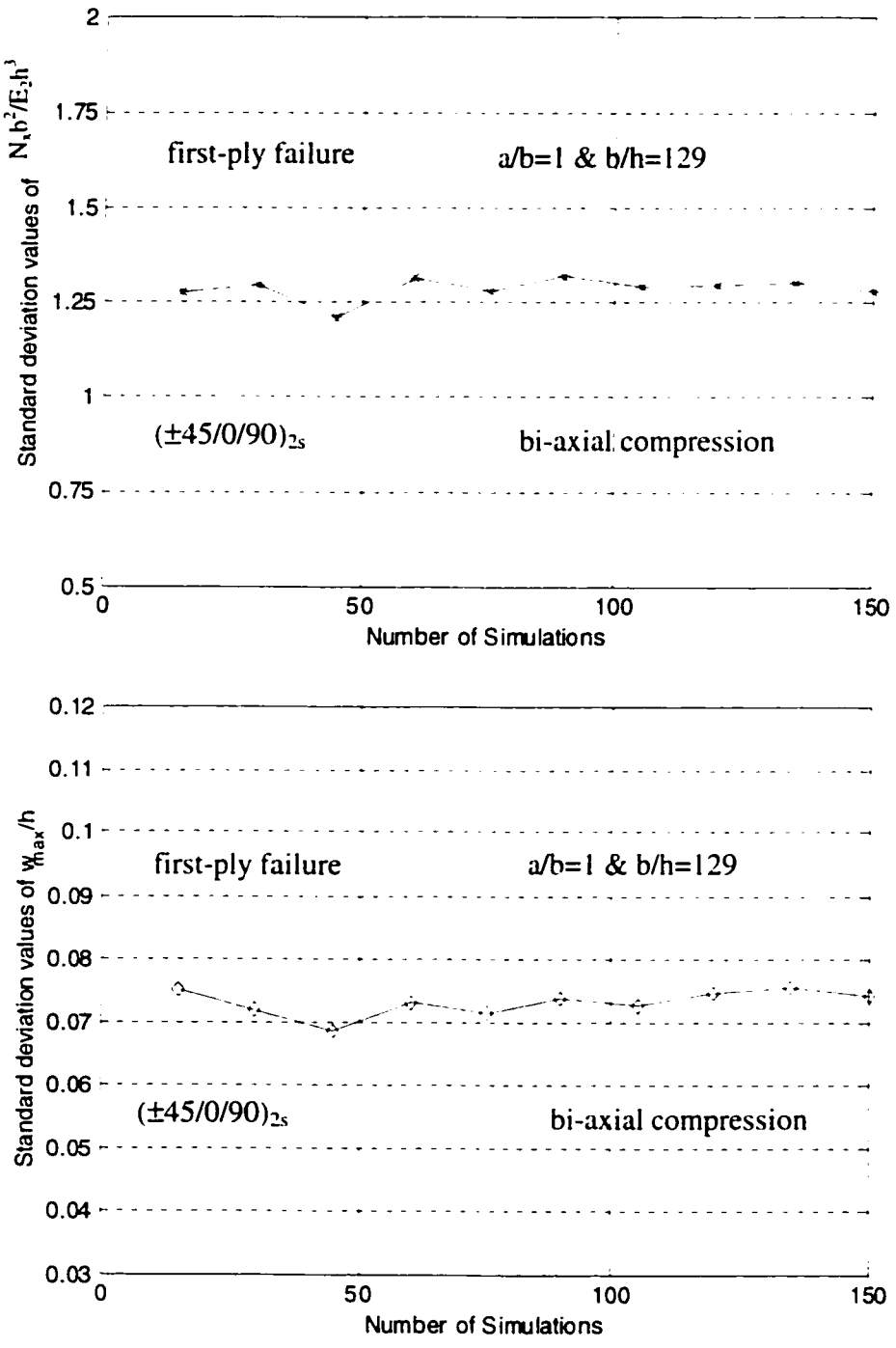

Figure 5-10 The standard deviation values of the first-ply failure load and the maximum deflection for $(\pm 45/0/90)_{2s}$ laminate under bi-axial compression

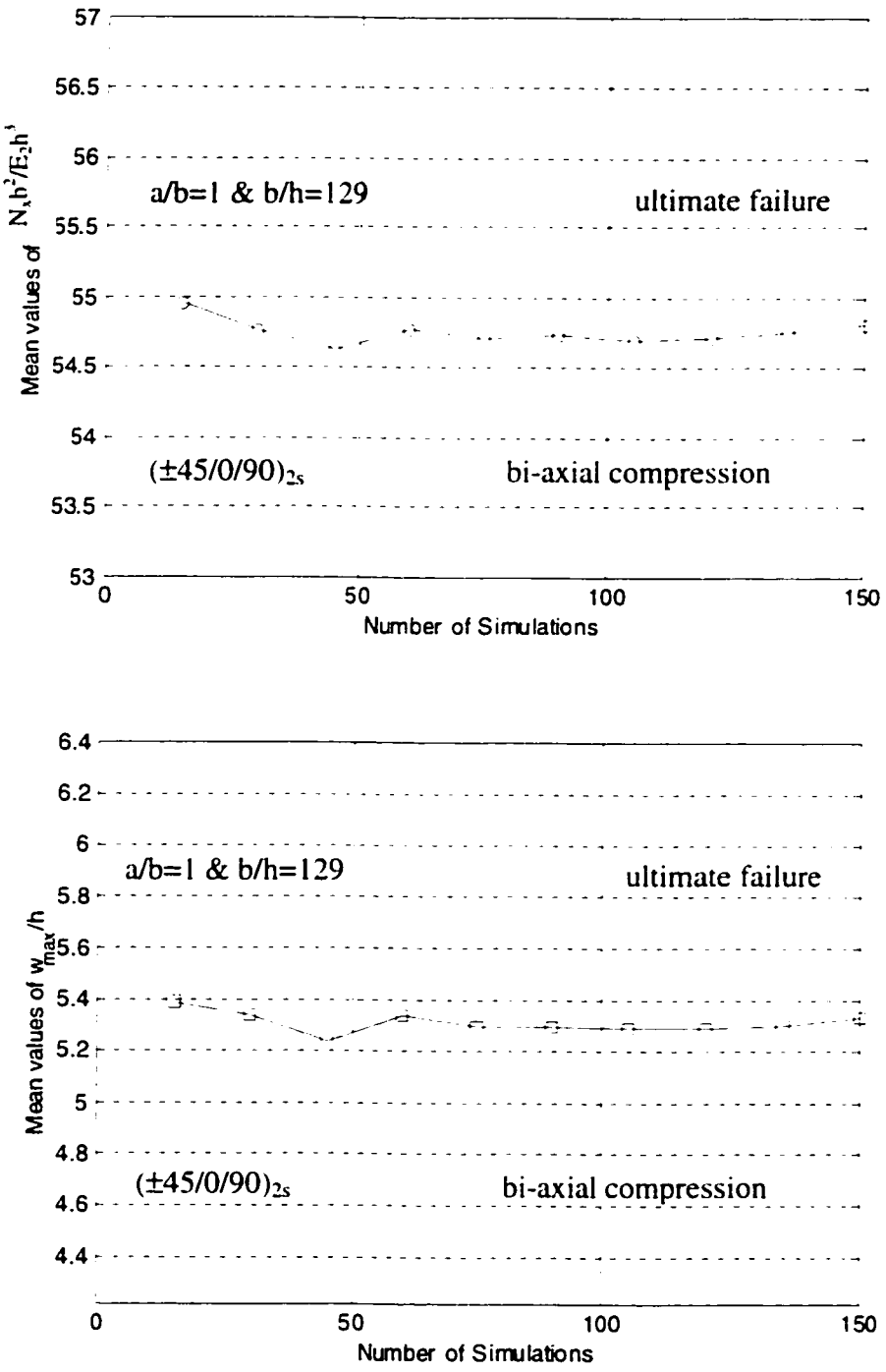

Figure 5-11 The mean values of the ultimate failure load and the maximum deflection for $(\pm 45/0/90)_{2s}$ laminate under bi-axial compression

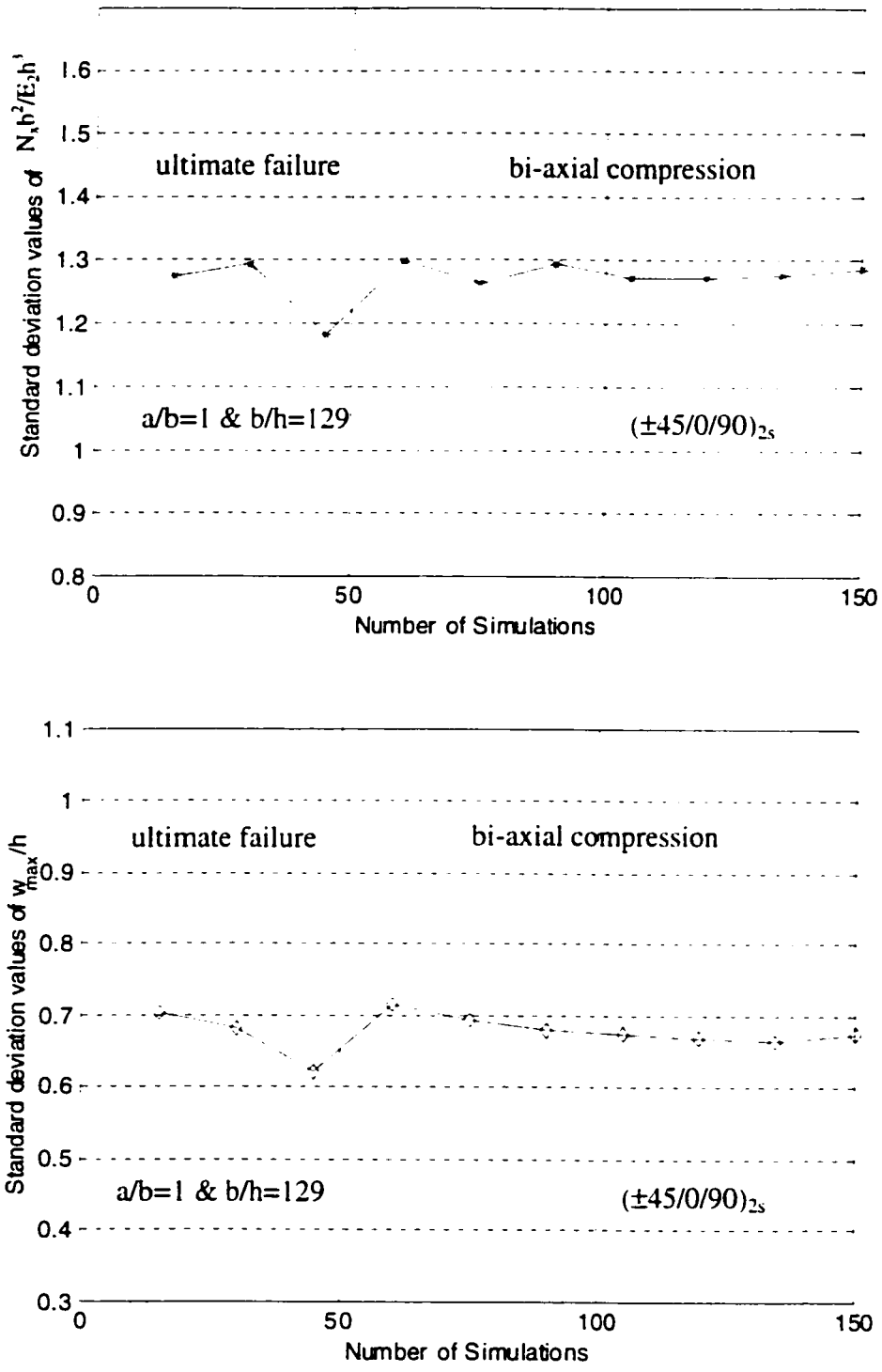

Figure 5-12 The standard deviation values of the ultimate failure load and the maximum deflection for $(\pm 45/0/90)_{2s}$ laminate under bi-axial compression

5.6 Conclusion

This thesis has investigated the progressive failure of composite laminates using a non-linear finite element formulation that also takes into account the effects due to shear deformation. The influences of randomness in the material property values on the first-ply and ultimate failure loads, and the corresponding maximum deflections of the laminate have also been investigated. The number of simulations seems to have a strong influence on the probabilistic characteristics of predicted failure loads and maximum deflection values when the number of simulations is less than 100. Considering the maximum value of the ratio of the mean value of the ultimate failure load to the mean value of the first-ply failure load for both the cases of uni-axial and bi-axial compression, it has been found that the case of uni-axial compression results in a higher value. This indicates that more reserve strength is available after the first-ply failure in this case. Considering the maximum value of the ratio of the standard deviation of the ultimate failure load to the standard deviation of the first-ply failure load for both the cases of uni-axial and bi-axial compression, it is found that the case of bi-axial compression results in a higher value. Therefore, the degree of randomness in the ultimate failure is almost the same as that in the first-ply failure. This indicates that considerable variations in the reserve strength are present in this case, suggesting that the reliability is low for this case.

Chapter 6

Conclusions and Recommendations

In the present thesis, the principle of minimum potential energy is used to derive the nonlinear finite element formulation. The finite element formulation is based on the first-order shear deformation theory and the von Karman geometric non-linearity hypothesis and also the finite element formulation employs a nine-node Lagrangian element having five degrees of freedom (two in-plane displacements, one transverse displacement and two rotational degrees of freedom) per node. The resulting nonlinear equations are solved using the Newton-Raphson technique.

For the stochastic failure analysis, a stochastic finite element methodology based on the Monte Carlo Simulation is used. The program that has been developed to conduct the non-linear finite element analysis is extended so as to incorporate the stochastic description of material properties and the stochastic finite element analysis. In the case of stochastic material properties, the mean values and the standard deviation values of failure loads are calculated.

For the case of uni-axial compression and bi-axial compression, the tensor polynomial form of the maximum stress criterion is used to predict the failure of the lamina. For the case of bi-axial compression combined with in-plane positive or negative shear loadings, the tensor polynomial form of the 3-D Tsai-Hill criterion is used to predict the failure of the lamina. The maximum stress criterion is used to predict the onset of delamination at the interface between two adjacent layers. The influences of plate aspect ratio, symmetric

and unsymmetric lay-ups, and fiber orientations on the deflection response, the first-ply failure load, the ultimate failure load, the failure mode and the maximum deflection associated with the failure loads are determined. In addition, progressive failure of $(\pm 45/0/90)_{2s}$, $(\pm 45)_{4s}$ and $(0/90)_{4s}$ laminates are analyzed.

Based on the study, the following main concluding remarks can be made:

- The maximum difference in the first-ply failure loads and the ultimate failure loads are strongly dependent on the type of laminate lay-up and aspect ratio value.
- Failure mode of the first-ply failure is associated with the localized matrix cracking and occurs primarily due to in-plane normal stresses acting in the direction transverse to the fiber direction irrespective of the laminate lay-up and aspect ratio value.
- The first-ply failure locations are found to be the most critical points of failure and they lie near the loaded edges of the plate.
- In $(\pm 45/0/90)_{2s}$ laminate (for all aspect ratio values) under the action of bi-axial compression combined with in-plane shear loading, the ultimate failure mode is delamination.
- The failure loads of laminates under the action of bi-axial compression are lesser than that for the laminates under the action of uni-axial compression. However, there is a small change in the first-ply and ultimate failure loads when the bi-axial compression is applied together with the shear load.

- Considering the maximum value of the ratio of the mean value of the ultimate failure load to the mean value of the first-ply failure load for both the cases of uni-axial and bi-axial compression, it has been noted that the case of uni-axial compression results in a higher value. This indicates that more reserve strength is available after the first-ply failure in this case.
- Considering the maximum value of the ratio of the standard deviation of the ultimate failure load to the standard deviation of the first-ply failure load for both the cases of uni-axial and bi-axial compression, it has been noted that the case of bi-axial compression results in a higher value. This indicates that considerable variations in the reserve strength are present in this case thereby indicating that the reliability is low for this case.

The following recommendations may be considered in the future studies:

- Progressive failure analysis using Hashin criterion or using Tensor polynomial criteria of maximum strain (Tsai-Wu) criterion has to be conducted.
- Using other stochastic models , laminate progressive failure analysis has to be conducted.
- Stochastic progressive failure analysis under the action of bi-axial compression combined with in-plane shear loading has to be conducted.

References:

[1] Reddy, J.N., Krishnamoorthy, C.S. and Seetharamu, K.N., "*Finite Element Analysis for Engineering Design-Lecture Notes in Engineering 37*", Springer-Verlag, Berlin, Heidelberh, 1988.

[2] Turvey, G.J., "*Flexural Failure analysis of Angle-ply Laminates of GFRP and CFRP*", Journal of Strain Analysis, Vol. 15, 1980, pp. 43-49.

[3] Turvey, G.J., "*An Initial flexural Failure Analysis of Symmetrically laminated Cross-ply Rectangular Plates*", International Journal of Solids and Structures, Vol. 16, 1980, pp. 451-463.

[4] Reddy, J.N. and Pandey, A.K., "*A First-ply Failure Analysis of Composite Laminates*", Computers and Structures, Vol. 25, 1987, pp. 371-393.

[5] Reddy, Y.S.N. and Reddy, J.N., "*Linear and Non-linear Failure Analysis of Composite Laminates with Transverse Shear*", Composites Science and Technology, Vol. 44, 1992, pp. 227-255

[6] Engelstad, S.P., Reddy, J.N. and Knight, Jr.N.F., "*Postbuckling Response and Failure Prediction of Graphite Epoxy Plates Loaded in Compression*", AIAA Journal., Vol. 30, 1992, pp. 2106-2113.

[7] Lee, H.H. and Hyer, M.W., "*Postbuckling Failure of Composite Plates with Holes*", AIAA Journal, Vol. 31, 1993, pp. 1293-1298.

[8] Kam, T.Y. and Sher, H.F., "*Nonlinear and First-ply Failure Analysis of Laminated Composite Cross-ply Plates*", Journal of Composite Materials, Vol. 29, 1995, pp. 463-485.

[9] Kaminski, B.E. and Ashton, J.E., "*Diagonal Tension Behaviour of Boron Epoxy Shear Panels*", Journal of Composite Materials, Vol. 5, 1971, pp. 553-558.

[10] Kobayashi, S., Sumihara, K. and Koyama, K., "*Shear Buckling Strengths of Graphite Epoxy Laminate Panels*", In "*Composite Materials*", Proceedings of the Japan-US Conference, Editors: Kawata, K. and Akaska, T..Tokyo, 1981, pp. 436-445.

[11] Agrawal, B.L., "*Postbuckling Behaviour of Composite Shear Webs*", AIAA Journal, Vol. 19, 1981, pp. 933-939.

[12] Zhang, Y. and Matthews, F.L., "*Postbuckling Behaviour of Anisotropic Laminated Plates Under Pure Shear and Shear Combined with Compressive Loading*", AIAA Journal, Vol. 22, 1984, pp. 281-286.

[13] Stein, M., "*Postbuckling of Long Orthotropic Plates in Combined Shear and Compression*", AIAA Journal, Vol. 23, 1985, pp. 788-794.

[14] Stein, M., "*Behaviour of Buckled Rectangular Plates*", ASCE Journal of Engineering Mechanics, Vol. 86, 1960, pp. 59-76.

[15] Prabhakar, M.K. and Kennedy, J.B., "*Non-linear Behaviour of Unsymmetric Angle-ply Rectangular Plates Under In-plane Shear Load*", Journal of Mechanical Engineering Science, Vol. 21, 1979, pp. 205-212.

[16] Kosteletos, S., "*Postbuckling Response of Laminated Plates Under Shear Load*", Composite Structures, Vol. 20, 1992, pp. 137-145.

[17] Lee, H.H. and Hyer, M.W., "*Postbuckling Failure of Composite Plates with Holes*", *AIAA Journal*, Vol. 31, 1293-1298.

[18] Singh, S.B., Kumar, A. and Iyengar, N.G.R., "*Progressive Failure of Symmetrically Laminated Plate Under Uni-axial Compression*", Structural Engineering and Structural Mechanics, Vol. 5, 1997, pp. 433-450.

[19] Singh, S.B., Kumar, A. and Iyengar, N.G.R., "*Progressive Failure of Symmetrical Laminates Under In-plane Shear, Part-1: Positive Shear*", Structural Engineering and Structural Mechanics, Vol. 6, 1998, pp. 143-159.

[20] Singh, S.B., Kumar, A. and Iyengar, N.G.R., "*Progressive Failure of Symmetrical Laminates Under In-plane Shear, Part-2: Negative Shear*", Structural Engineering and Structural Mechanics, Vol. 6, 1998, pp. 143-159.

[21] Stock, T.A., Bellini, P.X., Murthy, L.N. and Chamis, C.C., "*Probabilistic Composite Micromechanics*", Proceeding of the AIAA/ASME/ASCE/AHS/ASC 29th Structures, Structural Dynamics and Materials Conference (Williamsburg, VA), AIAA, Washington, DC, April 1988, Pt. 3, pp.1289-1293.

[22] Fukuda, H., "*Monte Carlo Simulation of the Strength of Hybrid Composite*", Journal of Composite Materials, Vol.16, 1982, pp. 371-385.

[23] Dzenis, Y.A., Joshi, S.P. and Bogdanocich, A.E., "*Damage Evaluation Modeling in Orthotropic Laminated Composites*", AIAA Journal, Vol. 32, No. 2,1994, pp. 357-364.

[24] Joshi, S.P. and Frantziskonis, G., "*Damage Evaluation in Laminated Advanced Composites*", Composite Structures, Vol. 17, No. 2,1991, pp. 127-139.

[25] Larder, R.A., "*The Stochastic Finite Element Simulation of Parallel Fiber Composites*", Journal of Composite Materials, Vol. 10, 1976, pp. 21-31.

[26] Cassenti, B.N., "*Probabilistic Static Failure of Composite Material*", AIAA Journal, Vol. 22, No. 1, 1984, pp. 103-110.

[27] Fukunaga, H. and Chou, T.W., "*Probabilistic Failure Strength Analysis of Graphite/Epoxy Cross-Ply Laminates*", Journal of Composite Materials, Vol. 18, 1984, pp. 339-351.

[28] Rosen, B.W., "*Tensile Failure of Fibrous Composite*", AIAA Journal, Vol. 2, No. 11, 1964, pp. 1985-1991.

[29] Zweben, C., "*Tensile Failure of Fiber Composite*", AIAA Journal, Vol. 6, No. 12, 1968, pp. 2325-2332.

[30] Harlow, D.G. and Phoenix, S.L., "*The Chain of Bundles Probability Model for the Strength of Fibrous Materials I: Analysis and Conjectures*", Journal of Composite Materials, Vol. 12, 1978, pp. 195-214.

[31] Harlow, D.G. and Phoenix, S.L., "*The Chain of Bundles Probability Model for the Strength of Fibrous Materials II: A Numerical Study of Convergence*", Journal of Composite Materials, Vol. 12, 1978, pp. 314-334.

[32] Contreras, H., "*The Stochastic Finite Element Method*", International Journal for Computers and Structures, Vol. 12, 1980, pp.341-348.

[33] Vanmarcke, E., Shinozuka, M., Nakagiri, S., Schueller, G.I., and Grigoriu, M., "*Random Fields and Stochastic Finite Elements*", Structural Safety, Vol. 3, 1986, pp. 143-166.

[34] Benaroya, H. and Rehak, M., "*Finite Element Methods in Probabilistic Structural Analysis: A Selective Review*", Applied Mech. Rev., Vol. 41, No. 5, May 1988, pp.201-213.

[35] Yamazaki, F., Shinozuka, M. and Dasgupta, G., "*Neumann Expansion for Stochastic Finite Element Analysis*", Journal of Engineering Mechanics, Vol. 114, No. 8, 1986, pp. 1335-1354.

[36] Ostoja-Starzewski, M., "*Micromechanics as a Basis of Stochastic Finite Elements and Differences: An Overview*", Applied Mech. Rev., Vol. 46, No. 2, November 1993, pp. S136-S147.

[37] Vanmarcke, E.H., "*Stochastic Finite Elements and Experimental Measurements*", Probabilistic Engineering Mechanics, Vol. 9, 1994, pp. 103-114.

[38] Iwan, W.D. and Jensen, H., "*On the Dynamic Response of Continuous Systems Including Model Uncertainty*", Journal of Applied Mechanics, Vol. 60, 1993, pp. 484-490.

[39] Koyluoglu, H.U., Nielsen, S.R.K. and Cakmak, A.S., "*Stochastic Dynamics of Geometrically Non-linear Structure with Random Properties Subject to Stationary Random Excitation*", Journal of Sound and Vibration, Vol. 190, 1996, pp. 821-841.

[40] Ramu, S.A. and Ganesan, R., "*A Galerkin Finite Element Technique for Stochastic Field Problems*", Computer Methods in Applied Mechanics and Engineering, Vol. 105, 1993, pp. 315-331.

[41] Zhu, W.Q., Ren, Y.J. and Wu, W.Q., "*Stochastic FEM Based on Local Averages of Random Vector Fields*", Journal of Engineering Mechanics, Vol. 118, No. 3, 1992, pp. 496-511.

[42] Jensen, H. and Iwan, W.D., "*Response of Systems with Unicertain Parameters to Stochastic Excitation*", Journal of Engineering Mechanics, Vol. 118, No. 5, 1992, pp. 1012-1025.

[43] Liu,W.K., Belytschko, T. and Mani,A., "*Applications of Probabilistic Finite Element Methods in Elastic/Plastic Dynamics*", Journal of Engineering for Industry, Vol. 109, 1987, pp. 2-8.

[44] Ghanem, R. and Spanos, P.D., "*Polynomial Chaos in Stochastic Finite Elements*", Journal of Applied Mechanics, Vol. 57, 1990, pp. 197-202.

[45] Ganesan, R., Sankar, T.S. and Ramu, S.A., "*Non-conservatively Loaded Stochastic Columns*", Int. Journal of Solids and Structures, Vol. 30, No. 17, 1993, pp. 2407-2424.

[46] Shinozuka, M., Kako, T. and Tsurui, A., "*Random Vibration Analysis in Finite Element Formulation*", Random Vibration-status and Recent Developments, Ed. I. Elishakoff and Lyon, R.H., Elsevier, New York, 1986.

[47] Ramu, S.A. and Ganesan, R., "*Free Vibration of a Stochastic Beam-column using Stochastic FEM*", International Journal for Computers and Structures, Vol. 41, No. 5, 1991, pp. 987-994.

[48] Ren, Y.J., Elishakoff, I. and Shinozuka, M., "*Finite Element Method for Stochastic Beams Based on Variational Principles*", Journal of Applied Mechanics, Vol. 64, 1997, pp. 664-669.

[49] Sankar, T.S., Ramu, S.A. and Ganesan, R., "*Variability of SIF and COD of Stochastic Structural Systems*", International Journal for Computers and Structures, Vol. 43, No. 6, 1992, pp. 1135-1145.

[50] Sankar, T.S., Ramu, S.A. and Ganesan, R., "*Stochastic Finite Element Analysis for High Speed Rotors*", Journal of Vibration and Acoustics, Vol. 115, 1993, pp. 59-64.

[51] Liaw, D.G., and Yang H.T.Y., "*Reliability of Initially Compressed Uncertain Laminated Plates in Supersonic Flow*", AIAA Journal, Vol. 29, No. 6, 1991, pp. 952-945.

[52] Ganesan, R. and Hoa, S.V., "*Stochastic Finite Element Analysis of Composite Structure*", CANCAM 95, 15th Canadian Congress of Applied Mechanics, May 95, Victoria, Canada.

[53] Nakagiri, S., Takabatake, H. and Tani, S., "*Uncertain Eigenvalue Analysis of Composite Laminated Plates by the Stochastic Finite Element Method*", Journal of Engineering for Industry, Vol. 109, 1987, pp. 9-12.

[54] Engelstad, S.P. and Reddy, J.N., "*Probabilistic Nonlinear Finite Element Analysis of Composite Structures*", AIAA Journal, Vol. 31, No. 2, 1993, pp. 362-369.

[55] Chang, C. and Yang, H.T.Y., "*Reliability of Uncertain Flexible Laminated Skewed Plates under Random Compressions*", AIAA Journal, Vol. 30, No. 2, 1992, pp. 464-472.

[56] Slattery, K., "*A Random-damage Finite Element for Modeling Failure in Advanced Composite Materials*", In: Composite Materials: Fatigue and Fracture, Vol. 5, Ed. R..H. Martin, ASTM, Philadelphia, 1995, pp. 231-245.

[57] Miki, M., Murotsu, Y. and Tanaka, T., "*Optimum Fiber Orientation Angle of Multiaxially Laminated Composites Based on Reliability*", AIAA Journal, Vol. 31, 1993, pp. 919-920.

[58] Shao, S., Miki, M. and Murotsu, Y., "*Optimum Fiber Angle of Unidirectional Composites for Load with Variations*", AIAA Journal, Vol. 30, 1992, pp. 189-196.

[59] Miki, M., Murotsu, Y. and Murayama, N., "*Application of Lamination Parameters to Reliability-based Stiffness Design of Composites*", AIAA Journal, Vol. 31, 1993, pp. 1938-1945.

[60] Kogiso, N., Shao, S. and Murotsu, Y., "*Effect of Correlation on Reliability-based Design of Composite Plate for Buckling*", AIAA Journal, Vol. 36, No. 9, 1998, pp. 1706-1713.

[61] Thomas, D.J. and Wetherhold, R.C., "*Reliability Analysis of Ceramic Matrix Composite Laminates*", Journal of Engineering for Gas Turbines and Power, Vol. 115, 1993, pp. 117-121.

[62] Cohen, David, "*Application of Reliability and Fiber Probabilistic Strength Distribution Concepts to Composite Vessel Burst Strength Design*", Journal of Composite Materials, Vol. 26, 1992, pp. 1984-2014.

[63] Tsai, S.W. and Wu, E.M., "*A General Theory of Strength for Anisotropic Materials*", Journal of Composite Materials, Vol. 5, No. 58, 1971.

[64] Christensen, R.M., "*Mechanics of Composite Materials*", John Wiley and Sons Inc., New York, 1979.

[65] Datoo, M.H., "*Mechanics of Fibrous Composites*", Elsevier Applied Science, London and New York, 1991.

[66] Ganesan, R. and Haque, Z., "*Stochastic Finite Element Analysis of Composite Laminates for Fracture*", CSME Forum, 2000, Montreal, Canada.